Republic of Iraq
Ministry of Higher Education and
Scientific Research
University of Diyala
College of Science
Department of Ph ysics

(Micro-Nano) Compartive Structure Characterization of Some Metallic Oxide Powders by Using Rietveld Method

A Thesis

Submitted to the Council of the College of Science University of Diyala in partial fulfillment for the requirement of the Degree of Master of Science in Physics

by

Noor Amer Hameed Al-Safar

B. Sc. 2009

Supervised by

Assistant Professor **Dr. Nabeel Ali Bakr**

Assistant Professor **Dr. Tagreed Muslim Marush**

2014 A.D. ***1435 A.H.***

بسم الله الرحمن الرحيم

﴿ فَأَمَّا الزَّبَدُ فَيَذْهَبُ جُفَاءً وَأَمَّا مَا يَنفَعُ النَّاسَ فَيَمْكُثُ فِي الأَرْضِ كَذَلِكَ يَضْرِبُ اللَّهُ الأَمْثَالَ ﴾

سورة الرعد
الآية ١٧

Dedication

I would like to dedicate my thesis to Imam Musa Al- Kadhim (AS) *and my family: parents, brothers and sister.*

Noor

Acknowledgment

First of all, praise be to Allah, the almighty for being my strength and guide in writing of this thesis. Without him, I would not have had the ability to complete this thesis successfully. Secondly, I offer my humblest and sincerest words of thanks to the prophet Muhammad (peace be upon him) whose way of life has been a continuous guidance for me.

I express my sincere thanks to my supervisor, Dr. Tagreed M. Marush for the great interest she shows in reading and commenting on this thesis. she analyzed my work critically and made valuable suggestions and revisions.

Thanks are also due to my supervisor, Dr. Nabeel A. Bakr for his esteemed supervision, incessant support, inspiration and constructive criticism throughout my project work.

I would like to express my gratitude to University of Diyala/ College of Sciences/ Deanery of the College and Department of Physics for giving me the chance to join the M.A program in physics. Extended thanks are to staff members to University of Baghdad/ College of education for Pure Science/ Ibn-Al-Haitham/ Department of Physics for enabling me to use their laboratories.

Dr. Ziyad T. Khodair is also worth my thanks for being my mentor and role model for tirelessly guiding me through every step of this work.

My deep and grateful thanks are due to Mr. Ismail and Mr. Haitham Akram for help me during my work.

Finally, I would also like to thank parents, for their continued support. I always looked to them for help and inspiration. I would like to give my brothers, Haider and Mustafa as well as my sister Aayah many thanks for aiding me in this thesis.

Papers Published

- N. A. Baker, T. M. Al-Saadi and N. A. Hameed, " Study of nanocrystalline structure and micro properties of ZrO_2 powders by using Reitveld method ", International Journal of Current Research, Vol. 6, Issue 03, pp.5743-5748, March 2014.

- T. M. Al-Saadi, N. A. Baker and N. A. Hameed, " Study of nanocrystalline structure and micro properties of ZnO powders by using Rietveld method ", International Journal of Engineering and Technical Research (IJETR) ISSN: 2321-0869, Vol. 2, Issue 4, pp. 191-195, April 2014.

Abstract

This study deals with nanocrystalline structure and micro properties for metallic oxide powders (ZrO_2 , ZnO , Al_2O_3) in nano and micro size by using Rietveld method for X-ray powder diffraction. These samples are chosen on the basis of different crystalline systems. The samples are scanned by using XRD before and after their treatment of heating at 1180°C for Al_2O_3 & ZrO_2 and 1200°C for ZnO. From the results peaks for XRD, indexing process is done by using two programs (Dicvol 91 and Treor 90) for determining space group, crystalline system, unit cell parameters and Miller indices for each o f the used samples. The obtained parameters from indexing process are used by coupling with intensity data in Fullprof program for crystalline structure refinement and obtaining fitting between observed and calculated diffraction patterns where reliability factors for ZrO_2 nano powder before heat treatment is 1.6 and after it is 1.5 for micro powder before heat treatment is 1.4 and after it is 1.7, for ZnO nano powder before heat treatment is 1.3 and after it is 1.1 for micro powder before heat treatment is 1.9 and after it is 1.4, for Al_2O_3 nano powder before heat treatment is 2.5 and after it is 1.9 for micro powder before heat treatment is 1.1 and after it is 2.4. The obtained data from Fullprof program is used in WinPLOTER program for drawing observed and calculated diffraction patterns after refinement process for the samples which the research dealt with is done. By using XRD data, we obtained grains size by using Debye-Scherrer formula, grains size and strain by using Williamson-Hall formula. The grains size is increased after heat treatment. Texture coefficient was calculated for each of the research samples.

Finally, SEM characterization for all samples before and after heat treatment. The pictures show that there is a change in the nature of grains shape and size.

List of Contents

Chapter Four: Results and Discussion

Chapter Five: Conclusion and Future Work

List of Figures

List of Tables

List of Abbreviations

Abbreviations	Definition
AFM	Atomic Force Microscope
CVDM	Chemical Vapor Deposition Method
FWHM	Full Width at Half Maximum
ICDD	International Centre for Diffraction Data
JCPDS	Joint Committee on Powder Diffraction Standards
PDF	Powder Diffraction File
SEM	Scanning Electron Microscope
SPM	Scanning Probe Microscope
SI	System International Unites
TC	Texture Coefficient
TEM	Transmission Electron Microscope
UV-VIS	UV-Visible Spectroscopy
W-H	Williamson-Hall
XRD	X-ray Diffraction
XRPD	X-ray Powder Diffraction

List of Symbols

Symbol	Definition
A_Θ	Absorption multiplier
μ	Absorption coefficient
A	Absorption correction factor
f_j	Atomic scattering factor
α_1	Angular aperture of a monochromater to sample collimator
α_k	Angle between the preferred orientation vector and the normal to the planes generating the diffracted peak.
β_D	Broadening due to small crystallite size
Y_{bi}	Background intensity
$B_i(obs)$	Background contribution
T_h	Bragg position
R_B	Bragg reliability factor
D	Crystallite size
Y_{ci}	Calculated intensity
α_2	Collimation between sample and detector
$u_1v_1w_1$ and $u_2v_2w_2$	Coordinates of atoms having structure factors f_1, f_2, respectively
Θ	Diffraction angle or Bragg's angle
$E_{hk\ell}$	Extinction multiplier
R_{exp}	Expected factor
X_j, y_j and z_j	Fractional atomic coordinates of the j^{th} atom in the model
β_k or FWHM	Full width at half maximum
χ^2	Goodness of fit

$I_{hk\ell}$	Intensity
L_p	Lorentz-polarization factor
L_Θ or $1/\sin^2 \Theta \cos \Theta$	Lorentz factor
ε	Microstrain
β	Mosaicity
$M_{hk\ell}$	Multiplicity factor
h,k,ℓ or H	Miller indices
I(hkℓ)	Measured relative intensity of a plane (hkℓ)
$\Phi_{pH}(2\Theta_i)$	Normalized profile function
P	Number of parameters
n	Number of diffraction peaks
Y_{obi}	Observed intensity
g_j	Occupancy factor
P_Θ or $1 + \cos^2 2\Theta$	Polarization factor
$P_{hk\ell}$	Preferred orientation factor
β_s	Peak broadening due to lattice strain
O_k	Preferred orientation function
Ø	Reflection profile function
R_F	R-structure factor
R_p	R-pattern factor
U,V and W	Refinable parameters
G_1 and G_2	Refinable parameter in the Rietveld method
I_o(hkℓ)	Standard intensity of the plane (hkl)
K	Scale factor
$F_{hk\ell}$	Structure factor or structure amplitude
T	Scattering variable

$\left\| F_{pH}(calc) \right\|^2$	Squared absolute value of the structure factor
e^{-2M}	Temperature factor
B_j	Temperature factor coefficient
α_3	Take-off angle of monochromator $2\Theta_m$
V_c	Unit cell volume
λ	Wavelength of Cukα radiation
w_i	Weight
R_{wp}	Weighted-profile reliability factor
n_1	ZrO_2 nano powder before heat treatment
n_2	ZrO_2 nano powder after heat treatment
m_1	ZrO_2 micro powder before heat treatment
m_2	ZrO_2 micro powder after heat treatment
n_3	ZnO nano powder before heat treatment
n_4	ZnO nano powder after heat treatment
m_3	ZnO micro powder before heat treatment
m_4	ZnO micro powder after heat treatment
n_5	Al_2O_3 nano before heat treatment
n_6	Al_2O_3 nano after heat treatment
m_5	Al_2O_3 micro before heat treatment
m_6	Al_2O_3 micro after heat treatment

Chapter One

Introduction

1-1 Introduction

The analysis of crystalline material and the determination of crystal structures is an important and a well known method since its beginning in the early 1930s. In the early 1920s, few examples of crystal structure analyses relied on single crystals with a rapid development in methods. The analysis today is highly automated and sophisticated, but it is still based on diffraction experiments with X-rays on single crystals in sizes around 100 μm. The development in methods of crystal structure analysis with the so-called direct methods make the determination of crystal structures . The main application of single crystal structure determination today is found in organic materials and proteins [1].

Powder diffraction is a very fast and a very versatile analytical method for identification and quantitative determination of crystalline phases found in powder and solid samples for so reasons. The first is that very often single crystals are not available, at least not in the quality or size required for single crystal work. Second, polycrystalline samples can be brought under “extreme” conditions, like high and low temperatures and high pressures without too much difficulties. Third, minor impurities are not a serious problem, and finally exposure times can be very short, even in terms of μs. Finally, the most important feature is that the complete diffraction pattern is recorded in a very short time [1-3].

Structure determination from powder diffraction data is much more difficult than from single crystal data because of the collapse of the three-dimensional reciprocal space of the individual crystallites on the one-dimensional 2θ axis and systematic overlapping of diffraction peaks due to symmetry conditions and considerable background which are difficult to define with accuracy and preferred orientation [4].

To develop an enhanced procedures for obtaining structural information from powder samples, in the late 1960s, Rietveld proposed a method for analysing the more complex patterns obtained from low-symmetry materials by means of a curve-fitting procedure. The least-squares refinement minimizes the difference between the observed and calculated profiles, rather than individual reflections. Refinement by the Rietveld method is now commonplace with both laboratory and synchrotron X-ray data [5].

1-2 Literature Review

The development of least-squares crystallographic structure-refinement methods occurred in 1960 because the growing availability of digital computers, was applied to the single-crystal data and powder data. In the same year, a number of laboratories, such as (UKAEA, Harwell), made widespread use of single-crystal codes for refining structures from powder data, and some of the codes were adapted to handle groups of non-equivalent overlapping reflections that could not be resolved experimentally. Such studies were used in the quantitative structural characterization of high-symmetry inorganic materials. The limitation of the integrated intensity method was due to the fact that it could not be applied to the complex patterns obtained from low-symmetry materials [5].

In the seventh congress of the IUCr in Moscow in 1966, Hugo M. Rietveld presented his first report on the method that was used to refine structures from data obtained by fixed wavelength neutron diffraction. The method was suggested to be applied to X-ray data but it was not encouraged. In 1969, Rietveld published full implementation of the method then attention which gained attention consequently. Before 1977, (Cheetham and Taylor), used Rietveld method to refine 172 structures from data obtained by fixed wavelength neutron diffraction. In 1977, (Malmros and Thomas, Young et al. and Khattak and Cox) , used Rietveld method to refine structures from X-ray data and it became generally accepted for X-ray as well as neutron powder diffraction [6].

In 1981, Wiles and Young [7], developed a new computer program for the application of the Rietveld method with X-ray data, or with neutron nuclear scattering data. The program accommodated either one or two wavelengths. It permitted simultaneous refinement of the structures of two phases and the background.

In 1982, Albinati and Willis published an article on the application of the Rietveld method in the four experimental technique, with neutrons or X-rays as the primary radiation and with the scattered intensity measured at a fixed wavelength or at a fixed scattering angle [8]. This article gave a good impression on the state of the method at that moment [6].

In the period (January 1987 to May 1989), a total of 341 papers were published with reference to using the Rietveld method, of which nearly half used neutron diffraction [6].

(Quantitative phase analysis of multi component mixtures using X-ray powder diffraction (XRPD) data has been approached with a modified version of the Rietveld computer program of Wiles & Young) and a new method discovered in 1988, by Bish and Howard [9]. This technique fits the complete diffraction pattern, it is less susceptible to primary extinction effects and minor amounts of preferred orientation. Additional benefits of this technique over traditional quantitative analysis methods include the determination of precise cell parameters and approximate chemical compositions, and the potential for the correction of preferred orientation and micro absorption effects.

In 1999, Mccusker et al. [10], reported a set of general guidelines for structure refinement using the Rietveld method which had been formulated by the international union of crystallography commission on powder diffraction.

In 1999, Daning et al. [11], studied crystal structure of zirconia by Rietveld refinement. It was found that a structural transition from monoclinic to tetragonal occurred when Y_2O_3 and CeO_2 were doped into zirconia. The space group of the pure ZrO_2 (monoclinic) is $P2_1/c$, Z=4, the lattice parameters were a=0.5146nm, b=0.5205nm, c=0.5313nm and β=99.1°. The space group of the tetragonal structure were $P4_2/nmc$, Z= 2. The lattice parameters were a = 0.3626nm, c =0.5226nm for CeO_2 doped zirconia and a = 0.360 2 nm, c ~0.5179 nm for Y_2O_3 doped zirconia, respectively.

In 2000, Bokhimi et al. [12], studied quantitative analysis of phase transformations in nano crystalline materials via Rietveld refinement by using the codes developed for microcrystalline materials. The software was corrected to incorporate the angle dependence of atomic scattering and polarization factors for each diffraction peak, and to model the amorphous phases that frequently coexist with the nano phases. It was found in yttria-doped samples annealed at 400°C, amorphous and crystalline structures coexisted with concentrations that depended on yttria content. In non-doped samples, the tetragonal phase was stabilized by the carboxyls involved in the synthesis.

Standard transition aluminas was studied in 2000, by Souza Santos et al. [13], by using transmission electron microscopy (TEM) and scanning electron microscopy (SEM). Selected area electron diffraction, in parallel with XRPD, was used for confirmation of the different transition aluminas types. The transition aluminas : χ, κ, γ, θ, δ and η were supplied by ALCOA central laboratory. It was found that the χ, κ, γ and δ-Al_2O_3 micro crystals are pseudo morphs from their respective precursors gibbsite and boehmite , θ-Al_2O_3 micro crystals are not pseudo morphs after the standard δ- Al_2O_3 sample and η-Al203 are not pseudo morphs after bayerite somatoids.

Polymeric precursor method was used in 2007 by Cava et al. [14], to prepare nanocrystalline Al_2O_3 powders. The prepared Al_2O_3 nano powders were

characterized by (XRD), micro-Raman spectroscopy and refinement of the structures through the Rietveld method . The results show that the identification of three steps on the γ-Al_2O_3 to α-Al_2O_3 phase transition and the particle size is closely related to γ -Al_2O_3 to α-Al_2O_3 phase transition.

The microstructure characterization of commercially available zirconia powders was studied in 2008 by Dercz et al. [15], using (XRD), (SEM) and (Hill and Howard) procedure which was applied for quantitative phase analysis. It was found that the good agreement of lattice parameters determined by Rietveld refinement method and these from international centre for diffraction data (ICDD) files for all involved phases and Rietveld refinement method appeared to be very useful in the characterization of complex, multiphases materials.

In 2009, Prasad and Jha [16] studied ZnO nanoparticles: synthesis and adsorption by using (XRD) and (TEM). (XRD and TEM) were performed to ascertain the formation of ZnO nanoparticles. Rietveld analysis of the X-ray data indicated that ZnO nanoparticles had hexagonal unit cell structure and individual nanoparticles had the size of 5-15 nm.

Phase quantification of mullite zirconia and zircon commercial powders was studied in 2010 by Rendtorff et al. [17], using the short range technique of the perturbed angular correlation (PAC) and the long range technique X-ray diffraction (Rietveld). The PAC technique, showed that zircon contained crystalline $ZrSiO_4$ and an important amount of a structurally distorted zircon, which also observed accompanying monoclinic zirconia in mullite zirconia. The XRD technique showed that after annealing treatment, important changes would occur in crystalline contents of the powders.

Nanostructural study of ZnO nanostructures was carried out in 2011 by Albores et al. [18], using Rietveld analysis and (SEM). The results obtained by (SEM) confirmed that the diameter of nanorods was affected directly by the

concentration of both zinc and OH sources. The result obtained by Rietveld refinement of grazing incidence XRD data evidence low-textured materials with oriented volumes less than 18% coming from (101) planes in Bragg condition.

In 2013, Krobthong et al. [19], prepared ZnO tetrapods by a rapid thermal oxidation from mixing metallic zinc powder into hydrogen peroxide at 1000 °C under atmospheric pressure. Single crystal structure analysis by Rietveld method showed that the ZnO tetrapods had the pure wurtzite hexagonal structure with lattice parameters *a* and *c* values of 0.3252 nm and 0.5211 nm, respectively.

1-3 Aim of thesis

Study of nano and micro crystalline structure for metallic oxide powders (Al_2O_3 , ZrO_2 , ZnO) by using Rietveld method through the use of the Fullprof program and study the effect of heat treatment on atomic position, lattice parameters, Miller indices, transition phases, crystallite size and comparison of results obtained.

1-4 Outline of the thesis

(1) Chapter one includes an introduction to the research, literature review, the aim of the thesis, outline of the thesis and methodology of the thesis.

(2) Chapter two contains a detailed description of X-ray powder diffraction, nanotechnology and Rietveld method .

(3) Chapter three includes the experimental part to raw materials, ((XRD), (SEM)) testing and analysis software.

(4) Chapter four contains the extracted results and discusses indexing of powder pattern, crystal structure refinement, parameters affecting refinement and ((XRD), (SEM)) characterization.

1-5 Methodology of the thesis

(1) Obtaining the samples for nano-powders of various metal oxides (Al_2O_3 , ZrO_2 , ZnO) and micro-powders for the same oxide are commercially available .

(2) Scan the samples by using ((XRD), (SEM)) systems.

(3) Perform the thermal treatment of the samples at different temperatures in order to convert them to other phases and scanning by using XRD and SEM.

(4) From X-ray diffraction define Bragg's angles, interplaner displacement and matching diffraction pattern with powder diffraction file (PDF) and then carry out the indexing process by using special software based on the Rietveld method to obtain Miller indices, space group and lattice parameters (a, b, c, α, β, γ) and from SEM define morphology of the surface and grains size.

(5) Refinement of the crystalline structure of each sample by Rietveld method through the Fullprof program**.**

(6) Study the effect of thermal treatment of the samples at different temperatures on the transition phases and the lattice parameters and the crystallite size.

(7) Explanation and comparison of results obtained.

Chapter Two

Theoretical Part

2-1 Introduction

This chapter shows the theoretical part which includes the explanation of nanotechnology, X-ray diffraction method and the explanation of Rietveld method.

2-2 Nanotechnology

The first use of the concepts in 'nano-technology' was in "There's Plenty of Room at the Bottom," a talk given by physicist Richard Feynman in the American Physical Society meeting at Caltech on December 29, 1959 [20].

Feynman spoke about the principles of miniaturization and atomic-level precision and how these concepts did not violate any known law of physics. He proposed that it was possible to build a surgical nanoscale robot by developing quarter-scale manipulator hands that would build quarter-scale machine tools analogous to those found in machine shops, continuing until the nanoscale was reached . He also discussed systems in nature that achieved atomic-level precision unaided by human design. Furthermore, he laid out some precise steps that might need to be taken in order to begin work in this uncharted field [21, 22].

The last two decades have seen the explosion of miniaturization, based on the development of nanotechnologies, and its use in an increasing number of scientific, technical fields, including biology, chemistry, microelectronics, high density data storage, optics and optoelectronics, sensors, photonics, etc. Nanofabrication and nano instrumentation are have recently been popular research topics in the development of nanotechnology. Nanotechnology is the chance for the realization of that purpose. Nanoscience and technology is a field that focuses on [23]:

(1) The development of synthetic methods and surface analytical tools for building structures and materials, typically on the sub-100 nanometer scale.
(2) The identification of the chemical and physical consequences of miniaturization.

(3) The use of such properties in the development of novel and functional materials and devices. This field is of greatest interest to handle nanoparticles, nanostructured materials, nanoporous materials, nanopigments, nanotubes, nanoimprinting, quantum dots, and has already led to many innovative applications, particularly in materials science. For basic investigations, an important role is played by manipulation or imaging nanoscale techniques (e.g., atomic force microscope(AFM) and SEM).

Nanotechnology can be defined as the design, synthesis, and application of materials and devices whose size and shape have been engineered at the nanoscale. It exploits unique chemical, physical, electrical, and mechanical properties that emerge when matter is structured at the nanoscale. In its original sense, 'nanotechnology' refers to the projected ability to construct items from the bottom up, using techniques and tools being developed today to make complete, high performance products. It is the ability to observe, measure, manipulate, and manufacture things at the nanometer scale. A nanometer (nm) is an system international unites (SI) unit of length 10^{-9} or a distance of one-billionth of a meter which is comparable to the size of atoms and molecules. It is the research and development of materials, devices, and systems that exhibit physical, chemical, and biological properties. These properties can be different from those found at larger scales those that are more than 100 nanometers [22, 24].

Three factors define nanotechnology: small size, new properties, and the integration of the technology into materials and devices. Nanotechnology covers a broad range of science, drawing concepts, knowledge and expertise, skills, and materials from all the three classical sciences, physics, chemistry, and biology [25].

2-3 Nanomaterials

Nanomaterials are a diverse class of small-scale substances. According to Siegel nanostructured materials can be generally grouped into [26, 27]:

(1) Zero-dimensional structures (i.e., quantum dots and core-shell nanostructures).

(2) One-dimensional structures (i.e., nanorods and nanowires).

(3) Two-dimensional structures (thin films).

(4) Three-dimensional structures (bulk materials with nanoscale building blocks). As shown in figure (2-1):

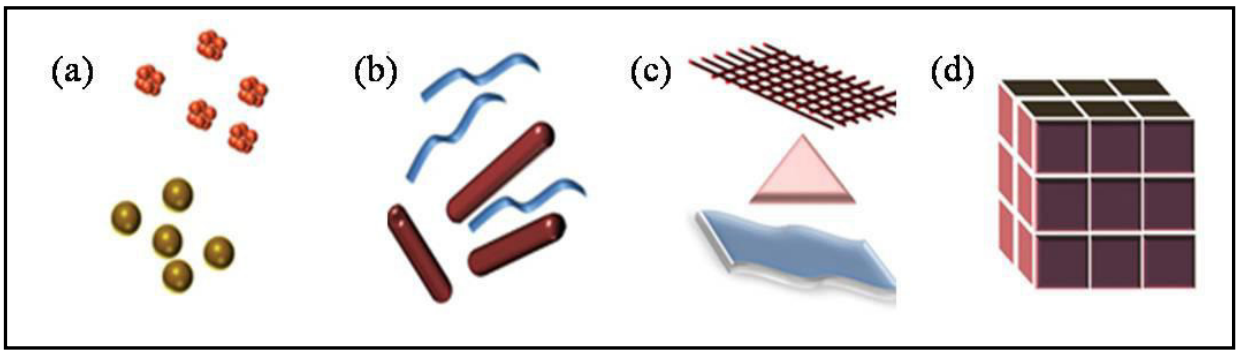

Fig. (2-1): Classification of Nanomaterials (a) 0D spheres and clusters. (b) 1D nanofibers, wires and rods. (c) 2D films, plates and networks. (d) 3D nanomaterials [28].

They can exist in single, fused, aggregated or agglomerated forms with spherical, tubular, and irregular shapes. Common types of nanomaterials include nanotubes, dendrimers, quantum dots and fullerenes. Nanomaterials have applications in the field of nano technology, and display different physical chemical characteristics from normal chemicals (i.e., silver nano, carbon nanotube, fullerene, photocatalyst, carbon nano, silica) [29].

The first discovered nanomaterials was prepared by vacuum evaporation of iron in inert gas and condensed in cooled substrates . Then many methods used to fabricate nanoparticles including inorganic ceramics and organic compound are developed. They include arc plasma torch to produce metallic powder , laser induced chemical vapor deposition method (CVDM) to produce special compounds, and microwave plasma enhanced to produce hard and brittle materials [30].

2-4 X-ray Powder Diffraction

X-ray powder diffraction is a powerful non-destructive testing method for determining a range of physical and chemical characteristics of materials [31].

A powder diffraction pattern contains in principle the same amount of information as a single-crystal diffraction data set does. XRD is an indispensable method for materials characterization and quality control. X-ray diffraction has been used in two main areas, for the fingerprint characterization of crystalline materials and the determination of their structure. Each crystalline solid has its unique characteristic X-ray powder pattern which may be used as a 'fingerprint' for its identification [2, 4, 32].

X-ray diffraction results from the interaction between X-rays and electrons of atoms depending on the atomic arrangement, interferences between the scattered rays are constructive when the path difference between two diffracted rays differ by an integral number of wavelengths. The relationship describing the angle at which a beam of X-rays of a particular wavelength diffracts from a crystalline surface is known as Bragg's law (as shown in figure (2-2)) this selective condition is described by the Bragg equation [33]:

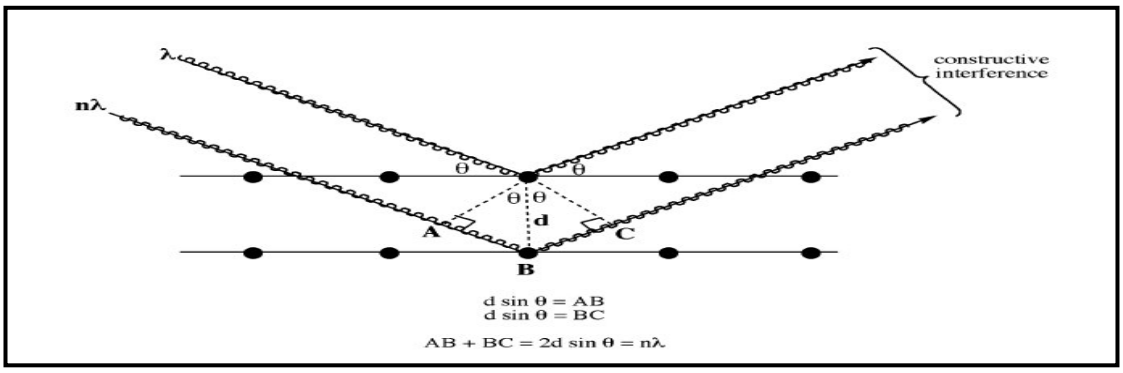

Fig. (2-2): Schematic representation of diffraction of X-rays by crystallographic plane [34].

Recently powder method has achieved remarkable success because of [1, 35]:

(1) Powder diffraction is a very fast and a very versatile analytical method.

(2) Polycrystalline samples can be brought under "extreme" conditions, like high and low temperatures and/or high pressures without too much difficulties.
(3) Minor impurities are not a serious problem.
(4) Exposure times can be very short, even in terms of μs.
(5) The exact description of the peaks in the pattern of powder diffraction [36].
(6) Optimization of measurement [36].

X-ray powder diffraction is most widely used in [37-40]:

(1) Determination of unit cell dimensions.
(2) Measurement of sample purity.
(3) Identification of single-phase materials - minerals, chemical compounds, ceramics or other engineered materials.
(4) Identification of multiple phases in microcrystalline mixtures.
(5) Recognition of amorphous materials in partially crystalline mixtures.
(6) Determination of the crystal structure of identified materials.

With specialized techniques, XRD can be used to [31,41]:

(1) Determine crystal structures using Rietveld refinement.
(2) Determine of modal amounts of minerals (quantitative analysis).
(3) Make textural measurements, such as the orientation of grains, in a polycrystalline sample.

A characteristic feature of powder diffraction is the collapse of the three-dimensional reciprocal space of the individual crystallites on the one-dimensional 2Θ axis. The resulting effects are [1, 41]:

(1) Systematic overlapping of diffraction peaks due to symmetry conditions.
(2) Accidental overlapping because of limited experimental resolution.
(3) Considerable background difficult to define with accuracy.

(4) Non-random distribution of the crystallites in the specimen, generally known as (preferred orientation).

(5) For mixed materials, detection limit is approximately 2% of sample [37].

2-5 Information Contained in a Diffraction Pattern

(1) Peak Positions: the peak positions give information about the translational symmetry (i.e. the size and shape of the unit cell).

(2) Peak Intensities: the peak intensities give information about the electron density inside the unit cell(i.e. where the atoms are located).

(3) Peak Shapes and Widths: the peak widths and shapes can give information on deviations from a perfect crystal (i.e. Knowledge crystallite size if it is less than roughly 100 – 200 nm and extended defects and microstrain) [35].

Figure (2-3) illustrates the amount of information which can be extracted from a powder diffraction pattern. The goal for a systematic evaluation of a powder pattern is to extract as much information as possible in a routine manner.

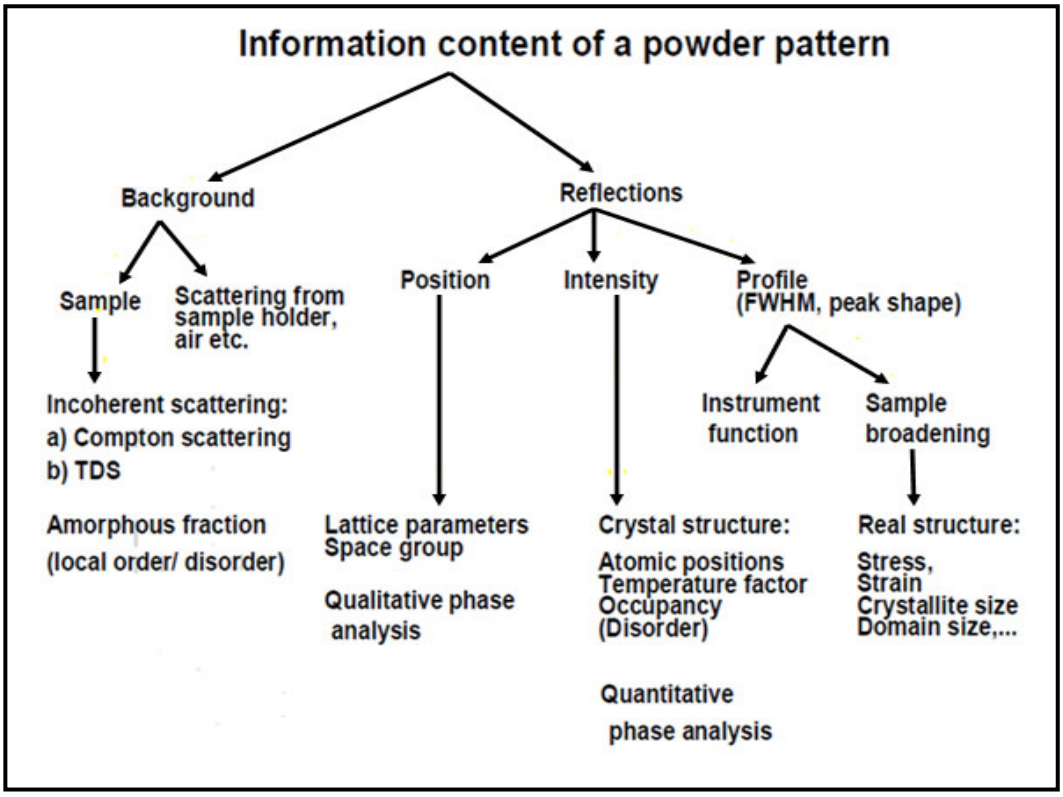

Fig. (2-3): Content of information of a powder diffraction pattern [2, 35]

2-6 Intensity of Powder Diffraction Peaks

Any powder diffraction pattern is composed of multiple Bragg peaks, which have different intensities in addition to varying positions and shapes. Numerous factors have either central or secondary roles in determining peak intensities[42].

These factors can be grouped as:

(1) Structural factors, which are determined by the crystal structure.

(2) Specimen factors owing to its shape and size, preferred orientation, grain size and distribution, microstructure and other parameters of the sample.

(3) Instrumental factors, such as properties of radiation, type of focusing geometry, properties of the detector, slit and/or monochromator geometry.

The two latter groups of factors may be viewed as secondary. They are less critical than the principal part defining the intensities of the individual diffraction peaks, which is the structural part. Structural factors depend on the internal (or atomic) structure of the crystal, which is described by relative positions of atoms in the unit cell, their types and other characteristics, such as thermal motion and population parameters.

2-7 Integrated Intensity

There are six factors affecting the relative intensity of the diffraction lines on a powder pattern[43-45]:

(1) Polarization factor.

(2) Structure factor.

(3) Multiplicity factor.

(4) Lorentz factor.

(5) Absorption factor.

(6) Temperature factor.

The integrated intensity, I, of a diffracted beam is [46]:

$$I = F^2 M (1+\cos^2 2\Theta / \sin^2 \Theta \cos \Theta) e^{-2M} \ldots\ldots\ldots (2\text{-}1)$$

Where

I : relative integrated intensity (arbitrary units).

F : is the structure factor.

M : is the multiplicity factor.

Θ : is the Bragg angle.

e^{-2M} : is the temperature factor.

$1/\sin^2 \Theta \cos \Theta$: is the Lorentz factor.

$1 + \cos^2 2\Theta$: is the polarization factor.

The term in parentheses is the Lorentz polarization factor.

Integrated Intensity is a function of the atomic structure, and it also depends on multiple factors, such as certain specimen and instrumental parameters. It represents the true intensity of Bragg peaks in powder diffraction. The intensity, $I_{hk\ell}$, scattered by a reciprocal lattice point ($hk\ell$) corresponds to the integrated intensity of the matching Bragg peak [42].

The above equation omitted factors which are constant for all lines of the pattern such as the intensity of the incident beam and the charge and mass of the electron. The intensity of a diffraction line is also directly proportional to the irradiated volume of the specimen and inversely proportional to the camera radius, but these factors are again constant for all diffraction lines and may be neglected. Omission of the temperature and absorption factors the above equation is valid only for the Debye-Scherrer method. It gives the relative integrated intensity, i.e. the relative area under the curve of intensity vs. 2Θ. That "integrated intensity" is not really intensity. It is expressed in terms of energy crossing unit area per unit of time. A beam diffracted by a powder specimen carries a certain amount of energy per unit time and one could quite properly refer to the total power of the diffracted beam [43].

The calculated integrated intensity in powder diffraction is expressed as the following product :

$$I_{hk\ell} = K\ M_{hk\ell}\ L_{\Theta}\ P_{\Theta}\ A_{\Theta}\ P_{hk\ell}\ E_{hk\ell}\ |F_{hk\ell}|^2 \ \ldots\ldots\ldots (2\text{-}2)$$

Where

K : is the scale factor.

$M_{hk\ell}$: is the multiplicity factor.

L_{Θ} : is the Lorentz factor.

P_{Θ} : is the polarization factor.

A_{Θ} : is the absorption multiplier.

$P_{hk\ell}$: is the preferred orientation factor.

$E_{hk\ell}$: is the extinction multiplier.

$F_{hk\ell}$: is the structure factor (or the structure amplitude).

2-7-1 Scale Factor

It is a multiplier required to normalize experimentally observed integrated intensities with absolute calculated intensities. Absolute calculated intensity is the total intensity scattered by the content of one unit cell in the direction (Θ), defined by the length of the corresponding reciprocal lattice vector. Therefore, the scale factor is constant for a given phase and is determined by the number spatial distribution and states of the scattering centers (atoms) in the unit cell. The scale factor is one of the important variables in structure refinement and its correctness is critical in achieving the best agreement between the calculated and observed intensities. Its value is also essential in quantitative analysis of multiple phase mixtures [42].

2-7-2 Multiplicity Factor

It is a multiplier which accounts for the presence of multiple symmetrically equivalent points in the reciprocal lattice, or, in other words, the number of

symmetrically equivalent reflections. The value of multiplicity factor depends on hkℓ and the crystal symmetry [44].

In the cubic system the highest multiplicity is 48, in the tetragonal system is 16, and in the orthorhombic system it is 8 [47, 48].

Multiplicity factor represents the number of the crystal planes, which have the same spacing and structure factors, but different orientation. When crystal orientations in powder samples are completely random, the probability of crystal orientations, which satisfy the Bragg condition is given by the ratio of multiplicity factors [49].

The number of equivalent planes cutting a unit cell in a particular hkℓ family is called the plane multiplicity factor and will directly affect the intensity. If the shape of the crystallites and the mounting technique do not produce any preferred orientation of the crystallites in a specimen , or if a solid polycrystalline specimen is not textured , then there will be as many crystallites oriented to diffract from the (100) plane as from the ($\bar{1}$00) [50].

In the powder method all planes of the same d-spacing superimpose to the same diffraction cone. It is given by the number of permutations of hkℓ indices that give the same sin2Θ values in the quadratic form for the crystal [51].

The multiplicity factor is defined as the number of permutations of position and sign of hkℓ for planes having the same d and F^2 (is the square of structure factor). It depends on the symmetry of the crystal. It is important because in a polycrystalline or powder specimen consisting of many randomly oriented grains diffraction can occur [46].

2-7-3 Polarization Factor

Polarization of X-rays like visible light, can be linearly polarized or partially. Polarized beams of X-rays can be obtained by scattering from a solid for a scattering angle of 90° [45].

The polarization factor (P) is given in the following form as a function of diffraction angle 2Θ [49]:

$$P= (1+C \cos^2 2\Theta)/(1+C)$$

where

C =1 for an unpolarized beam [44].

$$P= (1+\cos^2 2\Theta)/2 \text{ ……. (2-3)}$$

The relation given here is only valid in the case of an unpolarized incident beam. The beam used to irradiate the sample is sometimes diffracted beforehand by a single crystal acting as a monochromator, in which case the polarization factor's expression is more complex and depends in particular on the diffraction angle of the monochromator single crystal [45,52].

2-7-4 Lorentz Factor

When each lattice point on the reciprocal lattice intersects the diffractometer circle, a diffraction related to the plane represented will occurs. The diffractometer typically moves at a constant 2Θ rate, the amount of time each point is in the diffracting condition will be a function of the diffraction angle. As angles increase, the intersection approaches a tangent to the circle; thus at higher angles, much time is spent in the diffracting condition. This may be corrected by inserting the term $1/(\sin^2\Theta \cos\Theta)$ into the expression for calculating diffraction intensities, this is called the Lorentz factor [53].

The Lorentz factor for powder samples is given by the following equation as a function of diffraction angle [49,54]:

$$L_\Theta = 1 / \sin^2 \Theta \cos \Theta \text{ ……. (2-4)}$$

The Lorentz factor is used independently, and used in many cases as the Lorentz polarization factor by coupling with polarization factor, which is also a function of diffraction angle [49].

The Lorentz-polarization factor is the most important of the experimental quantities that control X-ray intensity with respect to diffraction angle. Its evaluation is essential to any analysis that depends on the intensities of X-ray diffraction maxima [55].

The Lorentz-polarization factor is a combination of two factors the Lorentz factor and the polarization factor that influence the intensity of the diffracted beam. The polarization factor is that the incident beam from the X-ray source is unpolarized. It may be resolved into two plane polarized components, and the total scattered intensity is the sum of the intensities of these two components, which depends on the scattering angle [46].

$$[\text{Lorentz-polarization factor } (L_p)] = 1 + (\cos^2 2\Theta / \sin^2 \Theta \cos \Theta) \quad \ldots\ldots\ldots (2\text{-}5)$$

The Lorentz-polarization factor varies strongly with Bragg angle (Θ) and the overall effect is that the intensity of reflections at intermediate Bragg angles is decreased compared to those at high or low angles. The Lorentz-polarization factor is important in all intensity calculations [46].

2-7-5 Absorption factor

This factor describes the loss of intensity of the incident and reflected X-ray beam within the crystal. The absorption factor (A) is given by a simple function of the absorption coefficient μ, but for various crystal and powder-sample shapes calculation of A is more complex.

If the crystal is thick enough to absorb all the initial beam, and if the reflective planes are parallel to the surface, absorption factor is simply given by [51]:

$$A = \frac{1}{2}\mu \quad \ldots\ldots\ldots \quad (2\text{-}6)$$

The absorption multiplier accounts for absorption of both the incident and diffracted beams and nonzero porosity of the powdered specimen. Absorption effects in powder diffraction are dependent on both the geometry and properties of the sample and the focusing method [52].

2-7-6 Temperature Factor

The temperature factor takes into consideration the effect of temperature on the intensity of the reflections in the x-ray diffraction pattern. At all temperatures the atoms in a crystal are undergoing thermal vibration about their mean positions. One of the effects of this vibration is that the intensities of the reflections decrease as the temperature increases [43]. At a fixed temperature (room temperature) the intensity decreases as d increases because at large Bragg angles planes with low values of d are diffracting. Hence, high-angle reflections are decreased in intensity relative to low-angle reflections. This effect is taken into account by the temperature factor e^{-2M}, where μ is a function of several variables, including μ and the diffraction angle [26].

2-7-7 Preferred Orientation Factor

It is a multiplier, which accounts for possible deviations from a complete randomness in the distribution of grain orientations [54].

2-7-8 Extinction Factor

It is a factor which accounts for deviations from the kinematical diffraction model. In powders, these are quite small and the extinction factor is always nearly neglected [54].

2-7-9 Structure Factor

The structure factor reflects the interference between atoms in the unit cell. All of the information regarding where the atoms are located in the unit cell is contained in the structure factor [48].

The scattering amplitude of a unit cell is determined by summing the scattering amplitudes, f , from all the atoms in the unit cell to all the atoms in the motif. Summing the scattering amplitudes must take into account the path or phase differences between all the scattered waves and is again expressed by a dimensionless number, $F_{hk\ell}$, the structure factor [56].

$$\text{Structure factor } F_{hk\ell} = \frac{\text{amplitude scattered by the atoms in the unit}}{\text{amplitude scattered by a single electron}} \quad \ldots\ldots\ldots (2\text{-}7)$$

$F_{hk\ell}$ expres on the amplitude of scattering from a reflecting plane with Laue indices $hk\ell$ and express the phase angle of the scattered wave . $F_{hk\ell}$ is therefore not a simple number, like f , but is represented as a vector or mathematically as a complex number. In the case of X-ray diffraction from crystals it is the structure factor, $F_{hk\ell}$, which expresses the interference effects from all the atoms in the unit cell which modulates the intensities of the diffracted beams [56].

The sum of the scattered waves from atoms in a unit cell can be computed using the generalized equation [47]:

$$F_{hk\ell} = \sum_{j=1}^{N} f_i \exp [2\pi i(hx_j + kx_j + lx_j) \quad \ldots\ldots\ldots (2\text{-}8)$$

where

N : is the total number of atoms involved in the unit cell.

f_j : is the atomic scattering factor.

$K_{hk\ell}$ can be defined as a structural constant of diffraction line ($hk\ell$) [57]:

$$K_{hk\ell} = (1/V_c^2) \cdot P_{hk\ell} \cdot |F_{hk\ell}|^2 \cdot Lp_{hk\ell} \quad \ldots\ldots\ldots (2\text{-}9)$$

where

V_c : unit cell volume.

The total intensity of a reflection summed up the waves that come from all the atoms. For the total intensity this may be accomplished by inserting the coordinates and I values of each atom in the unit cell in the structure-factor formula for I, which is proportional to the square of the absolute value of the amplitude of the diffracted ray [57]:

$$I \propto |F_{hk\ell}|^2 = [f_1 \cos 2\pi(hu_1 + kv_1 + lw_1) + f_2 \cos 2\pi(hu_2 + kv_2 + lw_2) + \cdots]^2 + [f_1 \sin 2\pi(hu_1 + kv_1 + lw_1) + f_2 \sin 2\pi(hu_2 + kv_2 + lw_2) + \cdots]^2 \quad \ldots\ldots\ldots (2\text{-}10)$$

Where

$u_1v_1w_1$, $u_2v_2w_2$: are the coordinates of atoms having structure factors f_1, f_2 respectively.

The above equation can be written as follows:

$$I \propto |F_{hk\ell}|^2 = [\sum_i f_i \cos 2\pi(hu_i + kv_i + lw_i)]^2 + [\sum_i f_1 \sin 2\pi(hu_i + kv_i + lw_i)]^2 \quad \ldots. (2\text{-}11)$$

2-7-9-1 Atomic Scattering Factor

When considering diffraction of X-rays from a crystal, one needs information about " atomic scattering factors" which provide a measure of the scattering ability of X-rays per atom. Since the nucleus of an atom is relatively heavy compared with an X-ray photon, it does not scatter X-rays. The scattering ability of an atom depends only on electrons, their number, and distribution [49].

The atomic scattering factors increase with the number of electrons on the atoms, the heavy atoms will contribute more to the structure factors. The positions of the heavy atoms may be obtained, and their contributions to the structure factors may be calculated. If the heavy atoms are heavy enough, they

may by themselves determine enough phases so that a Fourier map of the electron density will reveal the positions of some of the lighter atoms. If the structure has a center of symmetry, all that is necessary is that the heavy atom contribution gives the correct sign of a sufficient number of structure factors [58].

2-8 Preferred Orientation in Powder Diffraction

Powder diffraction is based on a fully random distribution of crystallites of equal size. Any deviation from a random distribution affects more or less the measured intensities in the diffraction pattern. These deviations are meant by "preferred orientation". Any preferred orientation shows up as an incorrect intensity distribution, but the peak positions will remain the same. When the shapes of crystallites are isotropic, random distribution of their orientations is not a problem, and deviations from an ideal sample are usually negligible. Quite often the shapes are anisotropic, the results in the introduction of distinctly nonrandom crystallite orientations due to natural preferences in packing of the anisotropic particles. The nonrandom particle orientation is called preferred orientation, and it may cause considerable distortions of the scattered intensity [59].

The problem can be reduced by [42, 44, 60]:

(1) Careful sample preparation (capillary sample will be less problematic than flat samples) .

(2) Use side-loading or back-loading,(i.e. the scattering surface is covered by a plate and the sample loaded from the side or from the bottom. After loading, the plate is removed and the sample is used as usual).

(3) Spinning the specimen around the normal to the specimen plane or by loose packing of the powder.

Quantitative information concerning the preferential crystal orientation can be obtained from the texture coefficient [61].

The texture coefficient (TC) represents the texture of the particular plane, deviation of which from unity implies the preferred growth. Quantitative information concerning the preferential crystallite orientation is obtained from the different texture coefficient TC(hkℓ) defined as [62]:

$$TC(hk\ell) = [I(hk\ell) / I_o(hk\ell)] / [N^{-1} \Sigma_n I(hk\ell) / I_o(hk\ell)] \ldots\ldots (2\text{-}12)$$

Where:

I(hkℓ) : is the measured relative intensity of a plane (hkl).

I_o(hkℓ) : is the standard intensity of the plane (hkl) taken from the Joint Committee on Powder Diffraction Standards (JCPDS) data.

N : is the reflection number.

n : is the number of diffraction peaks.

If TC(hkℓ)≈1 for all the (hkℓ) planes considered, then the films are with a randomly oriented crystallite similar to the JCPDS reference, while values higher than 1 indicate the abundance of grains in a given (hkℓ) direction. Values 0<TC(hkℓ)<1 indicate the lack of grains oriented in that direction. As TC(hkℓ) increases, the preferential growth of the crystallites in the direction perpendicular to the hkℓ plane is the greater [63].

2-9 Crystal Structure

A crystal defined as a substance that is crystalline in three dimensions and is bounded by plane faces, a crystal structure is a unique arrangement of atoms in a crystal. A crystal structure is composed of a unit cell, a set of atoms arranged in a particular way; which is periodically repeated in three dimensions on a lattice. The spacing between unit cells in various directions is called its lattice parameters [64]. The crystal systems are a method of classifying crystals according to their atomic lattice or structure. The atomic lattice is a three dimensional network of atoms that are arranged in a symmetrical pattern. The

shape of the lattice determines not only which crystal system the stone belongs to, but all of its physical properties and appearance [65]. There are seven crystal systems (Table 2-1), the simplest and most symmetric, the cubic (or isometric) system, has the symmetry of a cube, that is, the three axes are mutually perpendicular and of equal length. The other six systems, in order of decreasing symmetry, are hexagonal, tetragonal, rhombohedral (also known as trigonal), orthorhombic, monoclinic and triclinic [66].

Table (2-1): The crystal systems

Name of the system	Symmetric unit cell	
Triclinic	$a \neq b \neq c$	$\alpha \neq \beta \neq \gamma \neq 90^\circ$
Monoclinic	$a \neq b \neq c$	$\alpha = \beta = 90^\circ, \gamma \neq 90^\circ$
Orthorhombic	$a \neq b \neq c$	$\alpha = \beta = \gamma = 90^\circ$
Tetragonal	$a = b \neq c$	$\alpha = \beta = \gamma = 90^\circ$
Rhombohedral	$a = b = c$	$\alpha = \beta = \gamma \neq 90^\circ$
Hexagonal	$a = b \neq c$	$\alpha = \beta = 90^\circ, \gamma = 120^\circ$
Cubic	$a = b = c$	$\alpha = \beta = \gamma = 90^\circ$

Crystalline materials are ubiquitous both in nature and industry. One of their fundamental properties is seen from the crystallographic structure. It is well known that the material may change its crystal structure abruptly when the temperature or pressure varies, resulting in a discontinuous change in material properties. The crystalline phase transition, also known as the Martensitic phase transition, is a diffusionless, solid-to-solid phase transition where the lattice or molecular structure changes [67].

2-10 Indexing a Powder Pattern

XRPD is an ensemble analysis that is generally representative of a powder material, and utilizes powder samples that are often easier to produce than single crystals. For these reasons, XRPD is used routinely for the characterization of crystalline solids. XRPD indexing is one method that can be used to extract

information and aid the interpretation of XRPD patterns. Indexing is always the first step in analyzing a powder diffraction pattern. It is the process of determining the size and shape of the unit cell for a given phase. It involves assigning the correct Miller indices to each Bragg reflection [68].

Indexing makes use only of the positions of the observed peaks. Peak positions are determined by the dimensions and crystal symmetry, as well as the X-ray wavelength utilized. The complexity of the task depends on the symmetry of the phase, it is easy for cubic, tetragonal and orthorhombic systems, but gets significantly more complex when the angels are not 90. Other techniques, such as Rietveld refinement, may be used to extract additional information using the peak intensity information [68,69].

2-11 Sample Broadening

Diffraction peak broadening caused by microstresses in the crystal lattice can be separated into components due to strain in the crystal lattice and crystallite size. Separation of the broadening, from lattice strain and crystallite size is performed by using Fourier analysis of the diffraction peak profile and data collection sufficient to define precisely the shape of the entire diffraction peak. Analysis of the Fourier series terms allows separation of the components of the broadening attributable to lattice strain from that caused by reduction in the crystallite size. This method requires extensive data collection and depends on the precision with which the tails of the diffraction peak can be separated from the background intensity [70, 71].

Peak broadening comes from several sources [43]:

(1) Peak broadening due to crystallite size.

(2) Peak broadening due to strain (atoms deformed from ideal positions in a nonuniform manner).

(3) Peak broadening due to the instrumental effects.

Crystallite size broadening and strain broadening: according to Scherrer, it is possible to determine the average grain size of crystallites by measuring the FWHM of the diffraction peaks corrected for the contributions from the diffractometer. When the crystallite size is smaller than approximately 100 nm. XRD line profile broadening becomes a measurable effect by using relation for the calculation of crystallite size called the Debye-Scherrer's formula [41, 72-74]:

$$D = K\lambda / \beta_D \cos\Theta$$

$$\beta_D = K\lambda / D \cos\Theta \ldots\ldots\ldots (2\text{-}13)$$

where

λ : wavelength of radiation.

K : is a constant which depends on the assumptions made in the theory (e.g. the peak shape and crystallite habit, spherical crystallites being the easiest case to interpret) actually varies from 0.62 to 2.08, the most common values for it are: 0.94 for FWHM of spherical crystals with cubic symmetry 0.89 for integral breadth of spherical crystals / cubic symmetry, often taken as 0.9 [35, 41, 75, 76].

β_D : is the broadening due to small crystallite size.

The strain induced in powders due to crystal imperfection and distortion was calculated using the formula:

$$\varepsilon = \beta_s / 4\tan\Theta$$

$$\beta_s = 4\varepsilon \tan\Theta \ldots\ldots\ldots (2\text{-}14)$$

where

β_s : is the peak broadening due to lattice strain.

From eq. (2-13) and (2-14), it was confirmed that the peak width from crystallite size varied as $1/\cos\Theta$ strain varied as $\tan\Theta$. Assuming that the particle size and strain contributions to line broadening are independent on each other, the total peak broadening $\beta_{hk\ell}$ may be expressed as:

$$\beta_{hk\ell} = \beta_D + \beta_s$$

$$\beta_{hk\ell} = (K\lambda / D\cos\Theta) + (4\varepsilon \tan\Theta)$$

$$\beta_{hk\ell}\cos\Theta = (K\lambda / D) + (4\varepsilon \sin\Theta) \ldots\ldots\ldots (2\text{-}15)$$

The eq. (2-15) are W-H equations. A plot is drawn with $4\sin\Theta$ along the x-axis and $\beta_{hk\ell}\cos\Theta$ along the y-axis.

Correcting for instrumental effects: to perform an accurate analysis for size and/or strain effects one must accurately account for instrumental broadening. The manner of doing this differs depending on the peak shape.

(a) Lorentzian

$$\beta_{obs} = \beta_{size} + \beta_{strain} + \beta_{inst}$$

$$\{\beta_{obs} - \beta_{inst}\} = \beta_{size} + \beta_{strain} \ldots\ldots\ldots (2\text{-}16)$$

(b) Gaussian

$$\beta^2_{obs} = \beta^2_{size} + \beta^2_{strain} + \beta^2_{inst}$$

$$\{\beta^2_{obs} - \beta^2_{inst}\} = \beta^2_{size} + \beta^2_{strain} \ldots\ldots\ldots (2\text{-}17)$$

(c) Voigt, Pseudo-Voigt

Generally it is necessary to first deconvolute into gaussian and lorentzian fractions before subtracting out the instrumental effects [76].

2-12 Rietveld Method

Materials are essential to our technological society: semiconductors in the electronic industry, zeolites as catalysts in the petrochemical industry, ceramics in medicine and engineering, and, possibly in the future, high-temperature superconductors in electrical engineering. In order to understand the properties of these materials and to improve them, the atomic structure has to be known. An effective way to do this is by means of diffraction techniques using neutrons from nuclear reactors and particle accelerators or X-rays from X-ray tubes and synchrotrons. The single crystal diffraction technique, using relatively large crystals of the material, gives a set of separate data from which the structure can

be obtained. However, most materials of technical interest cannot grow large crystals, so one has to resort to the powder diffraction technique using material in the form of very small crystallites. The drawback of this conventional powder method is that the diffraction peaks grossly overlap, thereby preventing proper determination of the structure. The "Rietveld Method" creates a virtual separation of these overlapping peaks, thereby allowing an accurate determination of the structure [77].

In a high symmetry crystal system, very few peaks occur in the powder pattern, and they are often well resolved and well separated. It is then possible to measure their position and intensity with accuracy index the reflections and solve the structure. For larger and less symmetrical structures, far more reflections overlap considerably, and it becomes impossible to measure the intensities of individual peaks with any accuracy [78].

Rietveld analysis has been developed for solving crystal structures from powder diffraction data. The Rietveld method involves an interpretation (line position and line intensities), because there is so much overlap of the reflections in the powder patterns, the method developed by Rietveld involves analysing the overall line profiles. Rietveld formulates a method of assigning each peak a Gaussian shape and then allowing the Gaussians to overlap so that an overall line profile can be calculated. The method is originally developed for neutron diffraction [78].

Rietveld method can be used to solve a structure from the powder diffraction data. It starts by taking a trial structure, calculating a powder diffraction profile from it and then comparing it with the measured profile. The trial structure can then be gradually modified by changing the atomic positions and refined until a best-fit match with the measured pattern is obtained. The validity of the structure obtained is assessed by an R factor, and by a difference plot of the two patterns [79].

Rietveld method can be defined as a crystal structure refinement method, from powder diffraction data. A pattern is calculated from a series of structural parameters (cell, atomic coordinates, thermal motion, etc) and peak shape and width parameters (plus background, Lorentz-polarisation correction, etc), and compared with the observed data [71, 80].

The inherent drawbacks of the powder method, the loss of information as a result of overlap, can be effectively overcome by Rietveld's method, and powder diffraction can obviously compete with single crystal methods [1].

The basic idea behind the Rietveld method is the calculation of the entire powder pattern using a variety of different refinable parameters. The parameters can roughly be divided into three categories: structural parameters, which mainly affect the intensities of the Bragg reflections, profile parameters, which are determined by the instrument and the sample, and background parameters. The key problem in Rietveld analysis is the refinement strategy. In general, the profile, the background and the crystal structure parameters should be determined and refined separately at the beginning of the refinement. A typical strategy is to start with the refinement of the peak positions (lattice), followed by the profile parameters, the structural parameters, and finally the microstructure parameters like micro strain and domain size. Finally, all variable parameters should be refined simultaneously to obtain mathematically correct variances and covariances [35].

The Rietveld method holds several advantages over other peak intensity-based methods [81-83] :

(1) Differences between the experimental standard and the phase in the unknown are minimized. Compositionally variable phases are varied and fit by the software.

(2) Pure-phase standards are not required for the analysis.

(3) Overlapped lines and patterns may be used successfully.

(4) Lattice parameters for each phase are automatically produced, allowing for the evaluation of solid solution effects in the phase.

(5) The use of the whole pattern rather than a few selected lines produces accuracy and precision much better than traditional methods.

(6) Preferred orientation effects are averaged over all of the crystallographic directions, and may be modeled during the refinement.

The Rietveld method uses a model to calculate a diffraction pattern which is then compared with observed data. The difference between the two patterns is then reduced through least-squares method. The least-squares refinement leads to a minimal residual quantity S_y [60] :

$$S_y = \sum_i w_i(Y_{obi} - Y_{ci})^2 \quad \ldots\ldots\ldots \text{(2-18)}$$

Where:

Y_{obi} : is the observed intensity at point i^{th} of the observed powder pattern.

Y_{ci} : is the calculated intensity for the i^{th} data point.

w_i : The weight is based on the counting statistics.

The weighted sum of the squared differences between the observed and the calculated powder pattern is minimized by refining a selection of parameters using least squares methods [35].

$$\sum_i w_i(Y_{obi} - Y_{ci}) \rightarrow \text{Min} \ , \ W_i = \frac{1}{\sqrt{Y_i}} \quad \ldots\ldots\ldots \text{(2-19)}$$

The least-squares minimization procedure leads to a set of normal equations involving derivatives of all the calculated intensities (Y_{ci}) with respect to each refinable parameter. Because this problem is not linear in the parameters, approximate values for all parameters are required in the first refinement cycle. These are refined in subsequent refinement cycles until a certain convergence criterion has been met [84].

The least squares parameters are those varied in the model to achieve the best fit to the experimental data and include two groups [80, 84]:

(1) The profile parameters include: half-width parameters, counter zero point, cell parameters, asymmetry parameter and preferred orientation parameter.

(2) The structure parameters include: overall scale factor, overall isotropic temperature parameter, coordinates of all atomic units, atomic isotropic temperature parameter, occupation number and magnetic vectors of all atomic units, and symmetry operators.

2-13 The Variables of a Rietveld Refinement

These variables can be summarized as follows [82]:

(1) Peak shape function describes the shape of the diffraction peaks. It starts from a pure Gaussian shape and allows variations due to Lorentz effects, absorption, detector geometry, step size, etc.

(2) Peak width function starts with optimal FWHM values.

(3) Preferred orientation function defines an intensity correction factor based on deviation from randomness

(4) The structure factor is calculated from the crystal structure data and includes site occupancy information, cell dimensions, inter-atomic distances, temperature and magnetic factors. Crystal structure data is usually obtained from the ICDD database or other source. As with all parameters in a Rietveld refinement, this data is a starting point and may be varied to account for solid solution, variations in site occupancy, etc.

Many different statistical agreement factors have been proposed to judge the quality of a Rietveld refinement . The most common one is the so called weighted profile R-factor (R_{wp}). These factors measure not just how well the structural model fits the diffraction intensities, but also how well the background and the diffraction positions and peak shapes have been fit [35, 85].

2-14 Some Applications of the Rietveld Method

Rietveld method has many application as follows [47]:

(1) It has been used for structural investigations of polycrystalline materials having a variety of properties.

(2) It is a powerful tool for investigating phase transformations in solids as a function of temperature.

(3) Its contribution to an understanding of the structures of the high temperature oxide superconductors, due to the lack of suitable single crystals and the need to locate oxygen atoms, and their occupancy.

(4) It has been used for the refinement of incommensurate structures. The calculation of peak positions and structure factors for 1-dimensional incommensurate structures is based on four integers, hkℓm.

(5) Least-squares Rietveld refinement has been used for the study of intercalation or insertion phenomena in layered materials.

(6) The method is study of materials which undergo phase transitions and which often disintegrate when subjected to thermal treatment or produce multi-domain crystals not suitable for single-crystal studies.

2-15 Mathematical Aspects of Rietveld Refinement

The Rietveld method is considered a milestone in structure refinement from powder diffraction data. The basic idea behind the Rietveld method is the calculation of the entire powder pattern by using a variety of different refinable parameters [35].

It is based on the assumption that the measured diffraction pattern, normally given as intensity vs. scattering angle 2Θ, can be approximated by an analytical expression, containing instrumental and structural parameters [86].

The calculated intensity (y_{ci}):

(1) For a single phase [85, 87]:

$$Y_{ci} = S\sum_k L_k F_k Ø (2Θ_i-2Θ_k) O_k A + Y_{bi} \text{ ……. (2-20)}$$

Where:

for each i^{th} point (i=1 to a few thousands, for step-scans of $\Delta 2Θ = 0.02\text{-}0.05°$):

Ø : the reflection profile function(normally supplied in its analytical form, such as Gaussian, Cauchy (or Lorentzian), or as their combination, in the Voigt, pseudo-Voigt or Pearson VII formalisms).

O_k : is the preferred orientation function(which accounts for no ideal (i.e.., non-random) distribution of the crystalline orientations, leading to systematic enhancing of the peak intensities of a certain class of reflections).

Y_{bi} : is the background intensity at i^{th} step.

(3) For a mixture of phases [35]:

$$y_i(calc) = \sum_p [S_p .\sum_{pH} (M_{pH} . A_{pH} (2Θ_i) . P_{pH} . \left| F_{pH}(calc) \right|^2 . L_P(2Θ_i) . Φ_{pH}(2Θ_i))] + B_i(obs) \text{ …..(2-21)}$$

where:

at point i of the powder pattern is calculated from the contributions of all phases p contributing to the powder pattern and all Bragg reflections H of phase p.

$\left| F_{pH}(calc) \right|^2$: the squared absolute value of the structure factor.

$Φ_{pH}(2Θ_i)$: the normalized profile function.

$B_i(obs)$: the background contribution.

The structure factor contains the structural information , taken as [60]:

$$F_H = \sum f_j . g_j . \exp -2\pi I (hx_j+ky_j+\ell z_j) . \exp(-B \sin^2 Θ/\lambda^2) \text{ ……. (2-22)}$$

where:

H : represents the Miller indices for the Bragg reflection.

$\sum$: is over all atoms in the unit cell.

g_j : is the occupancy factor.

h, k and ℓ : Miller indices.

X_j, y_j and z_j : are the fractional atomic coordinates of the j^{th} atom in the model.

B_j : is the temperature factor coefficient.

The structure factor describes the way in which an incident beam is scattered by the atoms of a crystal unit cell, taking into account the different scattering power of the elements through the term fj. The atomic form factor or scattering power, of an element depends on the type of radiation considered as electrons interact with matter through different processes [88].

2-16 Reliability Factors

At the end of a refinement it is necessary to check whether the results are meaningful and whether they meet certain standard criteria**.** One of the ways to measure the agreement between the observed and calculated models is adjusting the various atomic parameters so that the calculated structure factors match the observed structure factors as closely as possible .The factors called (Reliability factors or agreement factors. There are several R values : R-structure factor (R_F), R-Bragg factor (R_B), R-pattern factor (R_p), the weighted-profile factor (R_{wp}) and the expected factor (R_{exp}) [1, 84, 88].

(1) Weighted-profile Reliability factors

$$R_{wp} = \sum_i W_i (y_{oi} - y_{ci})^2 / \sum_i W_i (y_{oi})^2 \quad \ldots\ldots\ldots (2\text{-}23)$$

The expression in the numerator of the Rwp is the minimal residual quantity being minimized ; therefore, it is the most expressive of the R's, and is the one which best reflects the fit of the calculated pattern diffraction [77,89,90].

(2) Expected Reliability factors

$$R_{exp} = [(N - P) / \sum_i W_i (y_{oi})^2]^{1/2} \quad \ldots\ldots\ldots (2\text{-}24)$$

Where

N : is the number of observations.

P : is the number of parameters.

In the perfect refinement, the final R_{wp} would equal R_{exp} [77,91].

(3) The goodness of fit (χ^2)

Is another numerical criterion frequently used for the evaluation of the success of the fit , the χ^2 term is then defined as the average of these values [4,78]:

$$\chi^2 = (1/N) \sum_i (y_{oi} - y_{ci})^2 / \sigma^2 (y_{oi}) \quad \ldots\ldots\ldots (2\text{-}25)$$

χ^2 can also be determined from the expected and weighted profile *R* factors :

$$\chi^2 = R_{wp} / R_{exp}$$

$\chi^2 = (R_{wp} / R_{exp})^2$ called Reduced Chi-squared [92].

During the refinement process, χ^2 starts out large and decreases as the model produces better agreement with the data. χ^2 should never drop below one, or equivalently, the smallest that R_{wp} should ever be is R_{exp} [85].

- If a refinement results is ($\chi^2<1$), then $(y_{oi} - y_{ci})^2$ is less than $\sigma^2 (y_{oi})$, which means that one of two cases below is true:

(1) The standard uncertainties for the data must be overestimated. or

(2) Many parameters have been introduced that the model is adjusting to fit noise which should be unlikely in powder diffraction .

- If at the end of a refinement ($\chi^2>>1$), then either:

(1) The model is reasonable but the s.u. values are underestimated.

(2) The model is incomplete because there are systematic effects (errors) in the data that are not expressed in the model .

(3) The model is wrong.

- If at the end of a refinement ($\chi^2>1$) this mean the higher-quality dataset may provide larger χ^2 or R_{wp} values.

(4) Bragg Reliability factors

The Bragg-intensity R value (R_B) is given by [4,7,92]:

$$R_B = \sum_{hk\ell} \left| I_{hk\ell}(obs) - I_{hk\ell}(calc) \right| / \sum_{hk\ell} \left| I_{hk\ell}(obs) \right| \quad \ldots\ldots\ldots (2\text{-}26)$$

Where

$I_{hk\ell} = MF^2_{hk\ell}$.

Its weighted equivalent can be used to monitor the improvement in the structural model. The label R_{Bragg} is sometimes used to refer to reflection intensity-based *R* factors, but this term is ambiguous, as it may refer to R_F, R_{F2}, or even R_I [85].

(5) Pattern Reliability factors

Based on the agreement between the observed and calculated structure factors ($F_{hk\ell}$) can also be calculated by distributing the intensities of the overlapping reflections according to the structural model [4,7,92].

$$F_{hk\ell} = \sum_{hk\ell} \left| I_{hk\ell}(obs) - I_{hk\ell}(calc) \right| / \sum_{hk\ell} \left| I_{hk\ell}(obs) \right| \quad \ldots\ldots\ldots (2\text{-}27)$$

2-17 The Rietveld Method Strategy

2-17-1 Peak-Shape Functions

The Cagliotti equation is used to calculate an approximate resolution function of the two axis diffractometer. The full width at half maximum (FWHM) of Bragg reflections varies with the scattering angle, 2Θ, following the expression [54,93]:

$$\beta_k = (U \tan^2\Theta + V \tan\Theta + W)^{1/2} \quad \ldots\ldots\ldots (2\text{-}28)$$

Where

β_k : is the FWHM (full width at half maximum).

U, V and W : are refinable parameters.

$$U = 4(\alpha_1^2 \alpha_2^2 + \alpha_1^2 \beta^2 + \alpha_2^2 \beta^2)/[\tan^2\Theta_m (\alpha_1^2 + \alpha_2^2 + 4\beta^2)] \quad \ldots\ldots\ldots (2\text{-}29)$$

$$V = -4\alpha_2^2 (\alpha_1^2 + 2\beta^2)/[\tan\Theta_m (\alpha_1^2 + \alpha_2^2 + 4\beta^2)] \quad \ldots\ldots\ldots (2\text{-}30)$$

$$W = [\alpha_1^2 \alpha_2^2 + \alpha_1^2 \alpha_3^2 + \alpha_2^2 \alpha_3^2 + 4\beta^2 (\alpha_2^2 \alpha_3^2)]/(\alpha_1^2 + \alpha_2^2 + 4\beta^2) \quad \ldots\ldots (2\text{-}31)$$

Where

α_1 : the angular aperture of a monochromater to sample collimator.

α_2 : the collimation between sample and detector.

α_3 : the take-off angle of monochromator $2\Theta_m$.

β : mosaicity.

X-ray data well-resolved show significant deviation from the simple Gaussian and have in addition pronounced asymmetry. Thus we need a more elaborate peak shape function. A particular peak shape will be generally denoted as $\Omega(x)$, the argument is $x=(T-T_h)$, (T is the scattering variable and T_h the Bragg position) and the FWHM will be called β_k.

Define explicitly the most important parameters defining the relevant peak shapes for microstructural analysis. The Voigt approximation is based on the assumption that the contribution of microstructural effects to the final peak shape can be approximated by a Voigt function: convolution of a Gaussian and a Lorentzian [60,93].

2-17-2 Preferred Orientation Correction

The presence of significant preferred orientation effects is often a consequence of using flat-plate geometry, which should normally be avoided if a preliminary microscopic examination indicates a platy or acicular crystal habit. Debye-Scherrer (capillary) geometry is superior in this respect [5].

Preferred orientation arises when there is a stronger tendency for the crystallites in a specimen to be oriented more one way, or one set of ways, than all others. Because preferred orientation produces systematic distortions of the reflection intensities, the distortions can be mathematically modeled with "preferred orientation functions ". This P_k is useful if the degree of preferred orientation is not large. When this function is used in Rietveld refinements with data from a standard Θ–2Θ X-ray diffractometer, the refined parameter changes sign [76,94].

$$P_k = \exp(-G_1 \alpha_k^2)$$

$$P_k = G_2 + (1+G_2) \exp(-G_1 \sin^3 \alpha_k)$$

$$P_k = G_2 + (1-G_2) \exp(-G_1 \sin^3 \alpha_k) \quad \ldots\ldots\ldots (2\text{-}32)$$

Where

G_1 and G_2 : are refinable parameter in the Rietveld method.

α_k : is the angle between the preferred orientation vector and the normal to the planes generating the diffracted peak.

In 1986, Dollase showed superior performance of the March function. One of the particular merits of this preferred orientation function is

$$P_k = (G_1^2 \cos^2 \alpha_k + 1/G_1 \sin^2 \alpha_k)^{-3/2} \quad \ldots\ldots\ldots (2\text{-}33)$$

The March distribution function is a model for fitting preferred orientation of cylinder or needle shaped crystals.

Chapter Three

Experimental Part

3-1 Introduction

This chapter shows the experimental part to raw materials, (XRD, SEM) testing and analysis software.

3-2 Raw Materials

The raw materials for three commercial metal ox ide powders:

(1) Commercial nano powder (Np) for ZrO_2, Al_2O_3 and ZnO.

(2) Commercial micro powder (Mp) for the same material.

The information of manufacturing for oxides is shown in table (3-1):

Table (3-1): Information of manufacturing for powders used

Powders	Samples	The information of manufacturing	Purity %
Nano	ZrO_2	Manufacture: Hongwu Nanometer Co. Ltd., Size: 40-50nm.	99.9
	ZnO		99.9
	Al_2O_3	Cust ID: Areej AlFurat Company, Product: Nano Al_2O_3 Powder α, Size: 20-30nm.	99
Micro	ZrO_2	Manufacture: Hongwu Nanometer Co. Ltd., Size: 70-80nm.	99.8
	ZnO		99.9
	Al_2O_3		99.5

The materials were chosen because of the difference in their crystalline systems. Scanning the samples by using (XRD and SEM) systems, then the samples were heated at different temperatures in order to convert them to other phases where ZrO_2 & Al_2O_3 are heated in furnace at 1180°C for 2h and ZnO is heated at 1200°C for 2h, then they were scanned by using XRD and SEM.

3-3 Phase Transition of Raw Materials

A phase transition is the system transformation from one phase or state of matter to another.

3-3-1 Zirconium Oxide (ZrO_2)

ZrO_2 exists in three different structure depending on pressure, temperature, impurity or doping content, growth conditions, etc [95] are: monoclinic, tetragonal and cubic. Pure zirconia is monoclinic at room temperature, (space group P21 /c), This phase is stable up to 1170°C (T < 1170 °C). Above this temperature 1170 < T < 2370 °C) it transforms into tetragonal (space group P42 /nmc) and then into cubic phase (T > 2370 °C) (space group Fm3m)[96-98]. Figure (3-1) shows scheme to phase transition for ZrO_2.

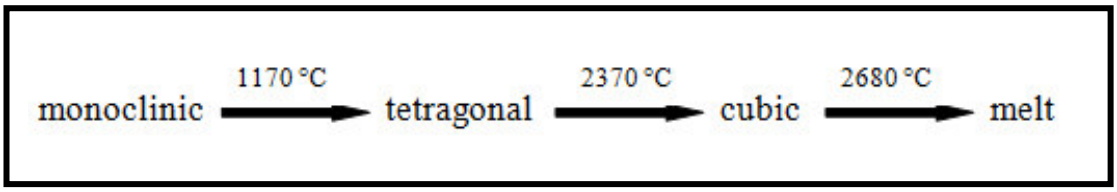

Fig. (3-1): Temperature related phase transformation of zirconia.

Phase transformations between cubic and tetragonal and monoclinic phases occur on cooling from high temperatures [99].

3-3-2 Aluminium Oxide (Al_2O_3)

Al_2O_3 appears in seven different structure: chi (χ-phase), kappa (κ-phase), gamma (γ-phase), delta (δ-phase), theta (θ-phase), eta (η-phase), and alpha (α-phase, also called corundum) [13]. Corundum is the most common naturally occurring crystalline form of aluminium oxide as an igneous and metamorphic mineral and is synthesized artificially by various high-temperature techniques. It is widely used as catalyst, catalyst support and adsorbent because of its high porosity and surface area [100]. Figure (3-2) shows scheme to phase transition for Al_2O_3.

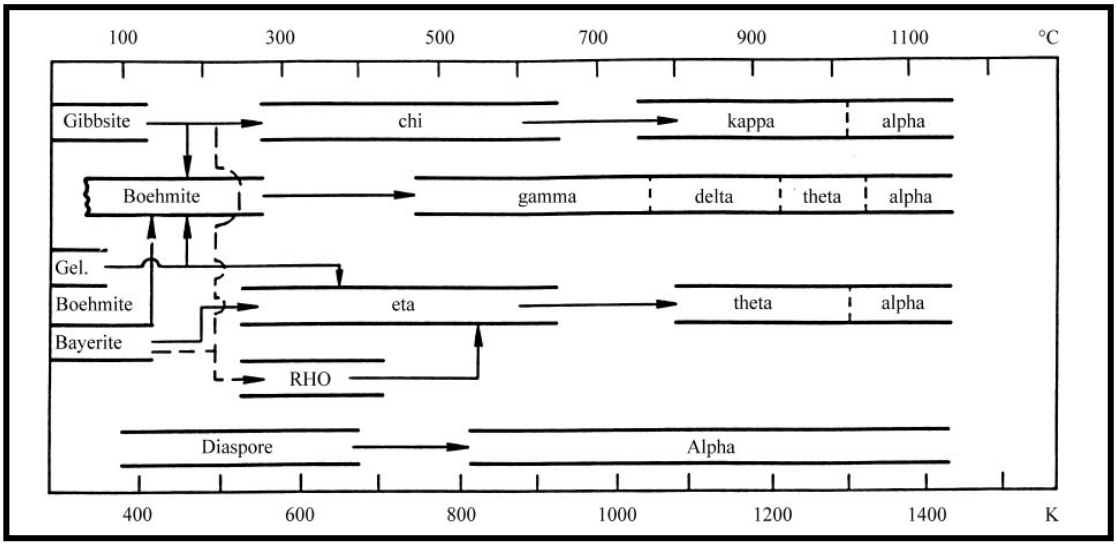

Fig. (3-2): Thermal transformation sequence of the aluminum hydroxides [13].

3-3-3 Zinc Oxide (ZnO)

Zinc oxide crystallizes in three forms [101]:

(1) Hexagonal wurtzite.

(2) Cubic zinc blende .

(3) Cubic rock salt.

At ambient pressure and temperature, ZnO crystallizes in the wurtzite structure. It has a hexagonal lattice, characterized by two interpenetrating hexagonal close packed (hcp), with lattice spacing a = 0.325 nm and c = 0.521 nm and space group $P6_3mc$. The lattice parameters of the unit cell have a c/a ratio of (1.602) which is 1.8 % off of the ideal hexagonal-close-packed structure of (1.633)[102-105]. At pressures of about 9 GPa and room temperature transforms into the cubic [106].

3-4 Instrument Used in the Tests

3-4-1 X-ray Diffraction

The collection of X-ray diffraction patternss was performed by the use (Shimadzu XRD-6000), max. tube voltage 60kV, max. tube current 80mA, generates X-ray wavelength (0.15406 nm) to the source of the target (Cu), step scan 0.02° and scanning angle range (2Θ=20°-100°) for ZnO and (2Θ=20°-80°) for ZrO_2 and Al_2O_3. The

instrument is available in University of Baghdad/ College of Education for Pure Science / Ibn -AL-Haitham/ Physics Department. Shimadzu XRD-6000 is shown in figures (3-3) and (3-4).

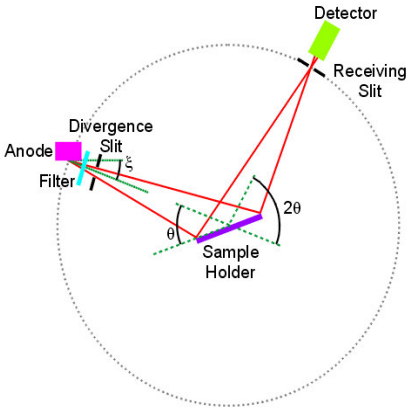

Fig. (3-3): Schematic diagram for XRD[107].

Fig. (3-4): Shimadzu XRD-6000 diffractometer.

3-4-2 Scanning Electron Microscope (SEM)

The scanning electron microscope used in imaging the nanoparticles is VEGA\\EasyProbe. The EasyProbe is a favorable combination of a scanning electron microscope and a fully integrated energy dispersive X-ray microanalyser. SEM specifications are electron gun Tungsten heated filament, resolution 3 nm at 30kV, magnification continuous form 6x to 100,000x, accelerating voltage 200 V to 30kV, probe current 1 pA to 2 µA, chamber (Internal size : Ø160 mm, Numbr of ports: 8) and stage (Motorized: X=45 mm , Y=45 mm , Rot=360°, manual: Z =27, eucentric tilt). The instrument is available in University of Technology / Nanotechnology and Advance Materials Research Center. VEGA\\EasyProbe is shown in figure (3-5). figure (3-6) shows schematic details of SEM.

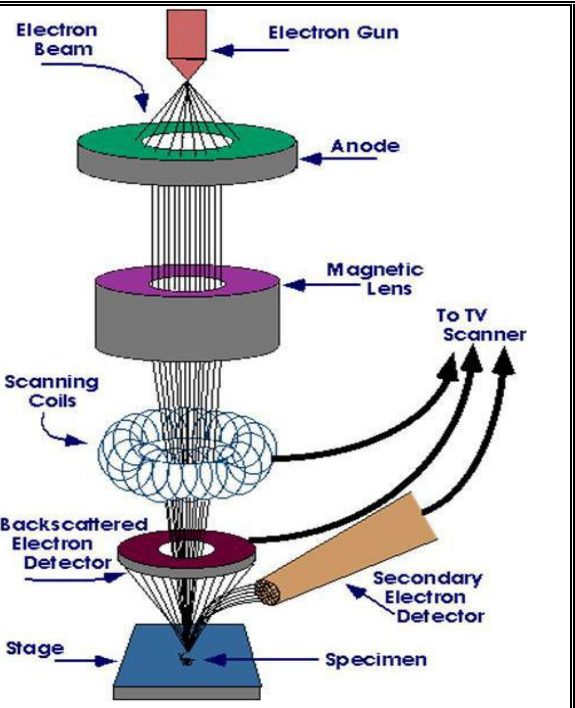

Fig. (3-5): Schematic details of SEM [108].

Fig. (3-6): Scanning electron microscope (VEGA\\EasyProbe)

3-5 Softwares Analysis Used in the Calculations

We use in this search several softwares prepared in different research centers by coupling with diffractometer to obtain crystalline structure, as in figure (3-7).

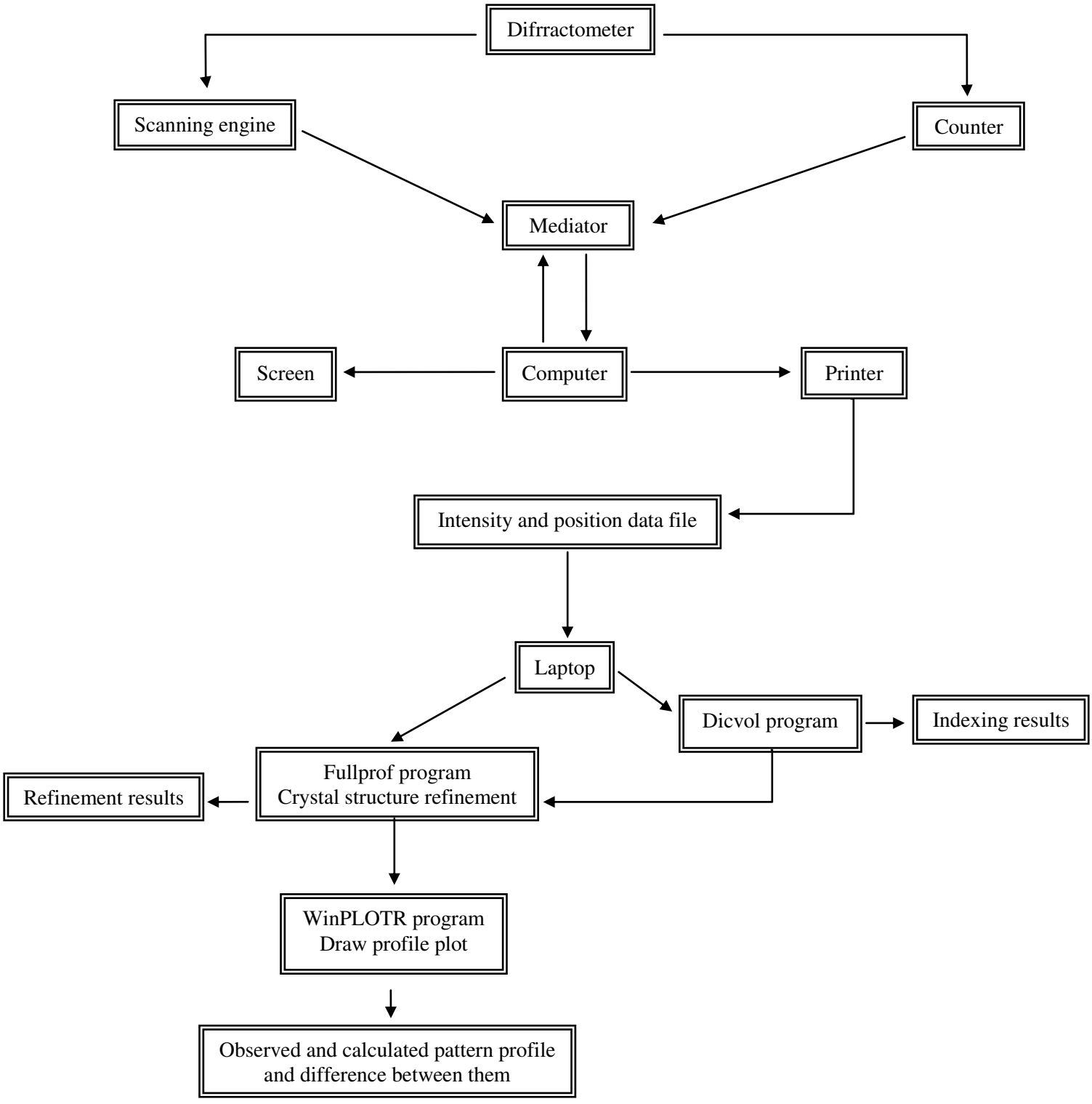

Fig. (3-7): A diagram which explains coupling diffractometer with software to obtain crystalline structure [36].

المخطط

3-6 The Steps Involved to Get the Results

After testing the samples by using X-ray diffractometer we get on a data that will be indexed by using Dicvol 91 program, that by inter angular position for Bragg's reflections (2Θ) and wavelength user we get a set of data that includes Miller indices, unit cell parameter (a,b,c,α,β,γ), crystal system and interplanar spacing.

After the formation of the input files, the process of crystal structure refinement can be started by using Fullprof program. Some output files Fullprof program such as step scan data, step width, wavelength user, intensity data and angular position data which are considered input for WinPLOTR program then draw observed and calculated diffraction patternss and plot difference between them. Other part from output Fullprof program includes unit cell parameters, atomic position and space group.

3-6-1 Indexing Program

3-6-1-1 Dicvol 91 Program

Dicvol is a powder indexing software that allows examine the dichotomy method for powder patterns indexing.

Dicvol 91 has an indexing approach based on the dichotomy method, introduced by D. Louër (version PC : 30/06/1992) . The original version of the program was written for orthorhombic and higher symmetry. Later, the method was extended to monoclinic and to triclinic symmetry. The dichotomy method was based on the variation in direct space, by finite increments, of the lengths of cell edges and of the interaxial angles (an m-dimensional search, where m is the number of unknown unit cell parameters): the variations were reduced when they contain a possible solution [2].

The Input data of Dicvol program included angular position observed for reflection Bragg (2Θ) and the wavelength of the beam used optional information such as molecular weight, density. Output included file called (file.cry) contains

crystal system, space group, unit cell parameter (a,b,c,α,β,γ) and other files included Miller indices, interplanar spacing, unit cell volume, zero shift and file called (file.pcr) used as input file for Fullprof program.

3-6-1-2 Treor 90 Program

An indexing program, Treor, mainly based on trial and error methods was described and introduced by Per-Eric Werner. The program contained separate routines for cubic, tetragonal, hexagonal, orthorhombic, monoclinic and triclinic symmetries. Ten years usage has been analysed to improve the original program. For monoclinic indexing a specific short-axis test has been developed. The over-all success rate of the program has been found to be better than 90%, and considerably more for orthorhombic. A number of programs to facilitate the indexing of powder patternss, based on trial-and-error methods, were written and described in the forties of the last century. The computer technology of that time did not allow a rigorous implementation of the principles. The original programs had to be coded in machine language, but in the 1974 the first version of a trial-and-error indexing program, TREOR, was written in Fortran [109].

3-6-2 Fullprof Program

Some materials under study suffer from bad crystallization because the presence of structural defects like dislocations, stacking faults, anti-phase domains, micro-strains and small crystallite sizes manifests in the diffraction patterns by a broadening of the Bragg peaks.

The Voigt approximation for peak broadening is sufficient to get quantitative explanation of the existing defects through the different hkℓ and angular dependence of the broadening through the treatment of microstructural effect using the program Fullprof [87].

The Fullprof program has been mainly developed for Rietveld analysis (structure profile refinement) of X-ray powder diffraction data collected at constant or variable step in scattering angle 2Θ. Single crystal refinement can

also be performed alone or in combination with powder data. Energy dispersive X-ray data can also be treated but only for profile matching.

The Fullprof program has been mainly developed for Rietveld analysis (structure profile refinement) of neutron (constant wavelength, time of flight, nuclear and magnetic scattering) or X-ray powder diffraction data collected at constant or variable step in scattering angle 2Θ [80, 110]. The program can be used as a profile matching tool, without the knowledge of the structure. Single crystal refinement can be performed alone or in combination with powder data. Energy dispersive X-ray data can be treated but only for profile matching . Last version program Fullprof.2k (version 5.30 – Mar 2012 – ILL JRC) .

Fullprof program contains several input and output files. Input files such as (file.pcr) Input control file, it must be in the current directory to run the program. This file contains the title and crystallographic data of the problem to be treated and must be prepared by user with a file editor. This file is normally up dated every time run the program. (file.dat) intensity data file, its format depends on instrument, useful to draw patterns calculation modes. (file.bac) background file, represents input file peak intensity and peak position. This file can also be generated by the program, its input file background intensity data. (file.hkℓ) represents input file Miller indices and angular position data. This file is optional and can also be generated by the program. (file.irf) file describes the instrumental resolution function and its content depends on the value of the parameter Res (Resolution function type). (file.int) single integrated intensity file when the program is used for refining with Cry (Single crystal job and refinement algorythm type =1, 2, 3) and Irf (Control the reflexion generation or the use of a reflexion file=4). (file.shp) providing a numerical table for calculating the peak shape and its derivatives.

Output files such as (file.out) is the main output file that contains all control variables and refined parameters. Its content depends on the values of flags set by the user. (file.prf) it is called sometimes CODFIL.prf, observed and calculated profile: to be fed into visualization programs, this file is used

automatically by WinPLOTR. In case of multiple patterns refinements a file (CODFIL_p.prf) is created for each patterns, where p is the ordinal number of the diffraction patterns. (file.sum) parameter list after last cycle: summary of the last parameters, their standard deviations and reliability factors, an analysis of the goodness of the refinement is included at the end if (Reliability of the refinement analysis =1) [111]. The program is available as an appendix.

3-6-3 WinPLOTR Program

WinPLOTR is a program to plot powder diffraction patternss. It can be used to plot raw or normalized data files coming from X-ray diffractometers as well as Rietveld files created by the Fullprof refinement program. WinPLOTR can also be used as a Graphical User Interface for programs used frequently in powder diffraction data analysis (ex: Fullprof, Dicvol ...) or other external programs defined by the user.

It has been developed for a Windows 9x/2k/NT environment. It takes advantage of this graphical environment to offer a powerful and user-friendly powder diffraction tool. The program is able to display and analyse many different kinds of diffraction patternss as well as calculated and observed profiles coming from the Windows/DOS version of the program Fullprof.

WinPLOTR has been developed to run on PC's with a 32-bit Microsoft Windows operating system. WinPLOTR supports Windows 9x/NT/XP. WinPLOTR has been build up with Lahey Fortran 95 compiler, using the Windows facilities of RealWin. Last version Oct. 13 [112].

WinPLOTR program contain Input file is (file.prf) prepared from Fullprof includes step scan data, step width, reflection number, the wavelength user, observed and calculated intensity data used to draw observed and calculated diffraction patterns.

Chapter Four

Results and Discussion

4-1 Introduction

This chapter includes the extracted results and discusses indexing of powder patterns, crystal structure refinement and parameters affecting refinement.

4-2 XRD Testing

Oxids	Heat treat.	2Θ(°)	Step (°)	intense diffraction line	Divergene slit (°)	Scattering slit (°)	Receivig slit (mm)
ZrO_2	1180 °C	20-80	0.02	5°/min	1	1	0.3
ZnO	1200 °C	20-100	0.02	5°/min	1	1	0.3
Al_2O_3	1180 °C	20- 80	0.02	5°/min	1	1	0.3

4-2-1 XRD for Zirconium Oxide (ZrO_2)

Figure (4-1) shows X-ray diffraction patterns of ZrO_2 nano powder before and after heat treatment at 1180 °C .

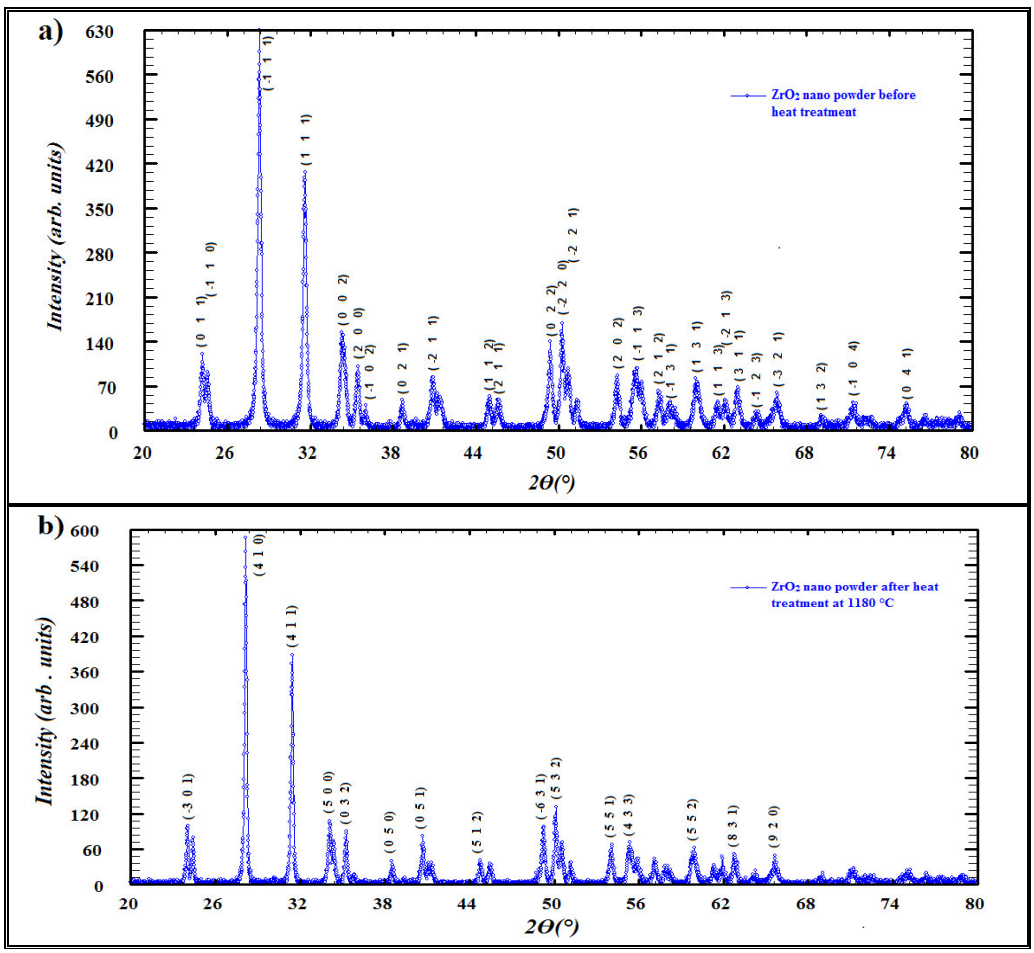

Fig. (4-1): X-ray diffraction patterns of ZrO_2 nano powder

a) before heat treatment. b) after heat treatment at 1180 °C .

XRD patterns exhibited strong diffraction peaks at (28.297°, 31.586°, 50.251°) and (28.123°, 31.411°, 50.089°) indicating ZrO_2 nano powder before and after heat treatment at 1180 °C respectively.

Figure (4-2) shows X-ray diffraction patterns of ZrO_2 micro powder before and after heat treatment at 1180 °C .

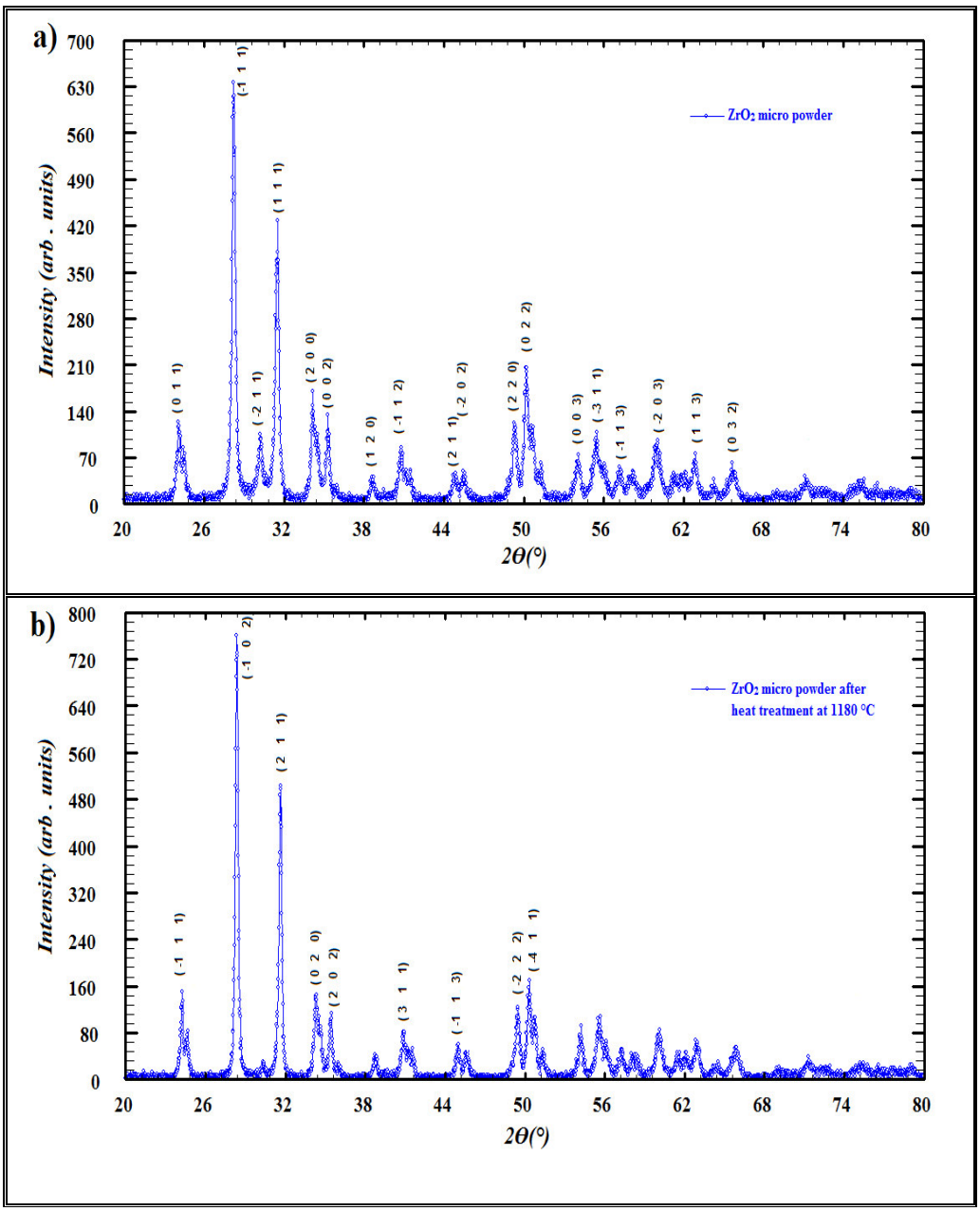

Fig. (4-2): X-ray diffraction patterns of ZrO_2 micro powder

a) before heat treatment. b) after heat treatment at 1180 °C .

XRD patterns exhibited strong diffraction peaks at (28.223°, 31.485°, 50.206°) and (28.324°, 31.605°, 50.286°) indicating ZrO_2 micro powde before and after heat treatment at 1180 °C respectively.

The results of indexing for ZrO_2 nano powder before and after heat treatment before crystal structure refinement performed by using (Dicvol 91) program are shown in table (4-1).

Table (4-1): The results of indexing for ZrO_2 nano powder before and after heat treatment at 1180 °C before crystal structure refinement

Sample ZrO_2 nano powder	Unit cell parameters (Å)			Phase	Space group	Angles (°)	
	a	b	c			α= γ	β
before heat treatment	5.142	5.205	5.312	Mono.	P2/m	90	99.22
after heat treatment	13.188	11.747	6.691	Mono.	P2/m	90	90.934

The results of indexing for ZrO_2 micro powder before and after heat treatment before crystal structure refinement performed by using (Dicvol 91 and Teror) programs are shown in table (4-2). We used Teror program because the material could not be indexed using Dicvol 91program.

Table (4-2): The results of indexing for ZrO_2 micro powder before and after heat treatment at 1180 °C before crystal structure refinement

Sample ZrO_2 micro powder	Unit cell parameters (Å)			Phase	Space group	Angles (°)	
	a	b	c			α= γ	β
before heat treatment	5.313	5.210	5.145	Mono.	P2/m	90	99.233
after heat treatment	7.355		11.166	Tetra.	P4/mmm	90	90

The detailed analysis of the XRD and the assignments of various reflections of ZrO_2 nano powder before and after heat treatment at 1180 °C are given in the table (4-3).

Table (4-3): Strongest three peaks for ZrO_2 nano powder before and after heat treatment at 1180 °C

Sample ZrO_2 nano powder	No.	Peak No.	2Θ (°)	d (Å)	FWHM (°)
before heat treatment	1	4	28.297	3.151	0.287
	2	6	31.586	2.831	0.281
	3	17	50.251	1.814	0.254
after heat treatment	1	2	28.123	3.171	0.171
	2	4	31.411	2.845	0.172
	3	16	50.089	1.819	0.173

The detailed analysis of the XRD and the assignments of various reflections of ZrO_2 micro powder before and after heat treatment at 1180 °C are given in the table (4-4).

Table (4-4): Strongest three peaks for ZrO_2 micro powder before and after heat treatment at 1180 °C

Sample ZrO_2 micro powder	No.	Peak No.	2Θ (°)	d (Å)	FWHM (°)
before heat treatment	1	3	28.223	3.159	0.139
	2	1	31.485	2.839	0.146
	3	2	50.206	1.815	0.135
after heat treatment	1	3	28.324	3.148	0.231
	2	5	31.605	2.828	0.240
	3	19	50.286	1.812	0.252

By comparing figure (4-1-a) with figure (4-1-b), figure (4-2-a) with figure (4-2-b) it shows that increase in intensity for some peaks and decrease in other peaks. By comparing ZrO_2 nano powder before heat treatment with after heat treatment the results are shown in table (4-3), and ZrO_2 micro powder before heat treatment with after heat treatment the results are shown in table (4-4) by using peak position it shows occurrence of shift in peaks position, because of the heat treatment atoms will acquire vibration energy which causes the atoms shift from their position. This is the reason for the increase in the intensity of some peaks and shift others after the heat treatment.

The results of indexing for ZrO_2 powders after crystal structure refinement are shown in table (4-5). Which show unit cell parameters, crystal system, space group and unit cell volume for ZrO_2 nano and micro powders before and after heat treatment.

Table (4-5): Unit cell parameters, crystal system, space group and unit cell volume for ZrO_2 powders after crystal structure refinement

Samples ZrO_2	Heat treatment at	Unit cell parameters (Å)			phase	Space group	Volume ($Å^3$)	Angles (°)	
		a	b	c				α= γ	β
n_1	-	5.142	5.205	5.312	Mono.	P2/m	544.619	90	99.22
n_2	1180 °C	13.192	11.755	6.692	Mono.	P 2/m	1037.805	90	89.078
m_1	-	5.313	5.201	5.145	Mono.	P2/m	140.621	90	99.233
m_2	1180 °C	7.283	7.283	10.984	Tetra.	P 4/m m m	582.691	90	90

Where

n_1 : ZrO_2 nano powder before heat treatment.

n_2 : ZrO_2 nano powder after heat treatment.

m_1 : ZrO_2 micro powder before heat treatment.

m_2 : ZrO_2 micro powder after heat treatment.

Through the matching diffraction patterns for ZrO_2 nano powder before heat treatment by using intensity and interplaner spacing, it shows that all diffraction data are in a good agreement with the Joint Committee on Powder Diffraction Standards (JCPDS) files (No. 24-1165).

When ZrO_2 nano powder is treated with heat at 1180°C, the material starts transition from monoclinic phase to tetragonal phase. Through the matching of diffraction patterns, it shows that all diffraction data are in a good agreement with JCPDS files (No. 36-0420) that has monoclinic phase and JCPDS files (No. 34-1084) that has tetragonal phase. This means that diffraction patterns is a mixture of two phases, monoclinic and tetragonal so unit cell parameters are not similar to unit cell parameters in any PDF files.

At matching diffraction patterns for ZrO_2 micro powder before heat treatment, it shows that all diffraction data are in full conformity with JCPDS files (No. 37-1484), this means that the powder has high purity. When ZrO_2 micro powder is treated with heat at (1180°C) and through the matching of diffraction patterns it shows that all diffraction data are in good agreement with JCPDS files (No. 02-0733) that have tetragonal phase and JCPDS files (No. 24-1165) that have monoclinic, because of non-completion of the phase transition from monoclinic to tetragonal.

From table (4-5) it is observed that the unit cell volume for ZrO_2 (nano and micro) powder after heat treatment has increased because of the growth of the crystal.

Table (4-6) shows texture coefficient and Miller indices for strongest three peaks for ZrO_2 nano powder before and after heat treatment.

Table (4-6): Texture coefficient and Miller indices for strongest three peaks for ZrO_2 nano powder

Before heat treatment			After heat treatment		
2Θ(°)	(h k ℓ)	TC	2Θ(°)	(h k ℓ)	TC
28.297	($\bar{1}$ 1 1)	0.855	28.123	(4 1 0)	0.883
31.586	(1 1 1)	0.907	31.411	(4 1 1)	0.938
50.251	($\bar{2}$ 2 0)	1.236	50.089	(5 3 2)	1.177

The texture coefficient has was estimated by using equation (2-12). From table (4-6) it shows that ZrO_2 nano powder before heat treatment on the basis of the texture coefficient has peak position (50.251°) which has Miller indices ($\bar{2}$ 2 0) is the most abundance and has an arrangement of the atoms. This is called preferred orientation. But for the ZrO_2 nano powder after heat treatment has peak position (50.089°) which has Miller indices (5 3 2) is the most abundance and has an arrangement of the atoms. By interpreting grain orientation.

Table (4-7) shows texture coefficient and Miller indices for strongest three peaks for ZrO_2 micro powder before and after heat treatment.

Table (4-7): Texture coefficient and Miller indices for strongest three peaks for ZrO_2 micro powder

Before heat treatment			After heat treatment		
2Θ(°)	(h k ℓ)	TC	2Θ(°)	(h k ℓ)	TC
28.223	($\bar{1}$ 1 1)	0.887	28.324	($\bar{1}$ 0 2)	0.891
31.485	(1 1 1)	0.861	31.605	(2 1 1)	0.964
50.206	(0 2 2)	1.251	50.286	($\bar{4}$ 1 1)	1.071

From table (4-7) it shows that the ZrO_2 micro powder before heat treatment on the basis of the texture coefficient has peak position (50.206°) which has Miller indices (0 2 2) is the most abundance and arrangement of the atoms. But for the ZrO_2 micro powder after heat treatment has a peak position (50.286°) which has Miller indices ($\bar{4}$ 1 1) is the most abundance and has an arrangement of the atoms.

Table (4-8) shows strain and grain size according to Williamson-Hall (W-H) and grain size according to Debye-Scherrer for ZrO_2 nano and micro powders before and after heat treatment.

Table (4-8): Strain and grain size according to W-H and grain size according to Debye-Scherrer for ZrO_2 powders

Samples ZrO_2	Heat treatment at	D (W-H) nm	ε (W-H)*10^{-4}	D (Scherrer) nm
n_1	-	23.1	-12.5	28.6
n_2	1180 °C	36.4	1	34.3
m_1	-	46.2	5	43.2
m_2	1180 °C	69.3	-2.5	52.3

The strain and grain size according W-H were estimated by using equation (2-15). the grain size according Debye-Scherrer has been estimated by using equation (2-13).

From table (4-8) it is show that the average grains sizes of the ZrO_2 after heat treatment for both powders is increased. The difference between grain size

according to W-H and grain size according to Debye-Scherrer occurs because W-H method takes into account the microstrain generated between atoms due to the defects and distortions in crystal. A negative value for the strain means lattice shrinkage [113].

Figure (4-3) shows strain and grain size according to W-H for ZrO_2 nano and micro powders before and after heat treatment.

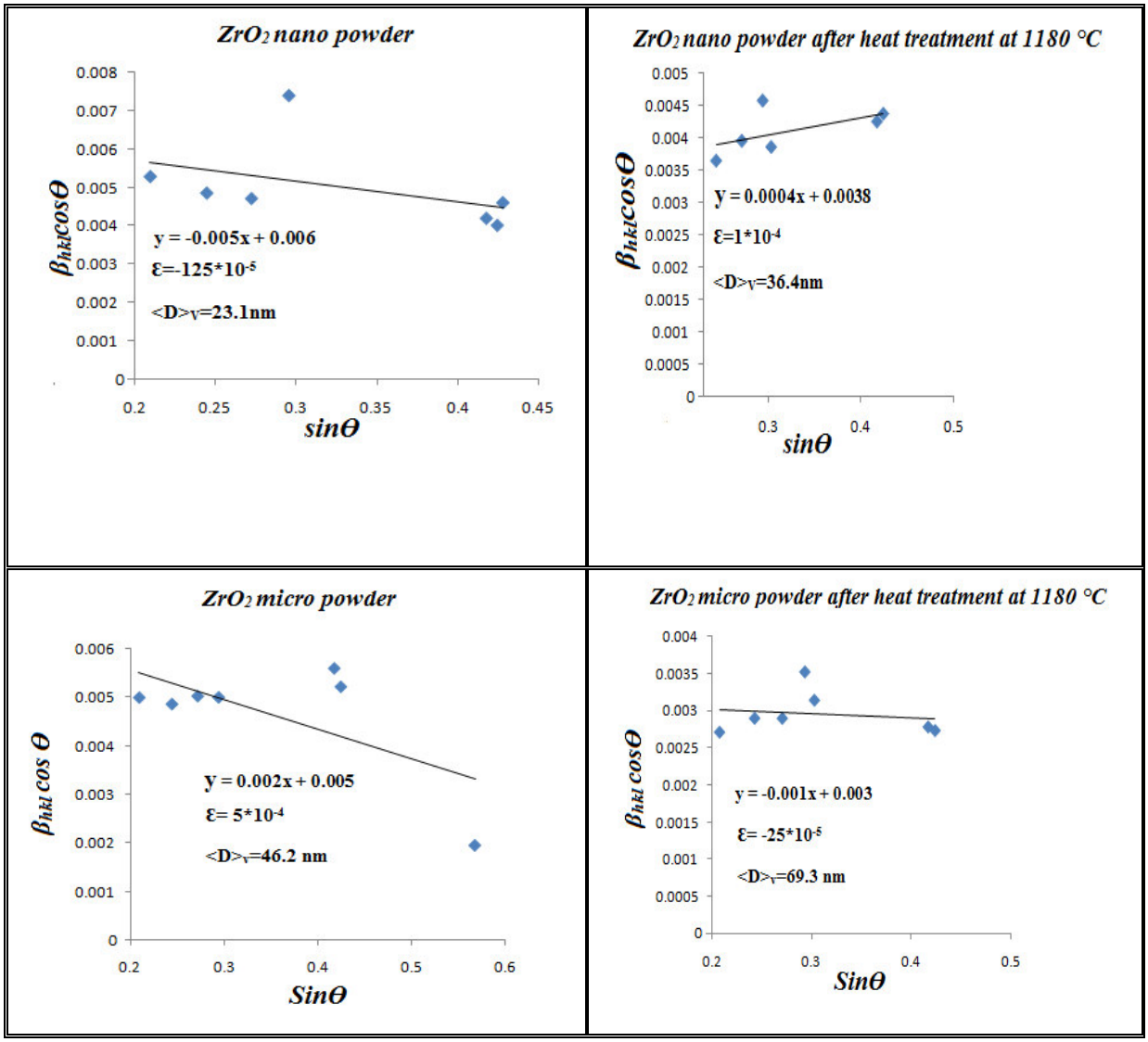

Fig. (4-3): Strain and grain size according to W-H for ZrO_2 powders

4-2-2 XRD for Zinc Oxide (ZnO)

Figure (4-4) shows X-ray diffraction patterns of ZnO nano powder before and after heat treatment at 1200 °C . XRD patterns exhibited strong diffraction peaks at (36.253°, 31.768°, 34.420°) and (36.261°, 31.772°, 34.438°) indicating ZnO nano powder before and after heat treatment at 1200 °C.

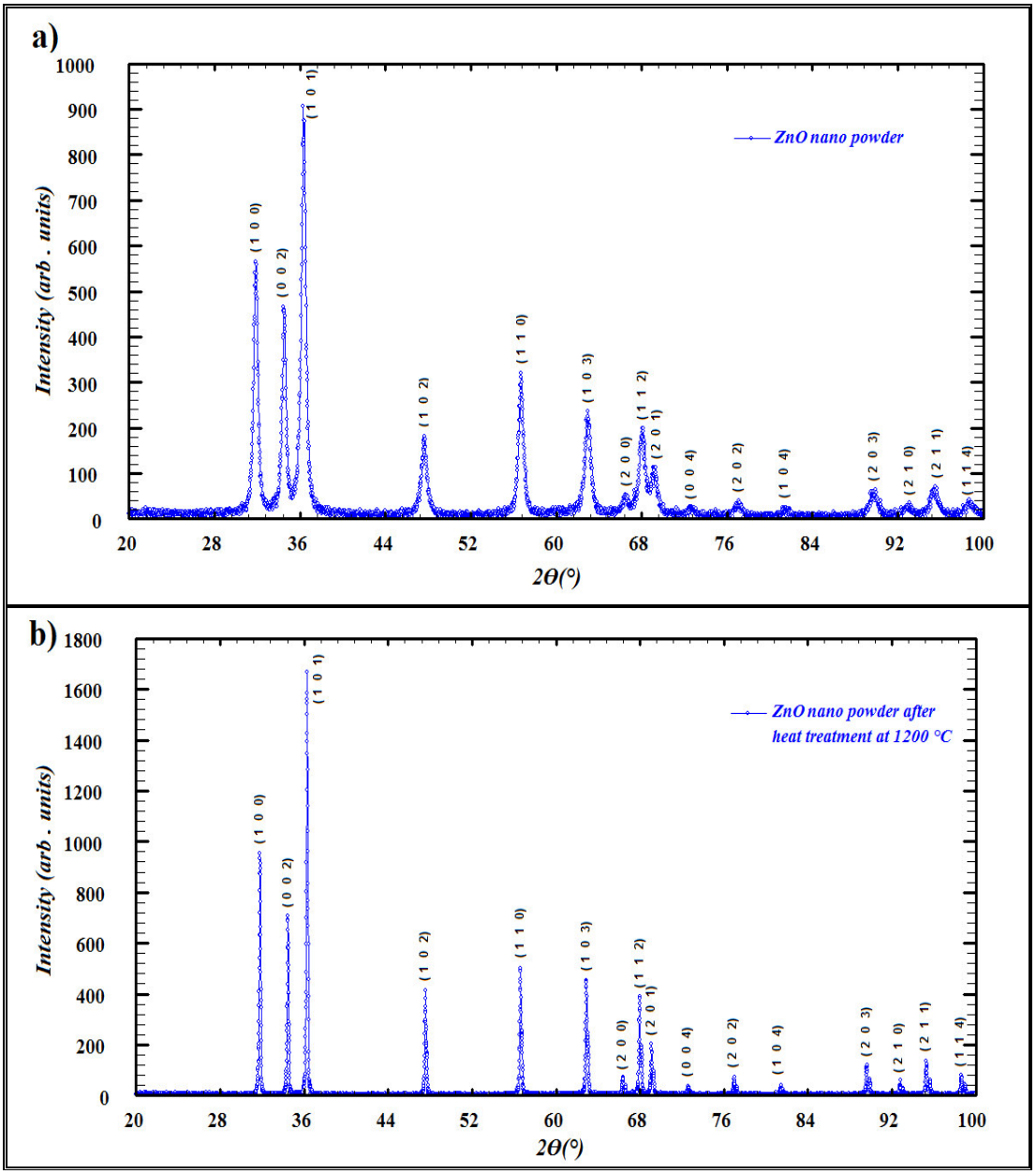

Fig. (4-4): X-ray diffraction patterns of ZnO nano powder

a) before heat treatment. b) after heat treatment at 1200 °C .

Figure (4-5) shows X-ray diffraction patterns of ZnO micro powder before and after heat treatment at 1200 °C. XRD patterns exhibited strong diffraction peaks at (36.494°, 31.818°, 34.331°) and (36.495°, 31.819°, 34.330°) indicating ZnO micro powder before and after heat treatment at 1200 °C.

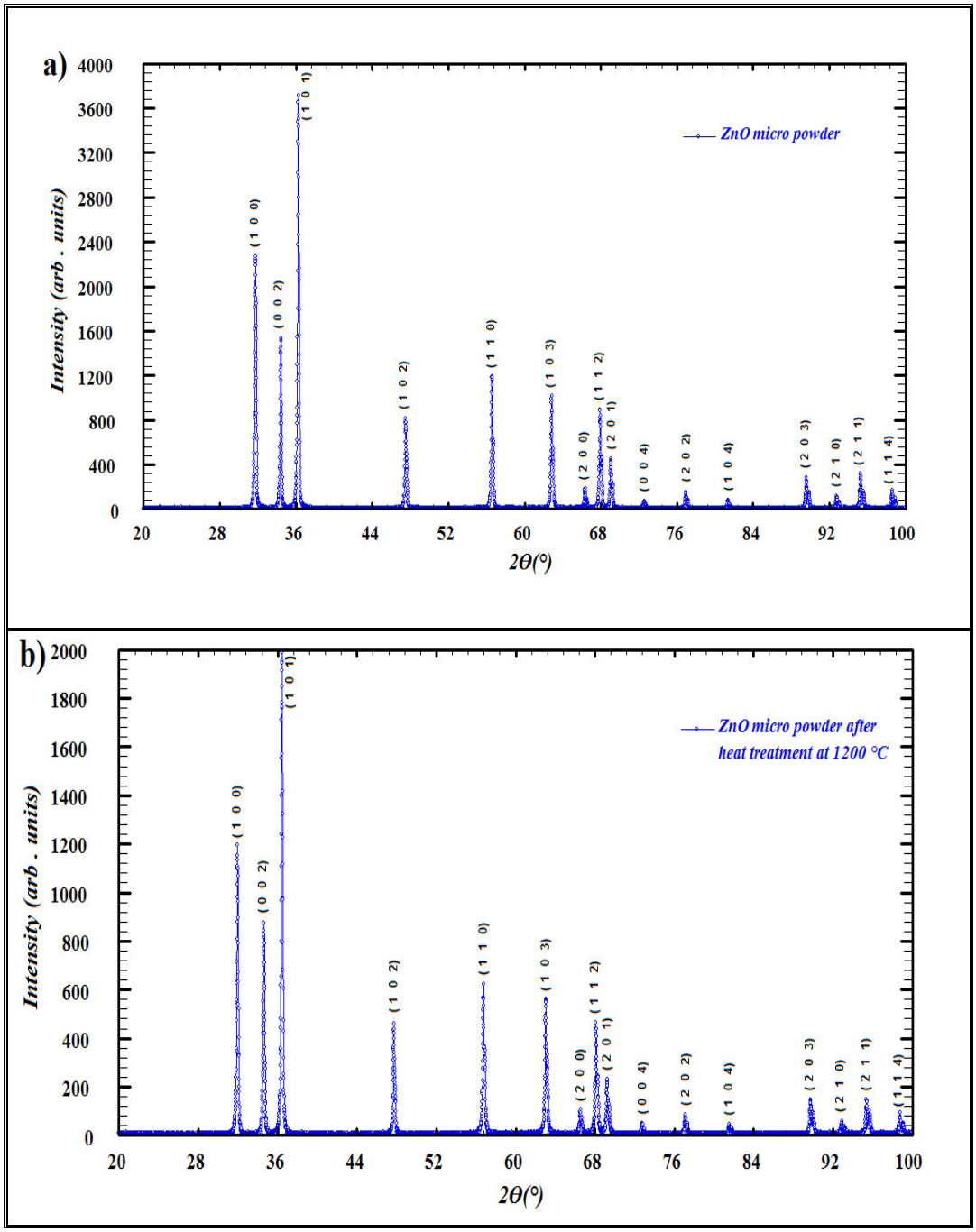

Fig. (4-5): X-ray diffraction patterns of ZnO micro powder

a) before heat treatment. b) after heat treatment at 1200 °C.

The results of indexing for ZnO nano powder before and after heat treatment before crystal structure refinement performed by using (Dicvol 91) program are shown in table (4-9).

Table (4-9): The results of indexing for ZnO nano powder before and after heat treatment before crystal structure refinement

Sample ZnO nano powder	Unit cell parameters (Å)		Phase	Space group	Angles (°)	
	a	c			α=β	γ
before heat treatment	3.249	5.206	Hex.	P 6_3 m c	90	120
after heat treatment	3.248	5.202	Hex.	P 6_3 m c	90	120

The results of indexing for ZnO micro powder before and after heat treatment before crystal structure refinement performed by using (Dicvol 91) program are shown in table (4-10).

Table (4-10): The results of indexing for ZnO micro powder before and after heat treatment before crystal structure refinement

Sample ZnO micro powder	Unit cell parameters (Å)		Phase	Space group	Angles (°)	
	a	c			α=β	γ
before heat treatment	3.248	5.202	Hex.	P 6_3 m c	90	120
after heat treatment	3.247	5.205	Hex.	P 6_3 m c	90	120

The detailed analysis of the XRD and the assignments of various reflections of ZnO nano powder before and after heat treatment at 1200 °C are given in the table (4-11).

Table (4-11): Strongest three peaks for ZnO nano powder before and after heat treatment at 1200 °C

Sample ZnO nano powder	No.	Peak No.	2Θ (°)	d (Å)	FWHM (°)
before heat treatment	1	4	36.253	2.471	0.482
	2	6	31.768	2.808	0.467
	3	17	34.420	2.598	0.422
after heat treatment	1	2	36.261	2.472	0.130
	2	4	31.772	2.809	0.131
	3	16	34.438	2.598	0.133

The detailed analysis of the XRD and the assignments of various reflections of ZnO micro powder before and after heat treatment at 1200 °C are given in the table (4-12).

Table (4-12): Strongest three peaks for ZnO micro powder before and after heat treatment at 1200 °C

Sample ZnO micro powder	No.	Peak No.	2Θ (°)	d (Å)	FWHM (°)
before heat treatment	1	3	36.494	2.472	0.139
	2	1	31.818	2.809	0.146
	3	2	34.331	2.599	0.135
after heat treatment	1	3	36.495	2.462	0.157
	2	5	31.819	2.797	0.164
	3	19	34.330	2.587	0.159

By comparing figure (4-4-a) with figure (4-4-b), figure (4-5-a) with figure (4-5-b) it is shown that increase in intensity for some peaks and decrease in other peaks. By comparing ZnO nano powder before heat treatment with after heat treatment the results are shown in table (4-11), and ZnO micro powder before heat treatment with after heat treatment the results are shown in table (4-12) by using peak position it shows occurrence of shift in peaks position, because of the heat treatment atoms will acquire vibration energy which causes the atoms shift from their position. This is the reason for increase in intensity the peaks and shift others after the heat treatment.

Table (4-13) shows unit cell parameters, crystal system, space group and unit cell volume for ZnO nano and micro powders before and after heat treatment after crystal structure refinement.

Table (4-13): Unit cell parameters, crystal system, space group and unit cell volume for ZnO powders after crystal structure refinement

Samples ZnO	Heat treatment at	Unit cell parameters (Å)		phase	Space group	Volume ($Å^3$)	$\frac{c}{a}$
		a=b	c				
n_3	-	3.247	5.206	Hex.	P 6_3 m c	47.54،	1.6021
n_4	1200 °C	3.249	5.204	Hex.	P 6_3 m c	47.626	1.6015
m_3	-	3.248	5.205	Hex.	P 6_3 m c	47.539	1.6014
m_4	1200 °C	3.259	5.202	Hex.	P 6_3 m c	47.548	1.6013

Where

n_3 : ZnO nano powder before heat treatment.

n_4 : ZnO nano powder after heat treatment.

m_3 : ZnO micro powder before heat treatment.

m_4 : ZnO micro powder after heat treatment.

Through the matching diffraction patterns for ZnO nano powder before by using peak position, intensity and interplaner spacing, it is shown that all diffraction data are in a good agreement with JCPDS files (No. 36-1451). At matching diffraction patterns for ZnO nano powder after heat treatment it is shows that all diffraction data are in full conformity with JCPDS files (No. 05-0664).

At matching diffraction patterns for ZnO micro powder before heat treatment it is shows that all diffraction data are in full conformity with JCPDS files (No. 01-1136). When ZnO micro powder is treated with heat at 1200°C, it shows that all diffraction data are in full conformity with JCPDS files (No. 01-1136). We note that the number PDF file for ZnO micro powder before heat treatment itself the number PDF file for ZnO micro powder before heat treatment this means failure to obtain phase transition.

Table (4-14) shows texture coefficient and Miller indices for strongest three peaks for ZnO nano powder before and after heat treatment.

Table (4-14): Texture coefficient and Miller indices for strongest three peaks for ZnO nano powder

Before heat treatment			After heat treatment		
2Θ(°)	(h k ℓ)	TC	2Θ(°)	(h k ℓ)	TC
36.253	(1 0 1)	0.767	36.261	(1 0 1)	1.035
31.768	(1 0 0)	0.952	31.772	(1 0 0)	0.999
34.420	(0 0 2)	1.279	34.438	(0 0 2)	0.965

The texture coefficient was estimated by using equation (2-12). From table (4-14) it shows that ZnO nano powder before on the basis of the texture coefficient has peak position (34.420°) which has Miller indices (0 0 2) is the most abundance and arrangement of the atoms. This is called preferred orientation. But for the ZnO nano powder after heat treatment has peak position (36.261°) which has Miller indices (1 0 1) is the most abundance and has an arrangement of the atoms. By interpreting grain orientation, the grains are non spherical and have different forms may be needle or sharpened etc.

Table (4-15) shows texture coefficient and Miller indices for strongest three peaks for ZnO micro powder before and after heat treatment.

Table (4-15): Texture coefficient and Miller indices for strongest three peaks for ZnO micro powder

Before heat treatment			After heat treatment		
2Θ(°)	(h k ℓ)	TC	2Θ(°)	(h k ℓ)	TC
36.494	(1 0 1)	1.191	36.495	(1 0 1)	1.029
31.818	(1 0 0)	0.956	31.819	(1 0 0)	1.011
34.331	(0 0 2)	0.851	34.330	(0 0 2)	0.959

From table (4-15) it shows that ZnO micro powder before heat treatment on the basis of the texture coefficient has peak position (36.494°) which has Miller indices (1 0 1) is the most abundance and has an arrangement of the atoms. But for the ZnO micro powder after heat treatment has a peak position (36.495°) which has Miller indices (1 0 1) is the most abundance and has an arrangement of the atoms.

Table (4-16) shows strain and grain size according to W-H and grain size according to Debye-Scherrer for ZnO nano and micro powders before and after heat treatment.

Table (4-16): Strain and grain size according to W-H and grain size according to Debye-Scherrer for ZnO powders

Samples ZnO	Heat treatment at	D (W-H) nm	ε (W-H)*10^{-3}	D (Scherrer) nm
n_3	-	17.33	-0.75	19.73
n_4	1200 °C	19.88	-3	33.96
m_3	-	46.21	-0.5	60.07
m_4	1200 °C	69.32	-0.25	64.48

The strain and grain size according to W-H have been estimated by using equation (2-15). The grain size according to Debye-Scherrer has been estimated by using equation (2-13).

From table (4-16) it is shown that the average grains sizes of the ZnO powders after heat treatment for both powders is increased. The difference between grain size according to W-H and grain size according to Debye-Scherrer occurs because W-H method takes into account the microstrain generated between atoms due to the defects and distortions in crystal. A negative value for the strain means lattice shrinkage.

Figure (4-6) shows strain and grain size according to W-H for ZnO nano and micro powders before and after heat treatment.

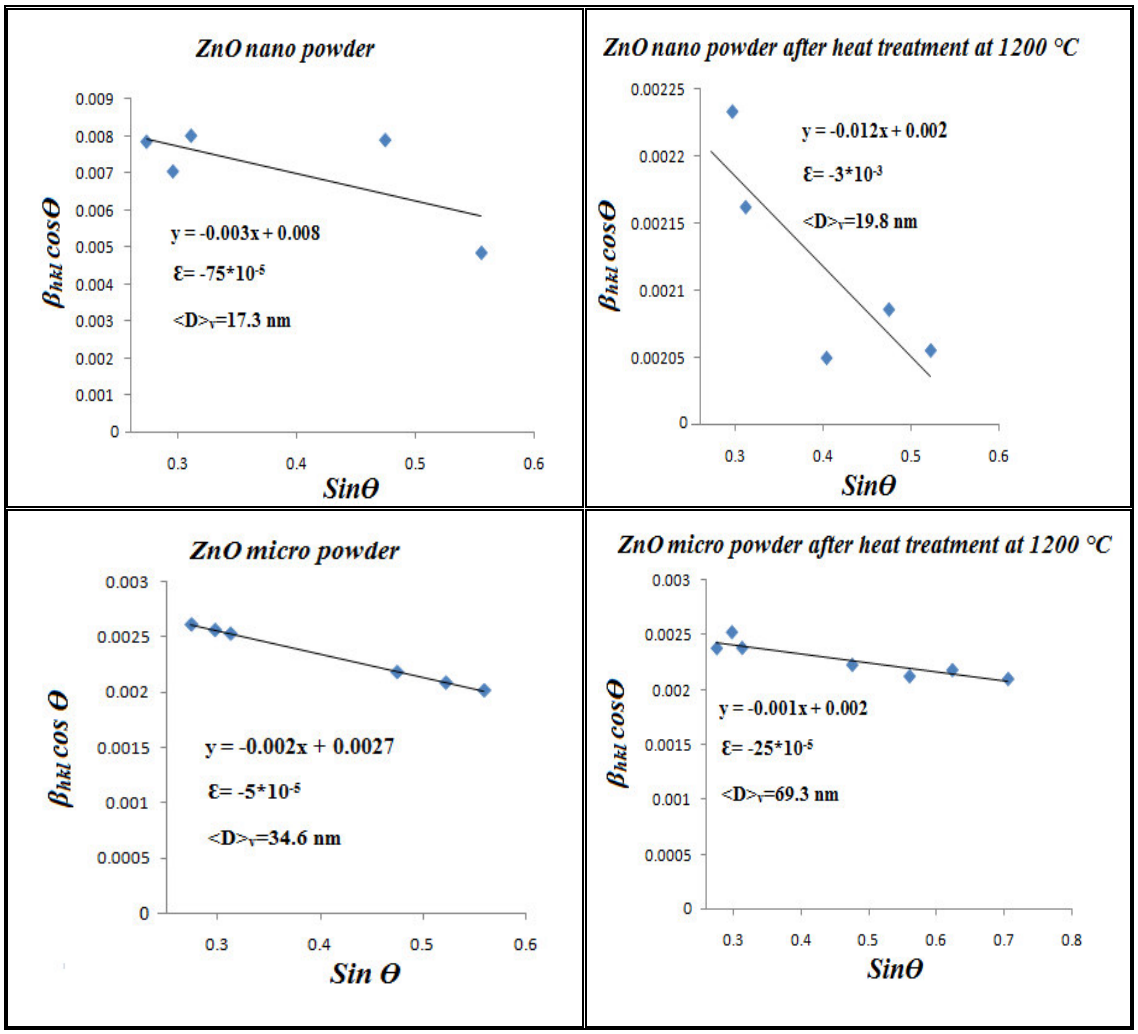

Fig. (4-6): Strain and grain size according to W-H for ZnO powders

4-2-3 XRD for Aluminium Oxide (Al_2O_3)

Figure (4-7) shows X-ray diffraction patterns of Al_2O_3 nano powder before and after heat treatment at 1180 °C. XRD patterns exhibited strong diffraction peaks at (43.317°, 35.117°, 66.266°) and (35.143°, 43.341°, 57.479°) indicating Al_2O_3 nano powder before and after heat treatment at 1180 °C.

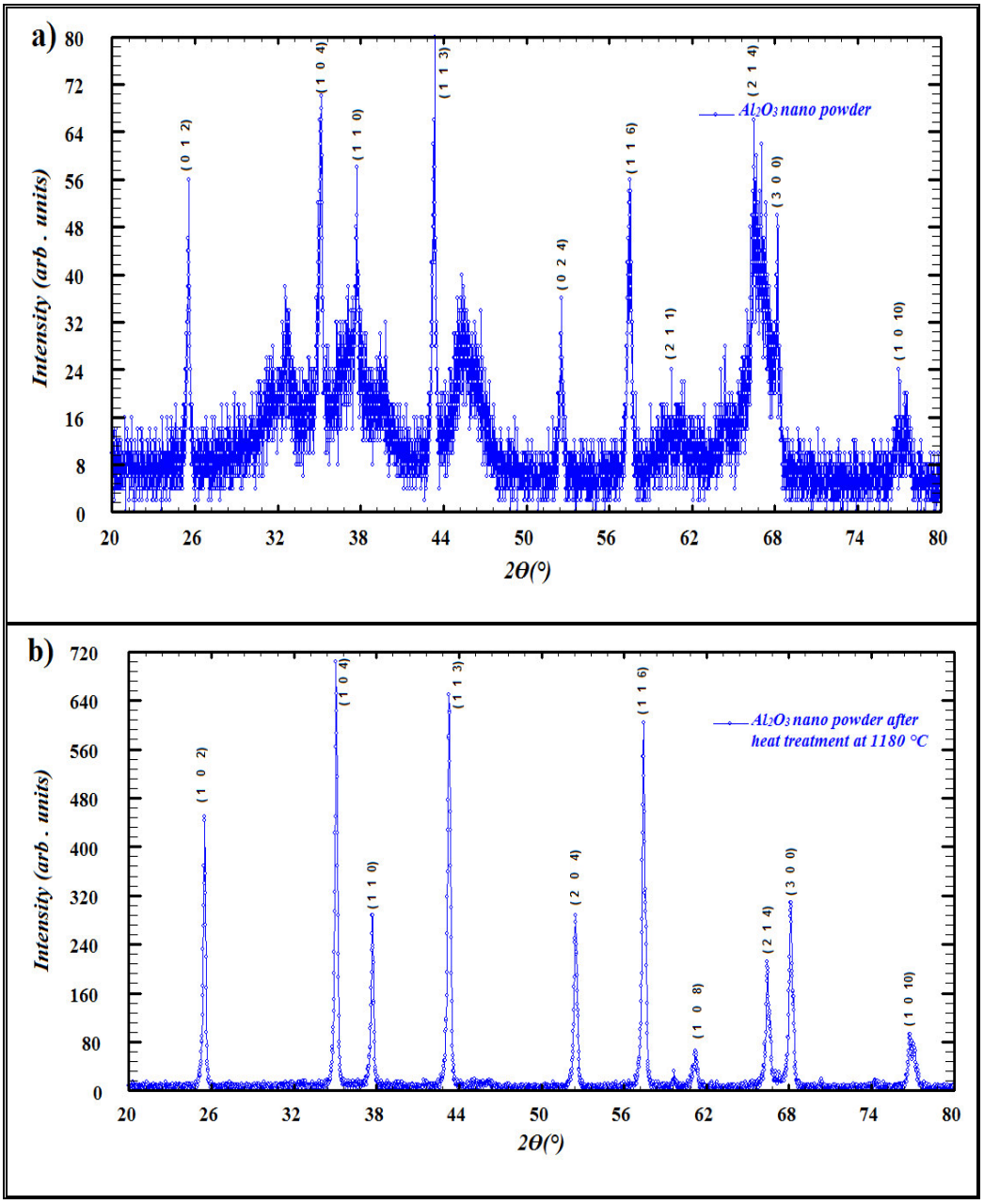

Fig.(4-7): X-ray diffraction patterns of Al_2O_3 nano powder

a) before heat treatment. b) after heat treatment at 1180 °C .

Figure (4-8) shows X-ray diffraction patterns of Al_2O_3 micro powder before and after heat treatment at 1180 °C. XRD patterns exhibited strong diffraction peaks at (67.042°, 37.475°, 45.710°) and (35.094°, 57.428° , 43.289°) indicating Al_2O_3 micro powder before and after heat treatment at 1180 °C.

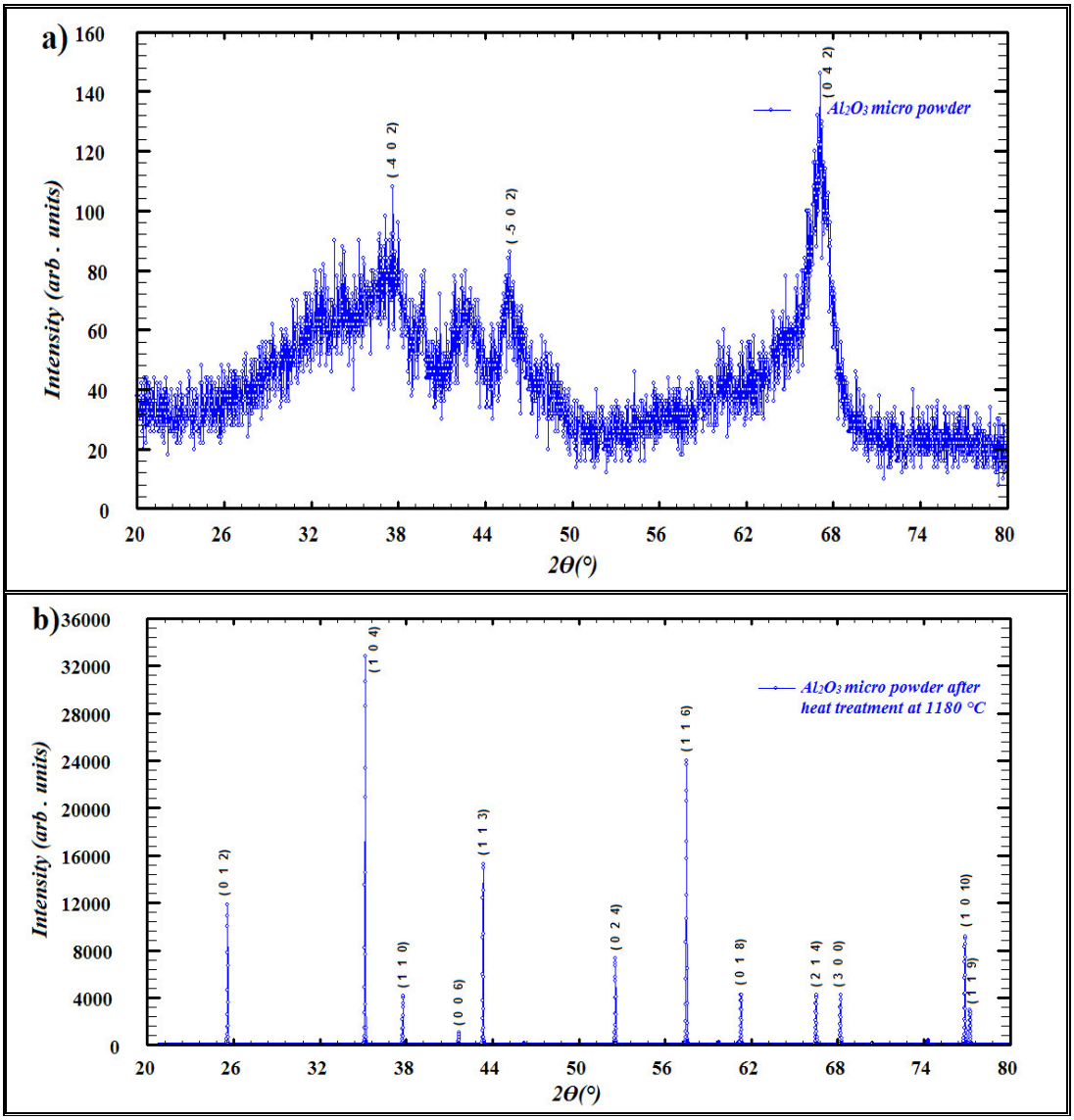

Fig.(4-8): X-ray diffraction patterns of Al_2O_3 micro powder

a) before heat treatment b) after heat treatment at 1180 °C.

The results of indexing for Al_2O_3 nano powder before and after heat treatment before crystal structure refinement performed by using (Dicvol 91 and Teror) programs are shown in table (4-17).

Table (4-17): The results of indexing for Al_2O_3 nano powder before and after heat treatment before crystal structure refinement

Sample Al_2O_3 nano powder	Unit cell parameters (Å)		Phase	Space group	Angles (°)	
	a	c			α=β	γ
before heat treatment	4.745	12.961	Hex.	R $\bar{3}$c	90	120
after heat treatment	4.759	12.993	Hex.	P6/mmm	90	120

The results of indexing for Al_2O_3 micro powder before and after heat treatment before crystal structure refinement performed by using (Dicvol 91) program are shown in table (4-18).

Table (4-18): The results of indexing for Al_2O_3 micro powder before and after heat treatment before crystal structure refinement

Sample Al_2O_3 micro powder	Unit cell parameters (Å)			Phase	Space group	Angles (°)	
	a	b	c			α= γ	β
before heat treatment	10.123	5.877	9.146	Mono.	P2/m	90	104.332
after heat treatment	4.758		12.992	Hex.	R $\bar{3}$c	90	120

The detailed analysis of the XRD and the assignments of various reflections of Al_2O_3 nano powder before and after heat treatment at 1180 °C are given in the table (4-19).

Table (4-19): Strongest three peaks for Al_2O_3 nano powder before and after heat treatment at 1180 °C

Sample Al_2O_3 nano powder	No.	Peak No.	2Θ (°)	d (Å)	FWHM (°)
before heat treatment	1	58	43.317	2.087	0.272
	2	32	35.117	2.553	0.260
	3	87	66.266	1.602	0.310
after heat treatment	1	2	35.143	2.551	0.177
	2	4	43.341	2.086	0.179
	3	16	57.479	1.602	0.194

The detailed analysis of the XRD and the assignments of various reflections of Al_2O_3 micro powder before and after heat treatment at 1180 °C are given in the table (4-20).

Table (4-20): Strongest three peaks for Al_2O_3 micro powder before and after heat treatment at 1180 °C

Sample Al_2O_3 micro powder	No.	Peak No.	2 Θ (°)	d (Å)	FWHM (°)
before heat treatment	1	3	67.042	1.394	1.560
	2	1	37.475	1.410	0.880
	3	2	45.710	2.397	1.720
after heat treatment	1	3	35.094	2.554	0.183
	2	19	57.428	1.603	0.192
	3	5	43.289	2.088	0.213

By comparing figure (4-7-a) with figure (4-7-b), figure (4-8-a) with figure (4-8-b), it is shows that increase in intensity for some peaks and decrease in other peaks. By comparing Al_2O_3 nano powder before heat treatment with after heat treatment the results are shown in table (4-19), and Al_2O_3 micro powder before heat treatment with after heat treatment the results are shown in table (4-20) by using peak position it shows occurrence of shift in peaks position, because of the heat treatment atoms will acquire vibration energy which causes the atoms shift from their position. This is the reason for increase in intensity the peaks and shift others after the heat treatment.

Table (4-21) shows unit cell parameters, crystal system, space group and unit cell volume for Al_2O_3 nano and micro powders before and after heat treatment.

Table (4-21): Unit cell parameters, crystal system, space group and unit cell volume for Al_2O_3 powders after crystal structure refinement

Samples Al_2O_3	Heat treatment at	Unit cell parameters (Å)			phase	Space group	Volume (Å^3)	Angles (°)		
		a	b	c				α	β	γ
n_5	-	4.745		12.961	Hex.	R $\bar{3}$c	252.735	90	90	120
n_6	1180 °C	4.759		12.993	Hex.	R $\bar{3}$c	254.935	90	90	120
m_5	-	10.108	5.877	9.145	Mono	P 2/m	526.481	90	104.312	90
m_6	1180 °C	4.758		12.992	Hex.	R $\bar{3}$c	254.792	90	90	120

Where

n_5 : Al_2O_3 nano before heat treatment

n_6 : Al_2O_3 nano after heat treatment

m_5 : Al_2O_3 micro before heat treatment

m_6 : Al_2O_3 micro after heat treatment

Through the matching of diffraction patterns for Al_2O_3 nano powder before heat treatment by using intensity and interplaner spacing, it shows that all diffraction data are in a good agreement with JCPDS files (No. 05-0712). When Al_2O_3 nano powder is treated with heat at 1180°C it shows that all diffraction data are in full conformity with JCPDS files (No. 10-0173).

At matching diffraction patterns for Al_2O_3 micro powder before heat treatment it shows that all diffraction data are in full conformity with JCPDS files (No. 34-0493). When Al_2O_3 micro powder after is treated with heat at 1180°C it shows that all diffraction data are in full conformity with JCPDS files (No. 10-0173).

Table (4-22) shows texture coefficient and Miller indices for strongest three peaks for Al_2O_3 nano powder before and after heat treatment.

Table (4-22): Texture coefficient and Miller indices for strongest three peaks for Al_2O_3 nano powder

Before heat treatment			After heat treatment		
2Θ(°)	(h k ℓ)	TC	2Θ(°)	(h k ℓ)	TC
43.317	(1 1 3)	0.944	35.143	(1 0 4)	0.998
35.117	(1 0 4)	1.017	43.341	(1 1 3)	0.953
66.266	(2 1 4)	1.038	57.479	(1 1 6)	1.048

The texture coefficient has been estimated by using equation (2-12). From table (4-22) which shows that Al_2O_3 nano powder before heat treatment on the basis of the texture coefficient has peak position (66.266°) which has Miller indices (2 1 4) is the most abundance and has an arrangement of the atoms and

this is called preferred orientation. But for the Al_2O_3 nano powder after heat treatment has peak position (57.479°) which has Miller indices (1 1 6) is the most abundance and has an arrangement of the atoms.

Table (4-23) shows texture coefficient and Miller indices for strongest three peaks for Al_2O_3 micro powder before and after heat treatment.

Table (4-23): Texture coefficient, Miller indices for strongest three peaks for Al_2O_3 micro powder

Before heat treatment			After heat treatment		
2Θ(°)	(h k ℓ)	TC	2Θ(°)	(h k ℓ)	TC
67.042	(0 4 2)	0.611	35.094	(1 0 4)	0.827
37.475	($\bar{4}$ 0 2)	0.903	57.428	(1 1 6)	1.253
45.710	($\bar{5}$ 0 2)	1.484	43.289	(1 1 3)	0.919

From table (4-23) it is shown that Al_2O_3 micro powder before heat treatment on the basis of the texture coefficient has peak position (45.710°) which has Miller indices ($\bar{5}$ 0 2) is the most abundance and has an arrangement of the atoms. But for the Al_2O_3 micro powder after heat treatment has peak position (57.428°) which has Miller indices (1 1 6) is the most abundance and has an arrangement of the atoms.

Table (4-24) shows strain and grain size according to W-H and grain size according to Debye-Scherrer for Al_2O_3 nano and micro powders before and after heat treatment.

Table (4-24): Strain and grain size according to W-H and grain size according to Debye-Scherrer for Al_2O_3 powders

Samples Al_2O_3	Heat treatment at	D (W-H) nm	ε (W-H)*10^{-4}	D (Scherrer) nm
n_5	-	34.6	5	33.3
n_6	1180 °C	39.6	-1.25	37.4
m_5	-	46.2	-25.2	40.5
m_6	1180 °C	57.7	-7.5	64.9

The strain and grain size according to W-H were estimated by using equation (2-15). The grain size according to Debye-Scherrer has been estimated by using equation (2-13).

From table (4-24) it is shows that the average grains sizes of the Al_2O_3 powders after heat treatment for both powders is increased. The difference between grain size according to W-H and grain size according to Debye-Scherrer occurs because W-H method takes into account the microstrain generated between atoms due to the defects and distortions in crystal. A negative value for the strain means lattice shrinkage.

Figure (4-9) shows strain and grain size according to W-H for Al_2O_3 nano and micro powders before and after heat treatment.

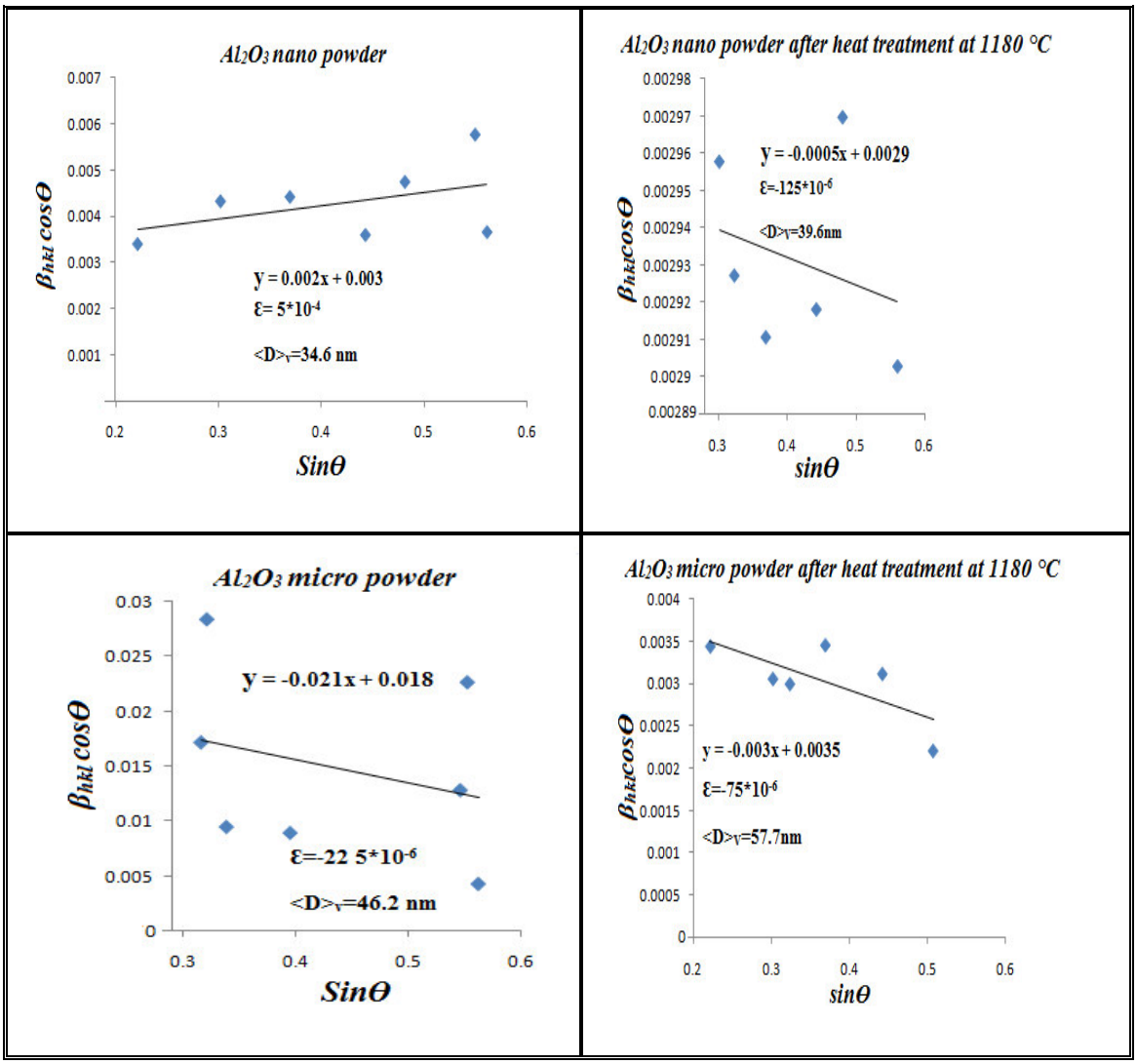

Fig. (4-9): Strain and grain size according to W-H for Al_2O_3 powders

4-3 Crystal Structure Refinement (Fitting between Observed and Calculated Pattern)

Crystal structure refinement performed through fitting method between the observed and calculated diffraction patterns by using Fullprof program through least square method. Refinement process includes diagram for observed and calculated diffraction patterns and best fit between them, Bragg's reflection and curve represents the difference between in them located down diagram.

4-3-1 Crystal Structure Refinement for ZrO_2

Figures (4-10-a) and (4-10-b) show the fitting between observed and calculated diffraction patterns after making crystal structure refinement process for ZrO_2 nano powder before and after heat treatment. The figures also show the Bragg's peak position and the difference between the observed and calculated patterns.

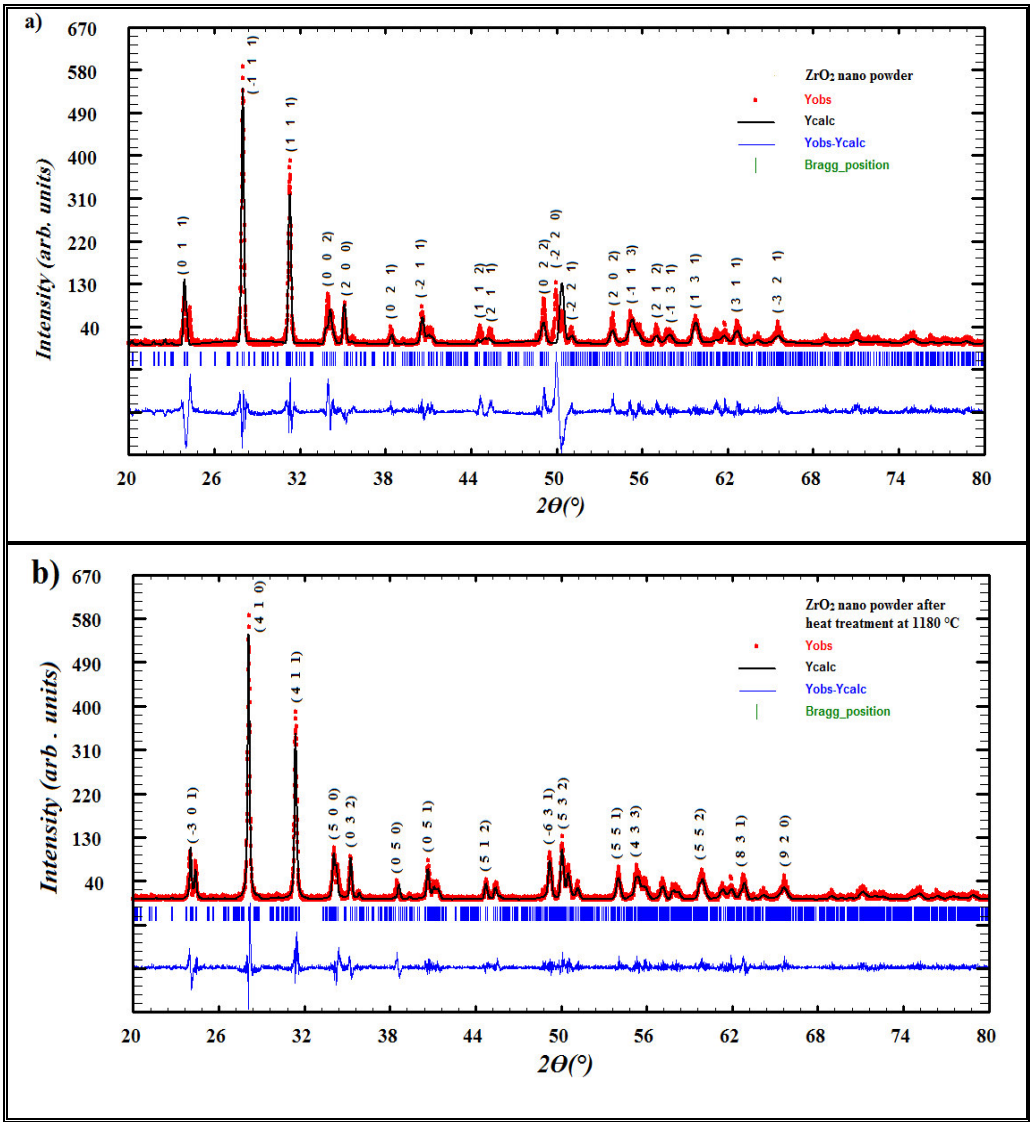

Fig. (4-10): The refined XRD patterns of ZrO_2 nano powder before and after heat treatment. The red line is the experimental data; the blue line is the theoretical data. The lowest trace indicates the difference between patterns. The middle vertical lines indicate the peak position.

Refinement results for ZrO_2 nano powder before and after heat treatment are shown in tables (4-25) and (4-26) respectively.

Table (4-25): Miller indices, observed and calculated intensity and difference between them for ZrO_2 nano powder before heat treatment.

N	2Θ	Miller indices	I_{obs}	I_{cal}	$I_{obs} - I_{cal}$
1	24.099	0 1 1	8.51	7.23	1.28
2	28.297	$\bar{1}$ 1 1	98.50	100	-1.5
3	31.586	1 1 1	65.01	64.92	0.09
4	34.147	0 0 2	10.43	10.37	0.06
5	35.318	2 0 0	8.72	8.53	0.19
6	38.581	0 2 1	1.17	1.16	0.01
7	40.757	$\bar{2}$ 1 1	3.12	3.01	0.11
8	44.856	1 1 2	1.71	1.02	0.69
9	45.526	2 1 1	3.01	2.94	0.07
10	49.291	0 2 2	1.42	1.45	-0.03
11	50.251	$\bar{2}$ 2 0	17.47	15.33	2.14
12	51.215	$\bar{2}$ 2 1	0.09	0.09	0
13	54.143	2 0 2	0.87	0.85	0.02
14	55.649	$\bar{1}$ 1 3	0.69	0.66	0.03
15	57.155	2 1 2	0.73	0.71	0.02
16	57.992	$\bar{1}$ 3 1	4.3	3.29	1.01
17	59.832	1 3 1	2.80	2.23	0.57
18	62.844	3 1 1	2.93	2.17	0.76

Table (4-26): Miller indices, observed and calculated intensity and difference between them for ZrO_2 nano powder after heat treatment.

N	2Θ	Miller indices	I_{obs}	I_{cal}	$I_{obs} - I_{cal}$
1	24.015	$\bar{3}$ 0 1	19.67	19.28	0.39
2	28.123	4 1 0	97.33	100	-2.67
3	31.411	4 1 1	17	16.24	0.76
4	33.948	5 0 0	2.53	2.41	0.12
5	35.236	0 3 2	18.14	17	1.14
6	38.242	0 5 0	1.14	1.14	0
7	40.631	0 5 1	11.54	11.54	0
8	44.827	5 1 2	4.18	3.29	0.89
9	49.202	$\bar{6}$ 3 1	11.04	10.91	0.13
10	50.089	5 3 2	16.75	15.73	1.02
11	54.106	5 5 1	4.06	3.68	0.38

Figures (4-11-a) and (4-11-b) show the fitting between observed and calculated diffraction patterns after making crystal structure refinement process for ZrO_2 micro powder before and after heat treatment.

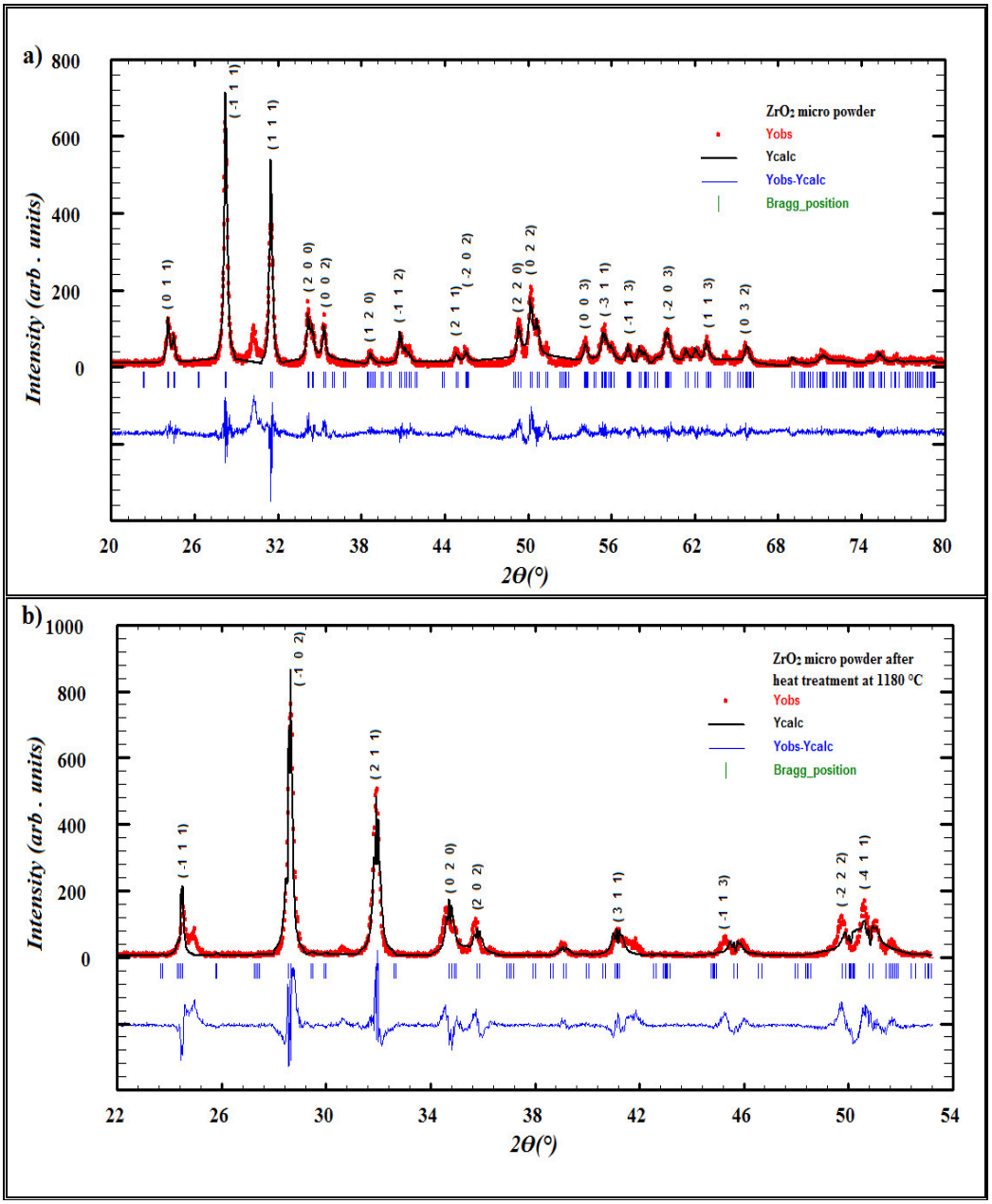

Fig. (4-11): The refined XRD patterns of ZrO_2 micro powder before and after heat treatment. The red line is the experimental data; the blue line is the theoretical data. The lowest trace indicates the difference between patterns. The middle vertical lines indicate the peak position.

Refinement results for ZrO_2 micro powder before and after heat treatment are shown in tables (4-27) and (4-28).

Table (4-27): Miller indices, observed and calculated intensity and difference between them for ZrO_2 micro powder before heat treatment.

N	2Θ	Miller indices	I_{obs}	I_{cal}	$I_{obs} - I_{cal}$
1	24.055	0 1 1	2.18	2.01	0.17
2	28.223	$\bar{1}$ 1 1	100	99.25	0.75
3	31.485	1 1 1	61.7	63.1	-1.4
4	34.072	2 0 0	11.9	11.5	0.4
5	35.211	0 0 2	3.12	3.01	0.11
6	38.409	1 2 0	0.3	0.3	0
7	40.644	$\bar{1}$ 1 2	0.75	0.76	-0.01
8	44.839	2 1 1	2.9	2.9	0
9	45.559	$\bar{2}$ 0 2	0.47	0.47	0
10	49.261	2 2 0	6.7	6.7	0
11	50.206	0 2 2	40.54	39.98	0.56
12	54.067	0 0 3	2.35	2.66	-0.31
13	55.028	$\bar{3}$ 1 1	0.8	0.8	0
14	57.151	$\bar{1}$ 1 3	1.4	1.3	0.1
15	59.799	$\bar{2}$ 0 3	3.8	3.9	-0.1
16	62.863	1 1 3	3.7	2.5	1.2
17	65.710	0 3 2	0.8	0.9	-0.1

Table (4-28): Miller indices, observed and calculated intensity and difference between them for ZrO_2 micro powder after heat treatment.

N	2Θ	Miller indices	I_{obs}	I_{cal}	$I_{obs} - I_{cal}$
1	24.078	$\bar{1}$ 1 1	37.73	37.59	0.14
2	28.324	$\bar{1}$ 0 2	100	96.94	3.06
3	31.605	2 1 1	9.73	9.73	0
4	34.474	0 2 0	12.08	11.94	0.14
5	35.278	2 0 2	13.57	13.50	0.07
6	40.738	3 1 1	8.03	7.96	0.07
7	44.813	$\bar{1}$ 1 3	16.41	16.20	0.21
8	49.311	$\bar{2}$ 2 2	3.12	3.05	0.07
9	50.286	$\bar{4}$ 1 1	37.73	37.59	0.14

Table (4-29) shows the reliability factors resultant from crystal structure refinement for ZrO_2 nano and micro powders before and after heat treatment.

Table (4-29): Reliability factors for ZrO_2 powders

Samples ZrO_2	Heat treatment at	R_{wp}	R_{exp}	R_p	χ^2
n_1	-	48.8	38.5	53.2	1.6
n_2	1180 °C	45.1	36.7	36.8	1.5
m_1	-	36.8	24.1	39.6	1.4
m_2	1180 °C	34.2	21.4	31.9	1.7

When comparing the diffraction patterns for ZrO_2 nano powder before and after heat treatment we note that the occurrence shift in intensity distribution for both diffraction patterns i.e. the peaks of diffraction patterns do not fall at the same angular position. This variation based on the diffraction files data where the powder before is matching with JCPDS files (No. 24-1165) and after heat treatment with JCPDS files (No. 36-0420), through the study diffraction files shows the material exhibits transition from phase to another and this is the reason behind the change in diffraction patterns. We note that the background intensity for both diffraction patterns are high at the small angular position can be attributed too the sample preparation method and preferred orientation existing in grains. This is same reason for ZrO_2 micro powder before and after heat treatment but the background intensity for ZrO_2 micro powder after heat treatment is high because of the quality of the sample scanned in terms of the method of preparation and the regularity of surface.

4-3-2 Crystal Structure Refinement for ZnO

Figures (4-12-a) and (4-12-b) show the fitting between observed and calculated diffraction patterns after making crystal structure refinement process for ZnO nano powder before and after heat treatment. The figures also show the Bragg's peak position and the difference between the observed and calculated

patterns. Refinement results for ZnO nano powder before and after heat treatment are shown in tables (4-30) and (4-31).

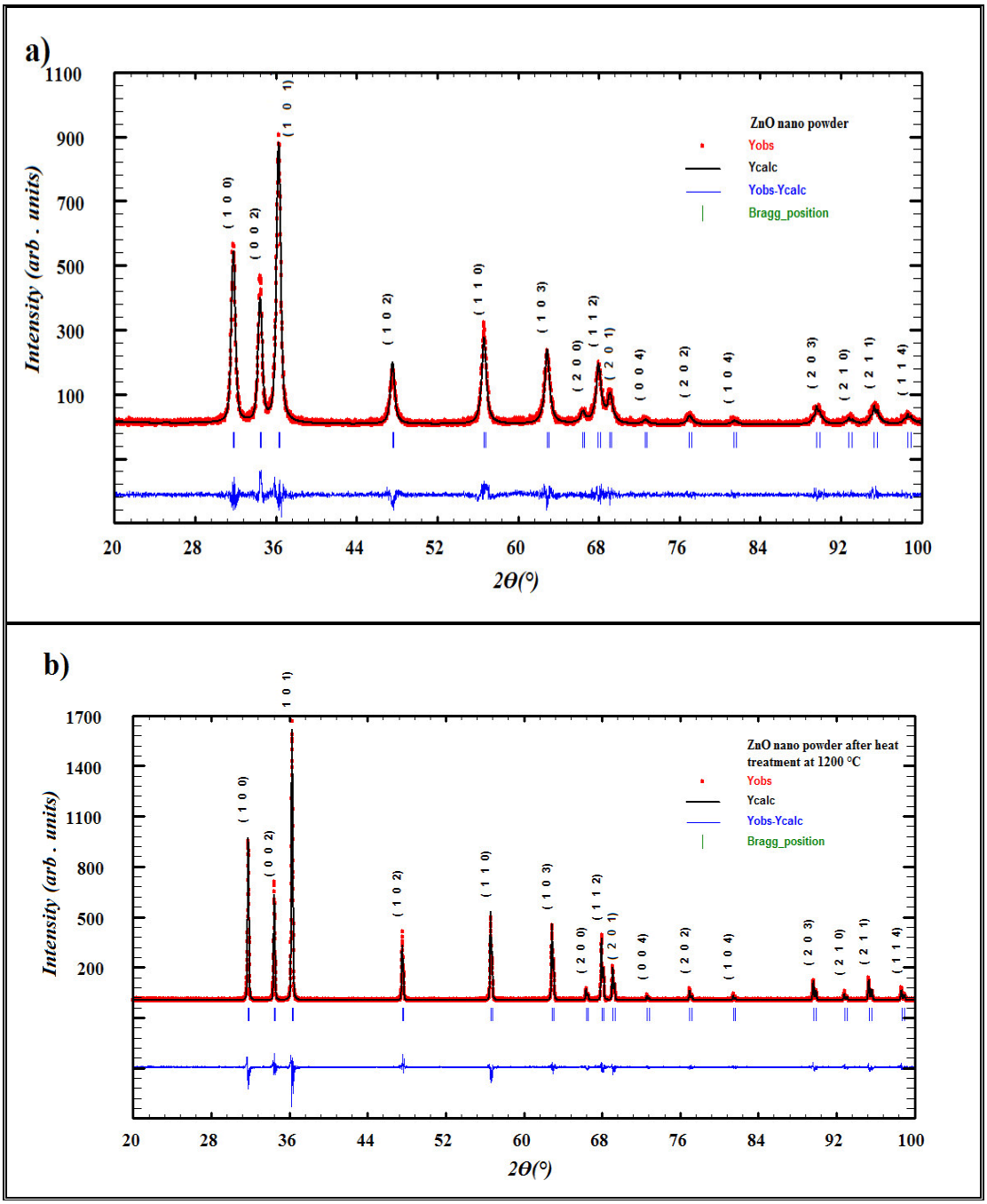

Fig. (4-12): The refined XRD patterns of ZnO nano powder before and after heat treatment. The red line is the experimental data; the blue line is the theoretical data. The lowest trace indicates the difference between patterns. The middle vertical lines indicate the peak position.

Table (4-30): Miller indices, observed and calculated intensity and difference between them for ZnO nano powder before heat treatment.

N	2Θ	Miller indices	I_{obs}	I_{cal}	$I_{obs} - I_{cal}$
1	31.768	1 0 0	58.85	58.28	0.57
2	34.420	0 0 2	44.74	42.59	2.15
3	36.253	1 0 1	100	98.59	1.41
4	47.538	1 0 2	24.88	24.00	0.88
5	56.595	1 1 0	39.92	36.68	3.24
6	62.855	1 0 3	35.51	33.62	1.89
7	66.375	2 0 0	5.26	5.18	0.08
8	67.946	1 1 2	28.67	28.13	0.54
9	69.085	2 0 1	14.31	13.53	0.78
10	72.563	0 0 4	2.80	2.20	0.6
11	76.958	2 0 2	5.65	4.58	1.07
12	81.382	1 0 4	3.18	2.30	0.88
13	89.610	2 0 3	11.61	10.44	1.17
14	93.081	2 1 0	4.04	3.57	0.47
15	95.305	2 1 1	11.48	10.42	1.06

Table (4-31): Miller indices, observed and calculated intensity and difference between them for ZnO nano powder after heat treatment.

N	2Θ	Miller indices	I_{obs}	I_{cal}	$I_{obs} - I_{cal}$
1	31.772	1 0 0	54.85	57.69	-2.84
2	34.438	0 0 2	40.541	38.27	2.271
3	36.261	1 0 1	95.35	100	-4.65
4	47.555	1 0 2	24.01	22.16	1.85
5	56.603	1 1 0	33.87	36.42	-2.55
6	62.883	1 0 3	32.78	31.92	0.86
7	66.385	2 0 0	5.58	5.11	0.47
8	67.965	1 1 2	27.66	26.62	1.04
9	69.098	2 0 1	13.64	14.11	-0.47
10	72.605	0 0 4	2.79	2.17	0.62
11	76.978	2 0 2	4.59	4.35	0.24
12	81.425	1 0 4	2.36	2.32	0.04
13	89.642	2 0 3	10.32	10.09	0.23
14	92.807	2 1 0	3.74	3.55	0.19
15	95.324	2 1 1	11.03	11.13	-0.1

Figures (4-13-a) and (4-13-b) show the fitting between observed and calculated diffraction patterns after making crystal structure refinement process

for ZnO micro powder before and after heat treatment. Refinement results for ZnO micro powder before and after heat treatment are shown in tables (4-32) and (4-33).

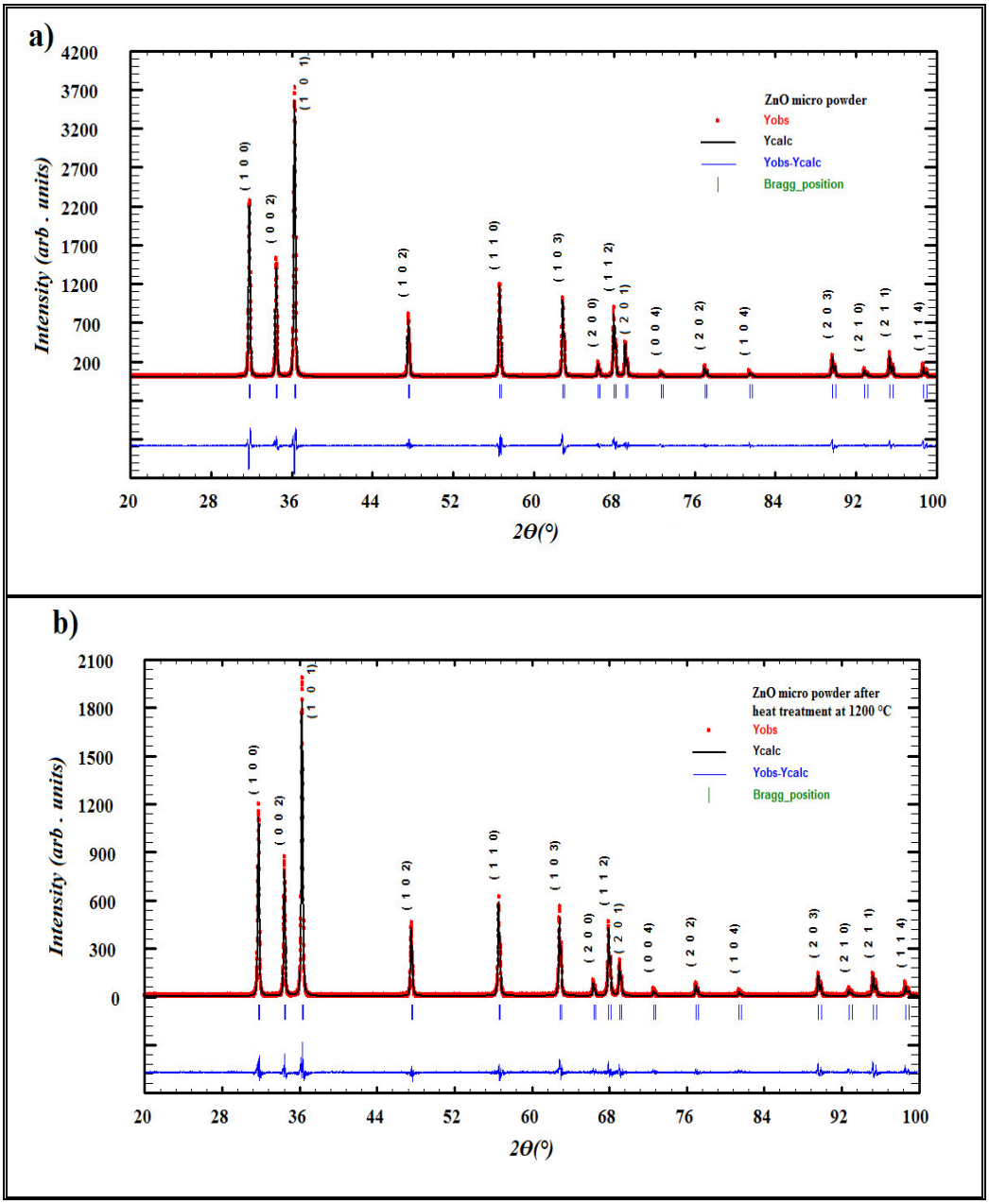

Fig. (4-13): The refined XRD patterns of ZnO micro powder before and after heat treatment. The red line is the experimental data; the blue line is the theoretical data. The lowest trace indicates the difference between patterns. The middle vertical lines indicate the peak position.

Table (4-32): Miller indices, observed and calculated intensity and difference between them for ZnO micro powder before heat treatment.

N	2Θ	Miller indices	I_{obs}	I_{cal}	$I_{obs} - I_{cal}$
1	31.818	1 0 0	59.29	59.68	-0.39
2	34.331	0 0 2	41.07	39.09	1.98
3	36.494	1 0 1	98.50	100	-1.5
4	47.573	1 0 2	23.69	22.40	1.29
5	56.622	1 1 0	36.48	37.02	-0.54
6	62.910	1 0 3	34.43	32.16	2.27
7	66.409	2 0 0	6.17	5.17	1
8	67.991	1 1 2	28.90	26.34	2.56
9	69.123	2 0 1	14.41	13.60	0.81
10	72.640	0 0 4	2.64	2.05	0.59
11	77.009	2 0 2	4.80	4.28	0.52
12	81.464	1 0 4	2.80	2.14	0.66
13	89.682	2 0 3	11.01	9.88	1.13
14	92.845	2 1 0	4.36	3.47	0.89
15	95.364	2 1 1	11.81	10.33	1.48

Table (4-33): Miller indices, observed and calculated intensity and difference between them for ZnO micro powder after heat treatment.

N	2Θ	Miller indices	I_{obs}	I_{cal}	$I_{obs} - I_{cal}$
1	31.819	1 0 0	58.70	56.90	1.8
2	34.330	0 0 2	41.39	40.87	0.52
3	36.495	1 0 1	100	97.67	2.33
4	47.544	1 0 2	23.85	24.67	-0.82
5	56.584	1 1 0	36.64	35.70	0.94
6	62.870	1 0 3	34.84	30.92	3.92
7	66.362	2 0 0	6.053	5.03	1.023
8	67.945	1 1 2	29.09	27.29	1.8
9	69.075	2 0 1	14.43	13.54	0.89
10	72.593	0 0 4	3.04	2.15	0.89
11	76.954	2 0 2	5.62	4.67	0.95
12	81.408	1 0 4	3.53	1.86	1.67
13	89.615	2 0 3	11.97	9.78	2.19
14	92.771	2 1 0	4.41	3.43	0.98
15	95.287	2 1 1	11.97	10.50	1.47

Table (4-34) show the reliability factors resultant from crystal structure refinement for ZnO nano and micro powders before and after heat treatment.

Table (4-34): Reliability factors for ZnO powders

Samples ZnO	Heat treatment at	R_{wp}	R_{exp}	R_p	χ^2
n_3	-	23.0	19.6	16.3	1.3
n_4	1200 °C	27.5	26.1	20.7	1.1
m_3	-	22.6	16.1	16.1	1.9
m_4	1200 °C	26.2	21.6	16.9	1.4

When checking the diffraction patterns for ZnO nano and micro powder before and after heat treatment we note that the intensity distribution for all diffraction is equal and the background intensity for all diffraction patterns are high at the small angular position, and this can be attributed to the sample preparation method and preferred orientation existing in grains.

4-3-3 Crystal Structure Refinement for Al_2O_3

Figures (4-14-a) and (4-14-b) show the fitting between observed and calculated diffraction patterns after making crystal structure refinement process for Al_2O_3 nano powder before and after heat treatment. The figures also show the Bragg's peak position and the difference between the observed and calculated patterns. Refinement results for Al_2O_3 nano powder before and after heat treatment are shown in tables (4-35) and (4-36).

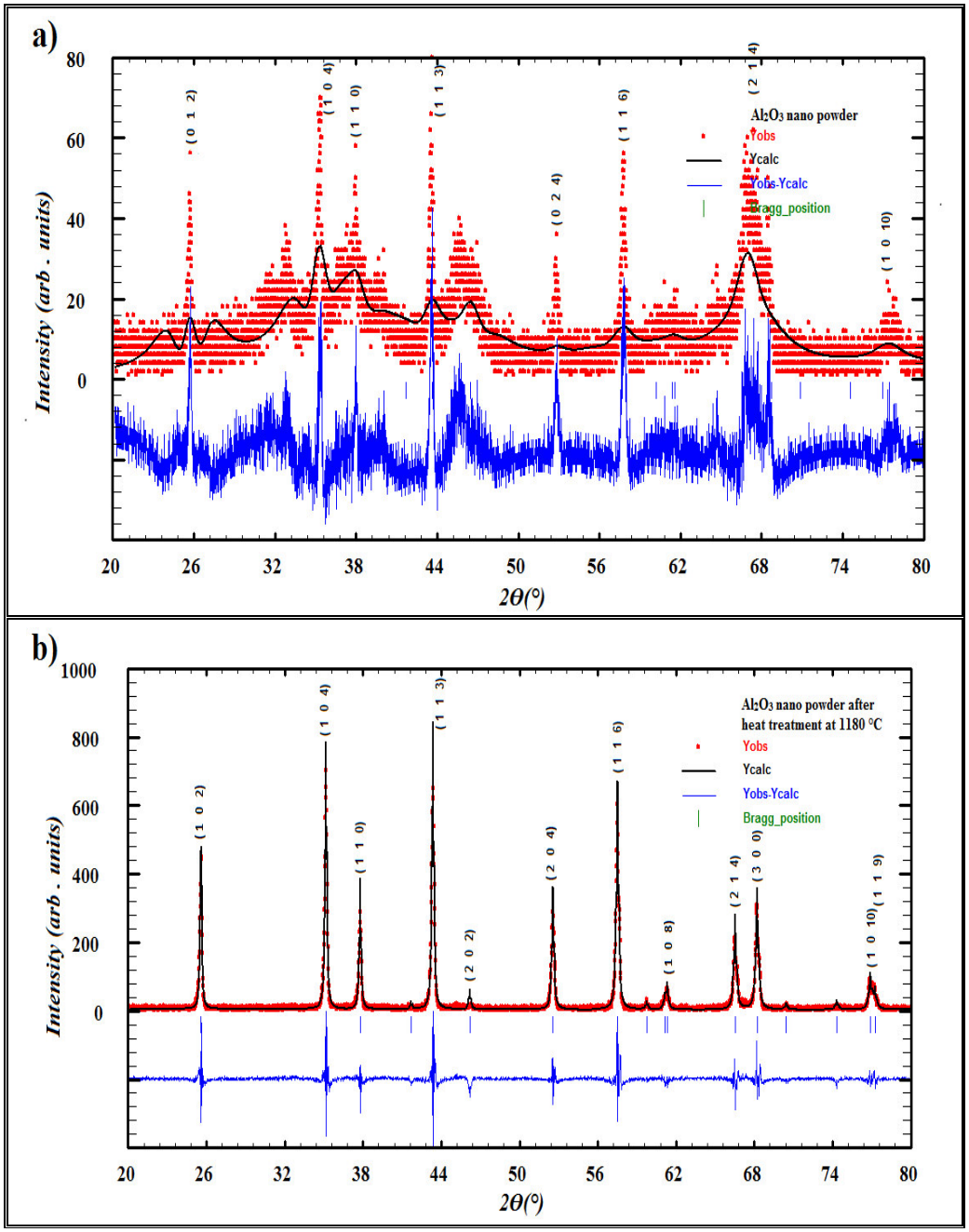

Fig. (4-14): The refined XRD patterns of Al_2O_3 nano powder before and after heat treatment. The red line is the experimental data; the blue line is the theoretical data. The lowest trace indicates the difference between patterns. The middle vertical lines indicate the peak position.

Table (4-35): Miller indices, observed and calculated intensity and difference between them for Al_2O_3 nano powder before heat treatment.

N	2Θ	Miller indices	I_{obs}	I_{cal}	$I_{obs} - I_{cal}$
1	25.707	0 1 2	50.05	49.70	0.35
2	35.117	1 0 4	85.15	80.32	4.83
3	38.046	1 1 0	34.10	34.63	-0.53
4	43.317	1 1 3	100	96.97	3.03
5	52.838	0 2 4	9.08	8.84	0.24
6	57.716	1 1 6	27.93	26.13	1.8
7	66.266	2 1 4	50.05	49.70	0.35
8	76.980	1 0 10	1.97	1.92	0.05

Table (4-36): Miller indices, observed and calculated intensity and difference between them for Al_2O_3 nano powder after heat treatment.

N	2Θ	Miller indices	I_{obs}	I_{cal}	$I_{obs} - I_{cal}$
1	25.572	1 0 2	60.55	62.29	-1.74
2	35.143	1 0 4	96.28	98.21	-1.93
3	37.770	1 1 0	41.98	42.39	-0.41
4	43.341	1 1 3	98.82	100	-1.18
5	46.170	2 0 2	7.73	7.83	-0.1
6	52.543	2 0 4	48.19	49.00	-0.81
7	57.479	1 1 6	90.83	91.55	-0.72
8	61.296	1 0 8	10.78	11.04	-0.26
9	66.506	2 1 4	44.73	45.90	-1.17
10	68.196	3 0 0	53.84	53.63	0.21
11	76.865	1 0 10	19.18	19.84	-0.66
12	77.226	1 1 9	10.78	11.19	-0.41

Figures (4-15-a) and (4-15-b) explain the fitting between observed and calculated diffraction patterns after making crystal structure refinement process for Al_2O_3 micro powder before and after heat treatment. The figures also show the Bragg's peak position and the difference between the observed and calculated patterns. Refinement results for Al_2O_3 micro powder before and after heat treatment) are shown in tables (4-37) and (4-38).

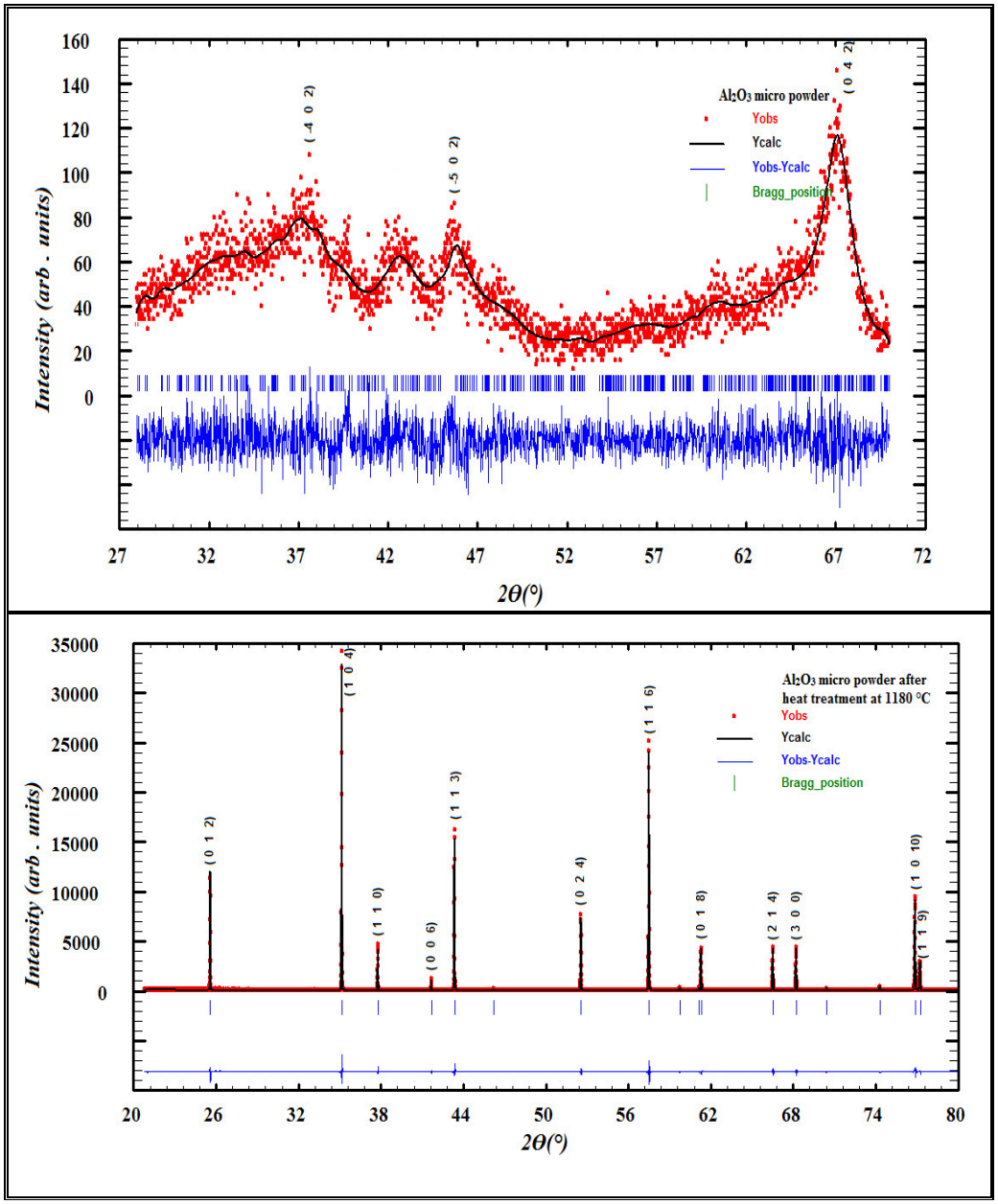

Fig. (4-15): The refined XRD patterns of Al_2O_3 micro powder before and after heat treatment. The red line is the experimental data; the blue line is the theoretical data. The lowest trace indicates the difference between patterns. The middle vertical lines indicate the peak position.

Table (4-37): Miller indices, observed and calculated intensity and difference between them for Al_2O_3 micro powder before heat treatment.

N	2Θ	Miller indices	I_{obs}	I_{cal}	$I_{obs} - I_{cal}$
1	37.475	$\bar{4}$ 0 2	29.06	29.01	0.05
2	45.710	$\bar{5}$ 0 2	15.28	15.21	0.07
3	67.042	0 4 2	100	99.84	0.16

Table (4-38): Miller indices, observed and calculated intensity and difference between them for Al_2O_3 micro powder after heat treatment.

N	2Θ	Miller indices	I_{obs}	I_{cal}	$I_{obs} - I_{cal}$
1	25.576	0 1 2	32.49	31.93	0.56
2	35.094	1 0 4	100	98.22	1.78
3	37.778	1 1 0	12.27	12.32	-0.05
4	41.675	0 0 6	0.06	0.06	0
5	43.289	1 1 3	50.32	49.81	0.51
6	52.552	0 2 4	25.64	25.67	-0.03
7	57.428	1 1 6	91.91	91.28	0.63
8	61.300	0 1 8	16.14	16.33	-0.19
9	66.520	2 1 4	17.01	17.24	-0.23
10	68.213	3 0 0	17.53	17.78	-0.25
11	76.871	1 0 10	43.57	43.65	-0.08
12	77.234	1 1 9	13.66	13.77	-0.11

Table (4-39) shows the reliability factors resultant from crystal structure refinement for Al_2O_3 nano and micro powders before and after heat treatment.

Table (4-39): Reliability factors for Al_2O_3 powders

Samples Al_2O_3	Heat treatment at	R_{wp}	R_{exp}	R_p	χ^2
n_5	-	48.8	30.3	34.9	2.5
n_6	1180 °C	37.2	26.9	28.6	1.9
m_5	-	15.5	14.2	11.8	1.1
m_6	1180 °C	11.9	7.6	8.3	2.4

When checking the diffraction patterns for Al_2O_3 nano powder before and after heat treatment we note that the occurrence shift in intensity distribution for both diffraction patterns i.e. the peaks of diffraction patterns do not fall at the same angular position. This variation based on the diffraction files data where the powder before was matching with JCPDS files (No. 05-0712) and after heat treatment with JCPDS files (No. 10-0173), through the study diffraction files shows the material exhibits transition from phase to another and this is the reason behind the change in diffraction patterns. We note that the background

intensity for all diffraction patterns increases with increasing the range of angular scanned because of thermal vibration and can be attributed too the sample preparation method and preferred orientation existing in grains.

Reduction the total intensity for all reflection in the diffraction patterns for Al_2O_3 nano and micro powder before and after heat treatment, in comparison nano powder before and after heat treatment we find the highest intensity of up to ≈70 cps for powder before heat treatment and ≈900 cps for powder after heat treatment . Also, we find the highest intensity of up to ≈150 cps for Al_2O_3 micro powder before heat treatment and ≈35000 cps for Al_2O_3 micro powder after heat treatment, this is proof that the material after heat treatment has high arrangement of crystalline and the information of powder exactly match the information of signal crystal.

4-4 SEM Characterization

4-4-1 SEM of ZrO_2 Nano Powder

The SEM images of the ZrO_2 nano powder before and after heat treatment are shown in figures (4-16) and (4-17).

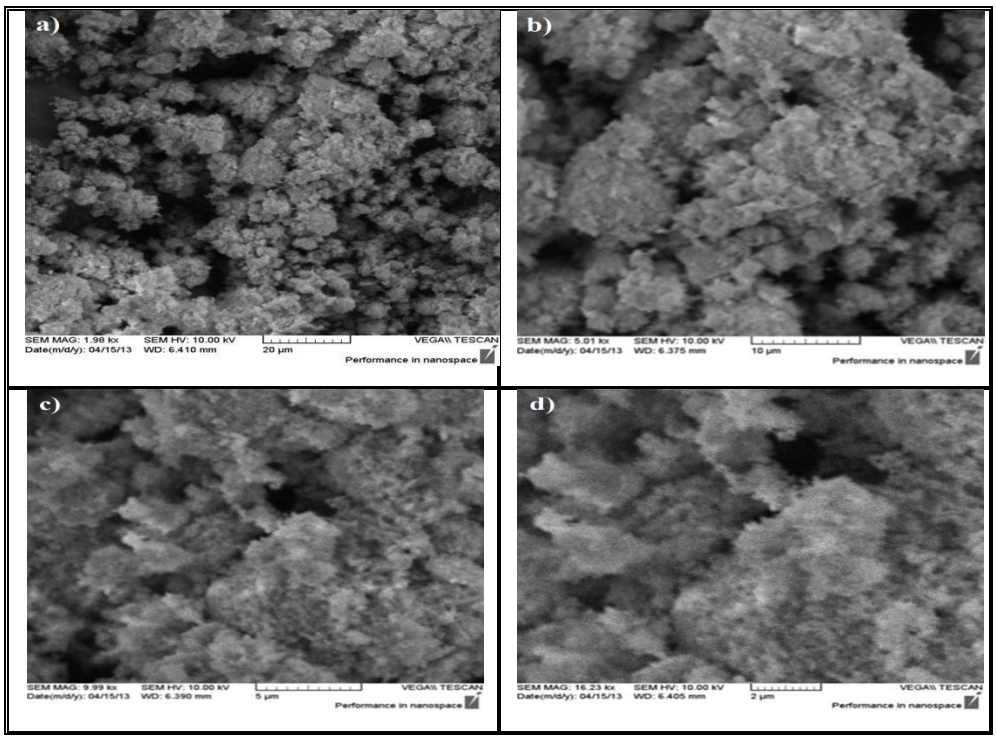

Fig. (4-16): SEM images of the ZrO_2 nano powder before heat treatment for different magnification.

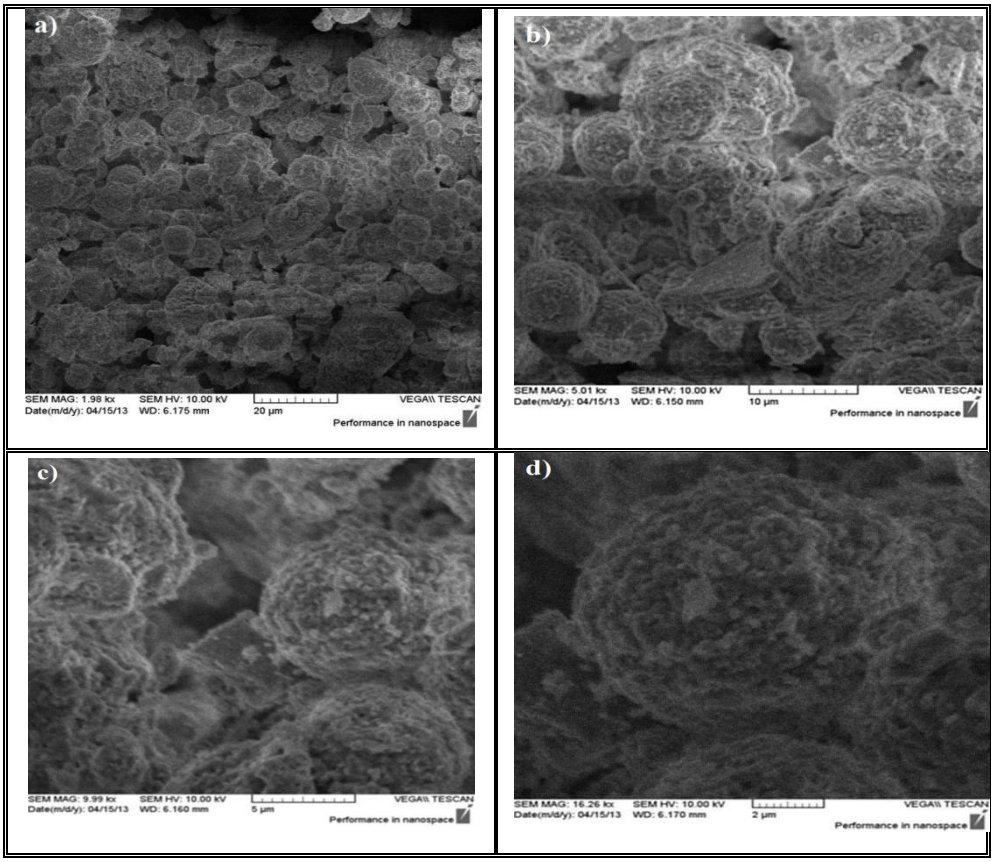

Fig. (4-17): SEM images of the ZrO_2 nano powder after heat treatment for different magnification.

SEM micrographs for ZrO_2 nano powder before heat treatment (Figure 4-16) show the particle morphology having homogenous irregular grains. The image appears to be similar to coral shape.

SEM images reveal the spherical shape of powder particles for ZrO_2 nano powder after heat treatment (Fig. 4-17). Differences in their morphology can be found from the analysis of the corresponding images obtained at different magnification.

4-4-2 SEM of ZrO_2 Micro Powder

The SEM images of the ZrO_2 micro powder before and after heat treatment are shown in figures (4-18) and (4-19).

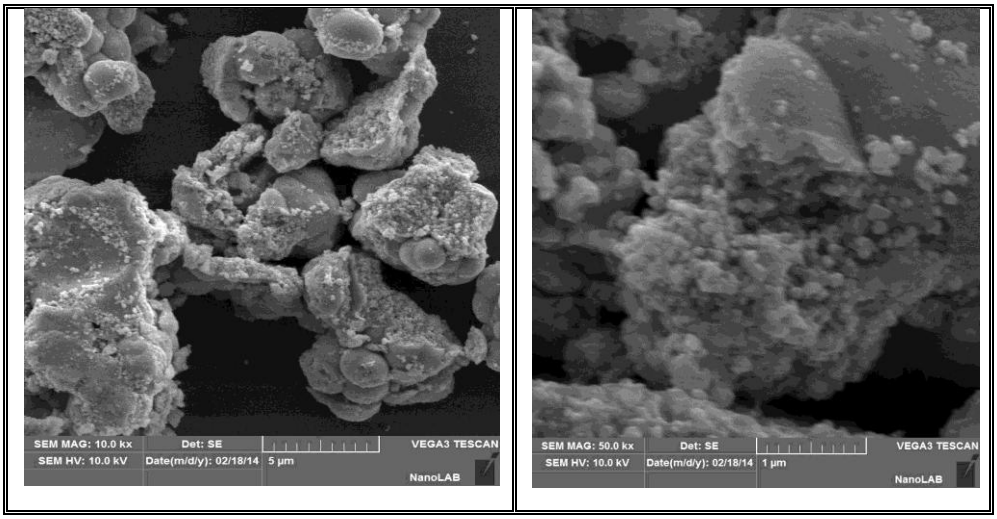

Fig. (4-18): SEM images of the ZrO_2 micro powder before heat treatment for different magnification.

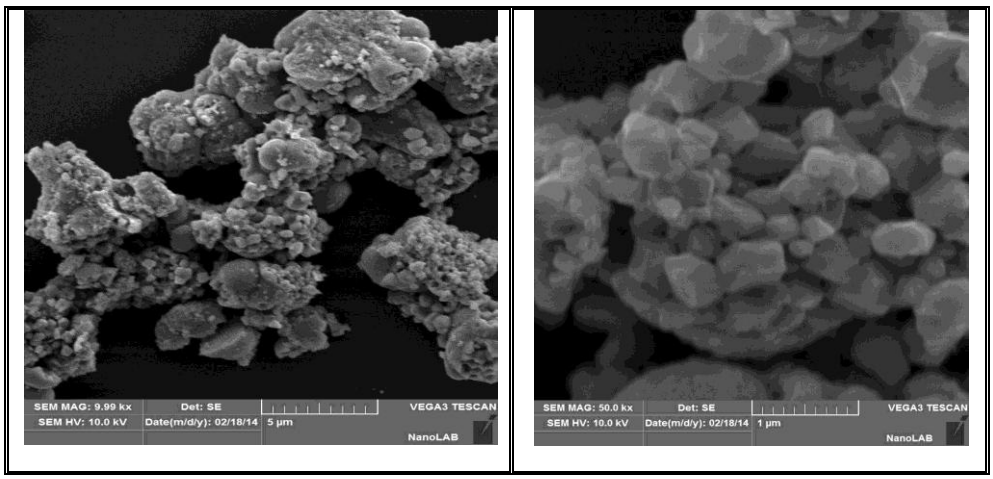

Fig. (4-19): SEM images of the ZrO_2 micro powder after heat treatment for different magnification.

From the figures (4-18) and (4-19) it can be observed that spherical particles are the predominant morphology; only a small number of them show a hollow or irregular shape.

4-4-3 SEM of ZnO Nano Powder

The SEM images of the ZnO nano powder before and after heat treatment are shown in figures (4-20) and (4-21).

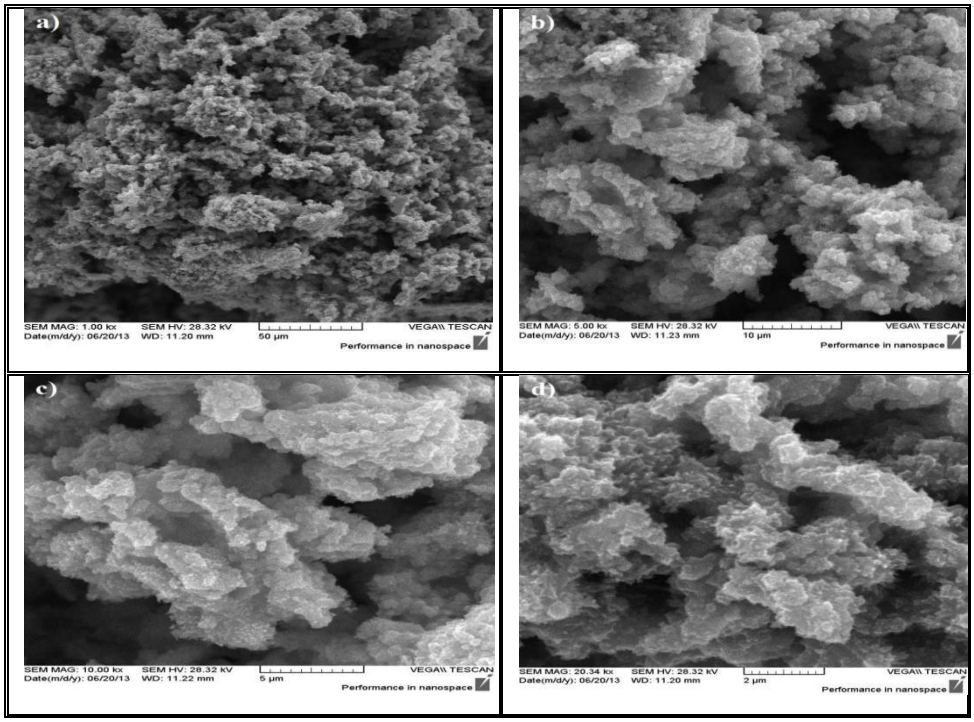

Fig. (4-20): SEM images of the ZnO nano powder before heat treatment for different magnification.

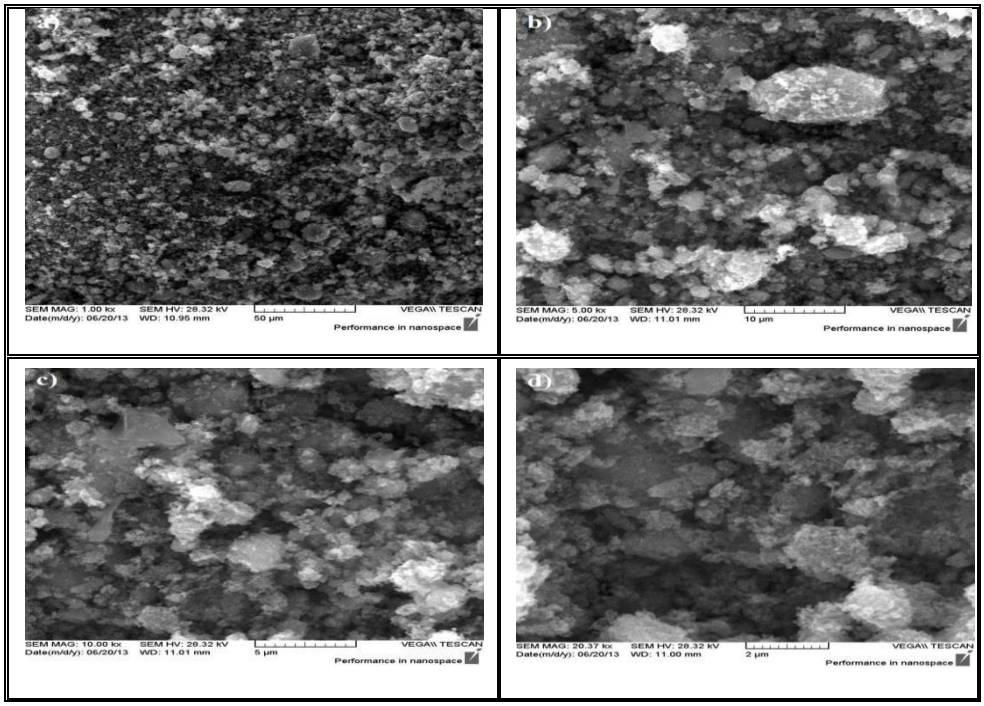

Fig. (4-21): SEM images of the ZnO nano powder after heat treatment for different magnification.

The figures (4-20) and (4-21) show that a network formation and agglomeration has taken place. The SEM micrographs clearly show the microstructural homogeneity and remarkably dense mode of packing of grains of ZnO nanoparticles.

4-4-4 SEM of ZnO Micro Powder

The SEM images of the ZnO micro powder before and after heat treatment are shown in figures (4-22) and (4-23).

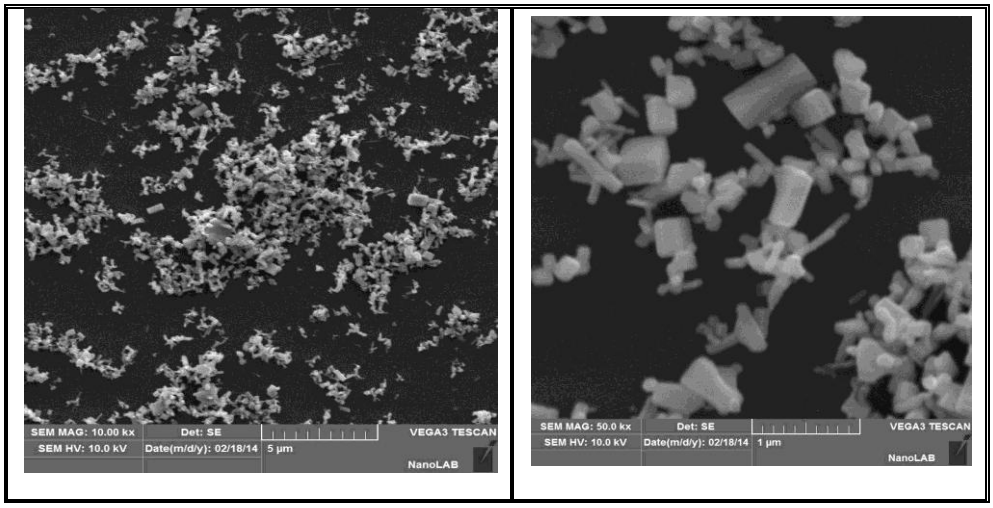

Fig. (4-22): SEM images of the ZnO micro powder before heat treatment for different magnification.

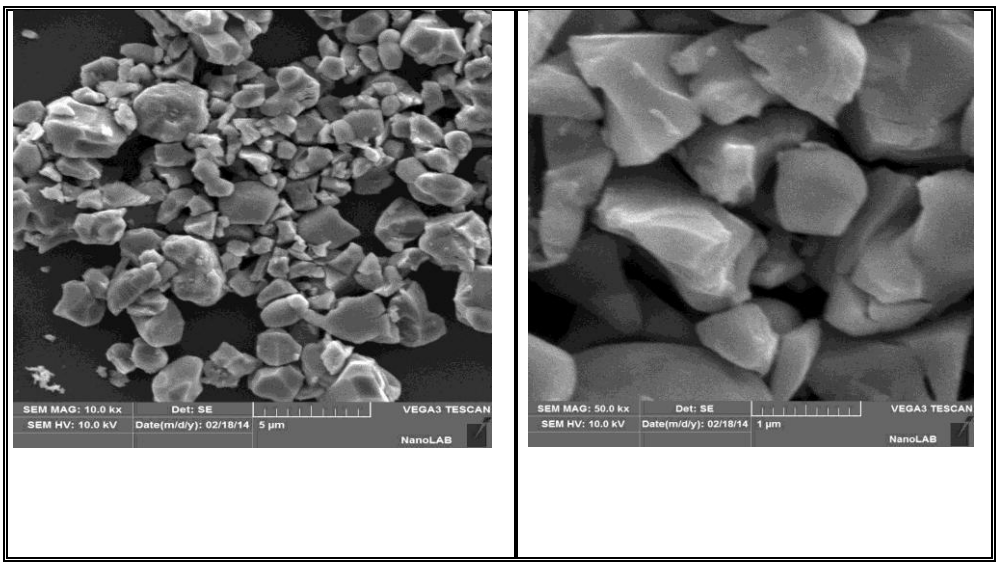

Fig. (4-23): SEM images of the ZnO micro powder after heat treatment for different magnification.

SEM micrographs for ZnO micro powder before heat treatment (Figure 4-22) show the particle that the columnar and polygon surface. After heat treatment SEM micrograph images show the grains have pyramid forms.

4-4-5 SEM of Al_2O_3 Nano Powder

The SEM images of the Al_2O_3 nano powder before and after heat treatment are shown in figures (4-24) and (4-25).

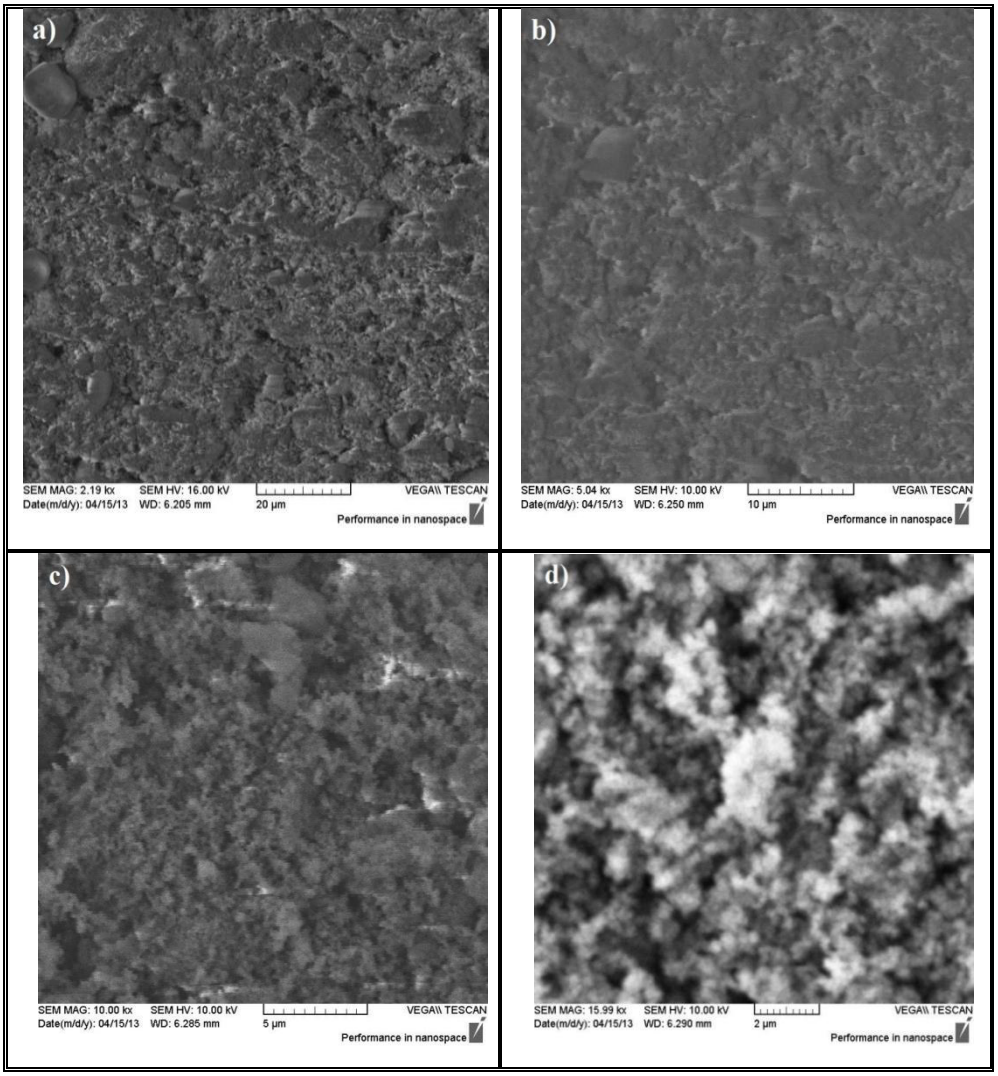

Fig. (4-24): SEM images of the Al_2O_3 nano powder before heat treatment for different magnification.

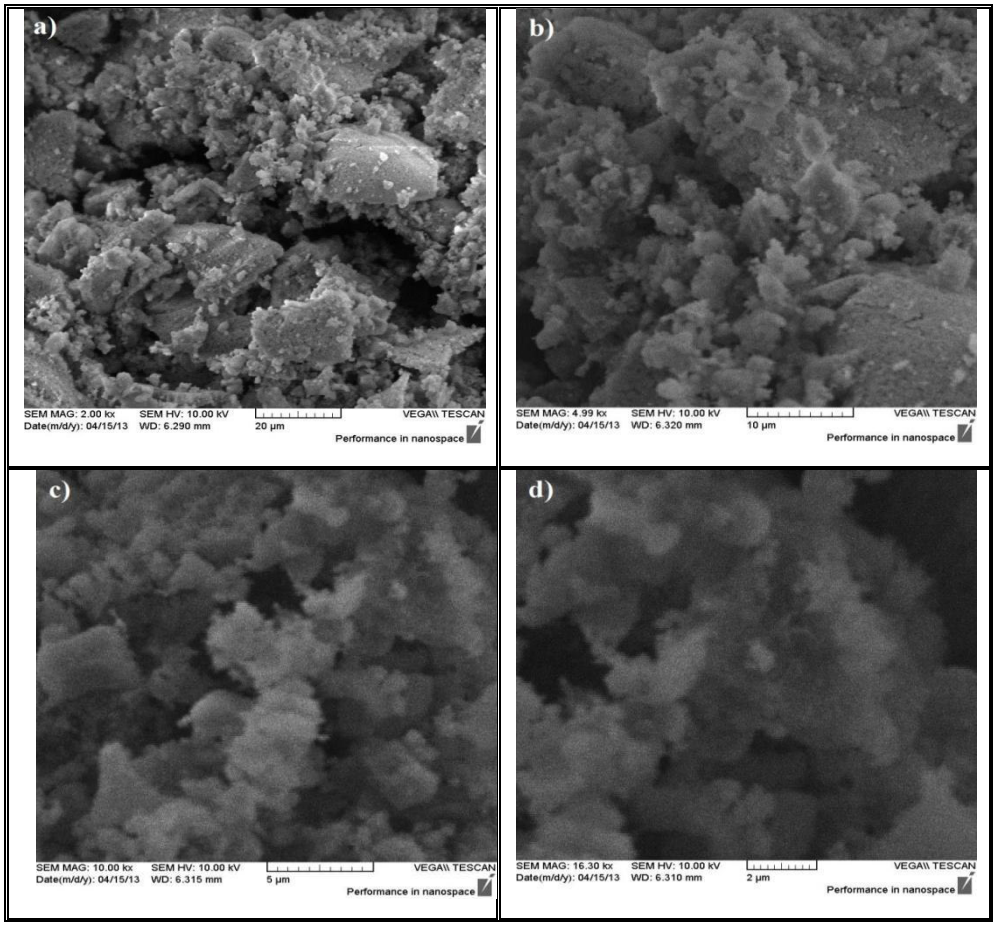

Fig. (4-25): SEM images of the Al_2O_3 nano powder after heat treatment for different magnification.

SEM micrograph image of Al_2O_3 nano powder before heat treatment show a homogeneous system with agglomerates of submicronic particles. After heat treatment SEM micrograph images show change in the positions of atoms so we observe a loss of the original morphology of the particles and particles are finer and more uniform as in figures (4-25).

4-4-6 SEM of Al_2O_3 Micro Powder

The SEM images of the Al_2O_3 nano powder before and after heat treatment are shown in figures (4-26) and (4-27).

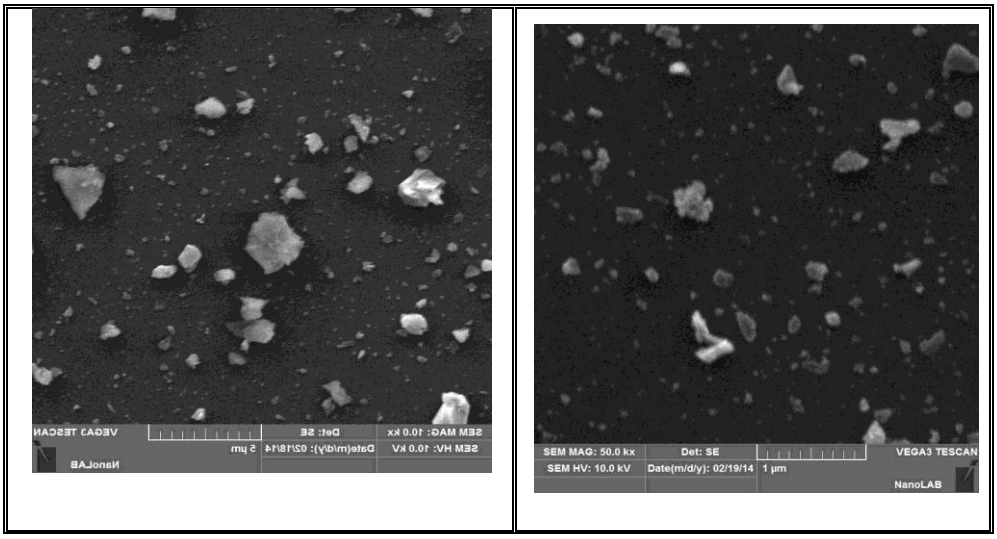

Fig. (4-26): SEM images of the Al_2O_3 micro powder before heat treatment for different magnification.

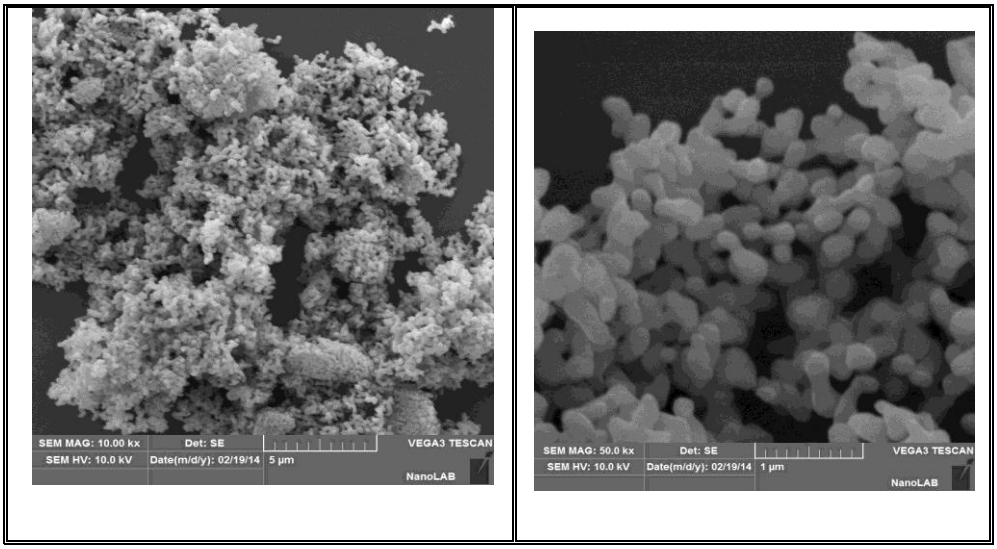

Fig. (4-27): SEM images of the Al_2O_3 micro powder after heat treatment for different magnification.

SEM micrograph image of Al_2O_3 micro powder before heat treatment show some grains are conglomerated. After heat treatment SEM micrograph images show the grains have finger shape is observed as in figures (4-27).

Chapter Five

Conclusion and Future Work

5-1 Introduction

This chapter shows the conclusions and future work for the thesis.

5-2 Conclusions

(1) The phase transition from monoclinic (P2/m phase group) to tetragonal (P4/mmm phase group) has been observed for the micro ZrO2 powder after heat treatment, while no phase transition occurred for the nano ZrO2 powder.

(2) No phase transition occurred for ZnO nano and micro powders before and after heat treatment because the powders need to heat treatment at high temperature.

(3) The phase transition from monoclinic (P2/m phase group) to hexagonal (R c phase group) has been observed for the micro Al_2O_3 powder after heat treatment, while no phase transition occurred for the nano Al_2O_3 powder.

(4) The results show that the grains size estimated by Debye-Scherrer formula and Williamson-Hall formula increases after heat treatment for all powders.

(5) The unit cell volume increase at heat treatment for all powders.

(6) SEM micrographs have proved convergence grain size measuring with what has been calculated from Debye-Scherrer and Williamson-Hall

(7) The Rietveld method does not require pure-phase standards for the analysis and it shows good precision for the qualitative analysis of phases present in powders used.

(8) The Rietveld analysis has numerous advantages: it does not require any standards or monitors, in addition to that, this method offers impressive accuracy and speed of analysis.

(9) Fullprof program efficiency in the refinement of crystal structure for powders give high resolution results which are very close to the results of

single crystal diffraction. This depends on the sample preparation method, degree of purity and specifications diffractometer.

5-3 Future Work

(1) Use GSAS program in crystal structure refinement instead of Fullprof program .

(2) Use other programs in indexing such as ITO, LZON and TAUP instead of DICVOL.

(3) Scan the samples in the ranges of high angle so as to be more accurate in the values of the unit cell parameters and reliability factors.

(4) Use powders prepared practically and not commercial.

(5) Use the Rietveld analysis in determining the crystal structures of the other powders.

References

[1] G. Will, " Powder diffraction: The Rietveld method and the two stage method to determine and refine crystal structures from powder diffraction data", Springer (2005).

[2] R. E. Dinnebier and S. J. L. Billinge, "Powder diffraction theory and practice", The royal society of chemistry (RSC), (2008).

[3] U. König and E. Spicer, " X-ray diffraction (XRD) as a fast industrial analysis method for heavy mineral sands in process control and automation-Rietveld refinement and data clustering", The 6th international heavy minerals conference 'back to basics', The Southern African Institute of Mining and Metallurgy, (2007).

[4] D. Gporob and T. Row, " Ab initio structure determination via powder X-ray diffraction", Proc. Indian Acad. Sci. (Chem. Sci.), Vol. 113, P. (435-444), (2001).

[5] W. I. F. David, K. Shankland, L. B. Mccusker and Ch. Baerlocher, " Structure determination from powder diffraction data ", Oxford university press, (2002).

[6] H. M. Rietveld, " The early days: a retrospective view ", in the Rietveld method, p. (39-42), ed. R. A. Young, Oxford: university press, (1993).

[7] D. B. Wiles and R. A. Young, "A new computer program for Rietveld analysis of X-ray powder diffraction patterns ", J. appl. cryst., Vol. 14, P. (149-151), (1981).

[8] A. Albinati and B. T. M. Willis, "The Rietveld method in neutron and X-ray powder diffraction", J. appl. cryst., Vol. 15, P. (361-374), (1982).

[9] D. L. Bish and S. A. Howard, " Quantitative phase analysis using the Rietveld method ", J. appl. cryst., Vol. 21, P. (86-91), (1988).

[10] L. B. Mccusker, R. B. Von Dreele, D. E. Cox, D. LoueÈr and P. Scardi, "Rietveld refinement guidelines", J. appl. cryst., Vol. 32, P. (36-50), (1999).

[11] W. Daning , G. Yongquan, L. Kaiming and T. Kun, "Crystal structure of zirconia by Rietveld refinement", Science in China (Series A), Vol. 42, P. (80-86), (1999).

[12] X. Bokhimi, A. Morales, O. Novaro, T. López, R. Gómez and A. Garcia-Ruiz, " Quantitative analysis of phase transformations in nanocrystalline

materials via Rietveld refinement ", JCPDS-International centre for diffraction data, Advances in X-ray analysis, Vol. 42, (2000).

[13] P. S. Santos, H. S. Santos and S.P. Toledo, " Standard transition aluminas. electron microscopy studies", Materials research, Vol. 3, P. (104-114), (2000).

[14] S. Cava, S.M. Tebcherani, I.A. Souza, S.A. Pianaro, C.A. Paskocimas, E. Longo and J.A. Varela, "Structural characterization of phase transition of Al_2O_3 nanopowders obtained by polymeric precursor method ", Materials chemistry and physics, Vol. 103, P.(394–399), (2007).

[15] G. Dercz, K. Prusik and L. Pająk, " X-ray and SEM studies on zirconia powders ", Journal of achievements in materials and manufacturing engineering, Vol. 31, P. (408-414), (2008).

[16] K. Prasad and A. Jha, " ZnO nanoparticles: synthesis and adsorption study", Natural science, Vol. 1, P. (129-135), (2009).

[17] N. M. Rendtorff, M. S. Conconi, E. F. Aglietti, C. Y. Chain, A. F. Pasquevich, P. C. Rivas, J. A. Martínez and M. C. Caracoche, " Phase quantification of mullite–zirconia and zircon commercial powders using PAC and XRD techniques ", Springer science and business media B.V., (2010).

[18] F. P. Albores, F. P. Delgado, W. A. Flores, P. A. Madrid, E. R. Valdovinos and M. M. Yoshida, "Microstructural study of ZnO nanostructures by Rietveld analysis", Journal of nanomaterials, P. (1-11), (2011).

[19] S. Krobthong, C. Bhoomanee, S. Choopun, A. Tubtimtae, S. Sujinnapram and S. Sutthana, " Antibacterial performance of ZnO tetrapods prepared by thermal oxidation ", Australian journal of basic and applied sciences, Vol. 7, P. (100-104), (2013).

[20] A. Nouailhat, "An Introduction to Nanoscience and Nanotechnology", Wiley, (2008).

[21] F. Allhoff, P. Lin and D. Moore, " What is nanotechnology and why does it matter from science to ethics", Wiley , (2010).

[22] C. Buzea, I. I. Blandino and K. Robbie, "Nanomaterials and nanoparticles: Sources and Toxicity", Biointerphases, Vol. 2, P. (17-172) , (2007).

[23] I. Capek, "Nanocomposite structures and dispersions science and nanotechnology - fundamental principles and colloidal particles", Elsevier, (2006).

[24] J. F. Mongillo, " Nanotechnology 101 ", Greenwood press , (2007).

[25] " Nanotechnolog applications guide ", Accelrys inc. (2004).

[26] G. Cao and S. J. Limmer, " Oxide nanowires and nanorods ", Encyclopedia of nanoscience and nanotechnology, Vol. 8, P. (377-396), (2004).

[27] M. N. Avadhanulu and P. G. Kshirsagar, "A textbook of engineering physics", S. Chand, (1992).

[28] P. Sharma and M. Bhargava, "Applications and characteristics of nanomaterials in industrial environment ", International Journal of Civil, Structural, Environmental and Infrastructure Engineering Research and Development (IJCSEIERD), Vol. 3, P. (63-72), (2013).

[29] N. Golovina, "Toxicity of nanoparticles", (2012).

[30] J. T. Lue, "Physical properties of nanomaterials", Encyclopedia of Nanoscience and Nanotechnology, Vol. X, P. (1-46), (2007).

[31] C. Y. Shen, "Structure determination from X-ray powder diffraction".

[32] Fultz, Brent, Howe and James, "Transmission electron microscopy and diffractometry of materials", Springer, (2013).

[33] K. Janssens and Van Grieken, "Comprehensive analytical chemistry XLII", Elsevier, (2004).

[34] G. M. Reeves, I. Sims and J. C. Cripps, " Clay materials used in construction", Geological Society, (2006).

[35] R. E. Dinnebier and K. Friese, "Modern XRD methods in mineralogy", Max-Planck Institute for Solid State Research, Stuttgart. FRG.

[36] T. M. Marush, " Crystal structure refinement of some metallic oxide powders using Rietveld analysis", University of Baghdad colloge of Education Department of Physics, (2005).

[37] B. L. Dutrow and C. M. Clark,"X-ray powder diffraction XRD", Geochemical Instrumentation and Analysis.

[38] J. R. Connolly, " Introduction to X-ray powder diffraction", Spring, (2007).

[39] Ch S. Vani, "Bioinspired study on morphosynthesis of calcium, barium and strontium carbonates – micro structures and nano crystallites", Acharya Nagarjuna University , (2011).

[40] P. G. Trust, " New portable X-ray diffraction/ X-ray fluorescence instrument (XRD/XRF)", The getty Conservation Institute, (2009).

[41] S. N. Danilchenko, O. G. Kukharenko, C. Moseke, I. Y. Protsenko, L. F. Sukhodub and B. S. Cleff, "Determination of the bone mineral crystallite size and lattice strain from diffraction line broadening ", Cryst. Res. Technol., Vol. 37, (2002).

[42] V. K. Pecharsky and P.Y. Zavalij, "Fundamentals of powder diffraction and structural characterization of materials ", Springer, (2009).

[43] B. D. Cullity, "Elements of X-ray diffraction", Addison-Wesley Publishing Company, INC., (1981).

[44] J. I. Langfordy and D. Louër, "Powder diffraction", Rep. Prog. Phys., Vol. 59, P. (131–234), (1696).

[45] A. Guinier, "X-ray diffraction in crystals, imperfect crystals, and amorphous bodies", W. H. Freeman and Company., (1994).

[46] C. Suryanarayana and M. G. Norton, "X-ray diffraction: A practical approach", Springer Science and Business Media, LLC, (1998).

[47] B. E. Warren, "X-ray diffraction", Dover Publications, INC., (1990).

[48] F. Sher, "Crystal structure determination II ", Pakistan Institute of Engineering and Applied Sciences, (2010).

[49] Y. Waseda, E. Matsubara and K. Shinoda, " X-ray diffraction crystallography introduction, examples and solved problems", Springer, (2011).

[50] R. Jenkins and R. L. Snyder, " Introduction to X-ray powder diffractometry ", John Wiley and Sons, INC., (1996).

[51] "X-Ray Diffraction Study of Ordering in CoPt System", 3.014 Materials Laboratory, (2006).

[52] R. Guinebretière, "X-ray diffraction by polycrystalline materials", ISTE Ltd, (2007).

[53] J. R. Connolly, "Diffraction basics, part 2", Spring, (2012).

[54] S. Speakman, "Fundamentals of Rietveld refinement: XRD pattern simulation", MIT Center for Materials Science and Engineering.

[55] R. C. Reynolds and JR., " The Lorentz-polarization factor and preferred orientation in oriented clay aggregates", Clays and Clay Minerals, Vol. 34, P. (359-367), (1986).

[56] C. Hammond, " The basics of crystallography and diffraction 3th edition ", Oxford University Press INc., New York, (2009).

[57] K. D. M. Harris, "Structure determination of molecular crystals directly from powder diffraction data", The Rigku Journal, Vol. 18, P. (23-33), (2001).

[58] D. E. Sands, "Introduction to crystallography", Dover pulications, INC., (1993).

[59] K. Rissanen, "Advanced X-ray crystallography", Spring, (2012).

[60] K. Ståhl, "Powder diffraction and the Rietveld method", Department of Chemistry Technical University of Denmark, (2008).

[61] S. IIican, Y. Caglar and M. Caglar, " Preparation and characterization of ZnO thin films deposited by sol-gel spin coating method", Journal of Optoelectronic and Advanced materials, Vol. 10, p.(2578 – 2583), (2008).

[62] M. Caglar, Y. Caglar and S. Ilican, "The determination of the thickness and optical constants of the ZnO crystalline thin film by using envelope method", Journal of Optoelectronic and Advanced Materials, Vol. 8, No. 4, p. (1410–1413), (2006).

[63] M. Mazhdi and P. H. Khani, "Structural characterization of ZnO and ZnO:Mn nanoparticles prepared by reverse micelle method", Int. J. Nano Dim., Vol. 2, p. (233-240), Spring 2012.

[64] M. F. C. Ladd and R. A. Palmer, "Structure Determination by X-Ray Crystallography", Plenum Press, (1995).

[65] U. Shmueli, "Theories and Techniques of Crystal Structure Determination", Oxford University Press Inc., NewYork, (2007).

[66] W. Massa, "Crystal Structure Determination", Springer, (2004).

[67] T. Ma and S. Wang, "Phase Transition Dynamics", Springer, (2014).

[68] R. B. Mcclurg and J. P. Smit, "X-ray powder diffraction pattern indexing for pharmaceutical applications", Tech. Europe, (2013).

[69] N. R. McLaren and N. C. Hyatt, "Peak indexing and lattice parameter refinement".

[70] P. E. Werner, L. Eriksson and M. Westdahl, " TREOR, a semi-exhaustive trial-and-error powder indexing program for all symmetries ", J. Appl. Cryst., Vol. 18, p. (367-370), (1985).

[71] H. M. Rietveld, "Line profiles of neutron powder-diffraction peaks for structure refinement", Acta Cryst., Vol. 22, p. (151-152), (1967).

[72] A. Monshi, M. R. Foroughi and M. R. Monshi, " Modified Scherrer equation to estimate more accurately nano-crystallite size using XRD ", World Journal of Nano Science and Engineering, Vol. 2, P. (154-160), (2012).

[73] J. Sakaliuniene, J. Cyviene, B. Abakeviciene and J. Dudonis, " Investigation of structural and optical properties of GDC thin films deposited by reactive magnetron sputtering", Acta physica polonica A, Vol. 120, (2011).

[74] M. Mukhtar, L. Munisa and R. Saleh, "Co-precipitation synthesis and characterization of nanocrystalline zinc oxide particles doped with Cu^{2+} Ions", Materials Sciences and Applications, Vol. 3, P. (543-551), (2012).

[75] W. Pabst and E. Gregorová, " Characterization of particles and particle systems ", ICT Prague, (2007).

[76] S. A. Speakman, "Estimating crystallite size using XRD", MIT Center for Materials Science and Engineering.

[77] R. A. Young, "The Rietveld method", Oxford University Press INc., New York, (1995).

[78] L. E. Smart and E. A. Moore, " Solid State Chemistry An Introduction, Fourth Edition", CRC pressTaylor & Francis group, (2012).

[79] L. E. Smart and E. A. Moore , " Solid state chemistry: an introduction, third edition", CRC Press Taylor & Francis group, (2005).

[80] H.M. Rietveld, **"**Profile refinement method for nuclear and magnetic structures", J. Appl. Cryst., Vol. 2, p. (65-71), (1969).

[81] U. Kolb, K. Shankland, L. Meshi, A. Avilov and W. David, "Uniting electron crystallography and powder diffraction", Spring, (2012).

[82] J. R. Connolly, "Introduction quantitative X-ray diffraction methods", Spring, (2003).

[83] T. A. Al-Dhahir, " Quantitative phase analysis for titanium dioxide from X-ray powder diffraction data using the Rietveld method ", Diyala Journal for Pure Sciences, Vol. 9, P.(108-119), (2013).

[84] E. Dova, "Structure determination of Fe(II) spin-crossover complexes from powder diffraction data with direct-space methods", Universiteit Van Amsterdam, (2003).

[85] B. H. Toby, " R factors in Rietveld analysis: How good is good enough?", Powder Diffraction, Vol. 21, (2006).

[86] N. Masciocchi, "The contribution of powder diffraction methods of structural crystallography :Rietveld and ab-initio techniques", The Rigaku Journal, Vol. 14, (1997).

[87] J. R. Carvajal, "Study of micro-structural effects by powder diffraction using the program Fullprof", Laboratoire Léon Brillouin (CEA-CNRS), France, (2003).

[88] R. Saravanan, M. P. Rani, "Metal and alloy bonding - An experimental analysis", Springer, (2012).

[89] D. L. Brsn and J. E. Posr, "Quantitative mineralogical analysis using the Rietvetd full-pattern fitting method", American Mineralogist, Vol. 78, p. (932-940), (1993).

[90] J. H. Bae, G. Heo, S. Taik Oh, E. Shin, B. S. Seong, C. H. Lee and K. Hwan Oh, " The quantitative analsys method of composite materials by Rietveld

method with texture", Material science forum, Vols. 408-412, p. (215-220), (2002).

[91] R. Snellings, L. Machiels, G. Mertens and J. Elsen, "Rietveld refinement strategy for quantitative phase analysis of partially amorphous zeolitized tuffaceous rocks", Geologica Belgica, Vol. 13, p. (183-196),(2010).

[92] "The Rietveld method", Short Reitveld Course, Atlanta, (2001).

[93] E. Thématique, "Structural analysis from powder diffraction data : The Rietveld method", Cristallographie et Neutrons, (1997).

[94] N. Sahu and S. Panigrahi, "Mathematical aspects of Rietveld refinement and crystal structure studies on $PbTiO_3$ ceramics", Bull. Mater. Sci., Vol. 34, p. (1495–1500), (2011).

[95] M. A. Taylor, R. E. Alonso, L. A. Errico, A. L´opez-Garc´ıa, P. de la Presa, A. Svane and N. E. Christensen, "Structural, electronic, and hyperfine properties of pure and Ta-doped m-ZrO_2", Physical Review B, Vol. 85, P.(1-11), (2012).

[96] G. Štefanić and S. Musić, "Factors influencing the stability of low temperature tetragonal ZrO_2", Croatica Chemical Acta (CCACAA), Vol. 75, P.(727-767), (2002).

[97] C. Piconi and G. Maccauro, "Zirconia as a ceramic biomaterial", Biomaterials, Vol. 20, P.(1 -25), (1999).

[98] A. S. Foster, V. B. Sulimov, F. L. Gejo, A. L. Shluger and R. M. Nieminen, "Structure and electrical levels of point defects in monoclinic zirconia ", Physical Review B, Vol. 64, P.(1-10), (2001).

[99] W. Zhu, R. Wang, G. Shu, P. Wu and H. Xiao, "First-principles study of the structure, mechanical properties, and phase stability of crystalline zirconia under high pressure", Struct Chem, Vol. 23, P.(601–611), (2012).

[100] A. Kumar, "Nanofibers", InTech, (2010).

[101] A. Khan, "Synthesis, characterization and luminescence properties of znic oxide nanostructures", (2006).

[102] S. Baruah and J. Dutta, "Hydrothermal growth of ZnO nanostructures", Sci. Technol. Adv. Mater., Vol. 10, (2009).

[103] M. M. Masıs, "Fabrication and study of ZnO micro- and nanostructures" , Wright State University Dayton-Ohio, (2007).

[104] C. Jagadish and S. J. Pearton, "Zinc Oxide Bulk, Thin Films and Nanostructures Processing, Properties, and Applications", Elsevier, (2006).

[105] Ü. Özgür, Y. I. Alivov, C. Liu, A. Teke, M. A. Reshchikov, S. Doğan, V. Avrutin, S.-J. Cho, H. Morkoç, S.-J. Cho and H. Morkoçd, "A comprehensive review of ZnO materials and devices", Journal of Applied Physics, Vol. 98, (2005).

[106] P. S. Sokolov, A. N. Baranov, Zh. V. Dobrokhotova and V. L. Solozhenko, "Synthesis and thermal stability of cubic ZnO in the salt nanocomposites" , Russian Chemical Bulletin, Vol. 59, Issue 2, P.(325-328), (2010).

[107] A. B. Pinto, "Novel ferromagnetic semiconductors: Preparation and characterization of bulk-and thin film samples of Cu-doped ZnO", Technische Universitat Munchen Walther - Meissner - Institut.

[108] R. R. Doshi , " Synthesis and characterization of some new perovskite type mixed oxide materials ", Saurashtra University, Rajkot, India , (2010).

[109] P. -E. Werner, L. Erikssonon and M. Westdahl, "TREOR, a semi-exhaustive trial-and-error powder indexing program for all symmetries", J. Appl. Cryst., Vol. 18, P. (367-370), (1985).

[110] H. M. Rietveld, "Line profiles of neutron powder-diffraction peaks for structure refinement", Acta Cryst., Vol. 22, p. (151-152), (1967).

[111] J. R. Carvajal, "An Introduction to the Program FullProf 2000 ", Laboratoire Léon Brillouin (CEA-CNRS), (2001).

[112] T. Roisnel1 and J. R. Carvajal, "WinPLOTR: a Windows tool for powder diffraction patterns analysis".

[113] A. K. Zak, W. H. A. Majid, M. E. Abrishami and R. Yousefi, "X-ray analysis of ZnO nanoparticles by Williamson-Hall and size-strain plot methods", Solid State Sciences, Vol. 13, P. (251-256), (2011).

Appendix

- Fullprof Program . 2k (Version 5.40 – May 2014 – ILL JRC).

الخـلاصـة

تم في هذا البحث دراسة البنية البلورية النانوية والخصائص المجهرية لمساحيق اكاسيد معدنية ($ZnO - ZrO_2 - Al_2O_3$) بالحجم النانوي والمايكروي بإستخدام طريقة ريتفيلد لحيود الشعاع السيني للمسحوق وقد تم إختيار هذه العينات بناءاً على إختلاف أنظمتها البلورية.

إجري مسح للعينات بإستخدام جهاز حيود الشعاع السيني قبل وبعد معاملتها حرارياً لدرجات 1180°C لـ $ZrO_2 - Al_2O_3$ و 1200°C لـ ZnO . من القمم الناتجة لحيود الشعاع السيني إجريت عملية الفهرسة بإستخدام برنامجي Dicvol 91 و Treor 90 لتحديد المجموعة الفضائية والنظام البلوري ومعلمات الشبيكة ودلائل ميلر لكل عينة من العينات المستخدمة.

المعلمات المستحصلة من عملية الفهرسة(Indexing process) تستخدم بالاقتران مع بيانات الشدة في برنامج Fullprof لتصفية البنية البلورية والحصول على موائمة بين أطياف الحيود الملاحظة والمحسوبة حيث كانت عوامل الموثوقية (Reliability factors) لـ ZrO_2 nano powder قبل المعامله الحرارية قد بلغ ١,٦ وبعدها بلغ ١,٥ ولـ micro powder قبل المعاملة الحرارية ١,٤ وبعدها بلغ ١,٧ ولـAl_2O_3 nano powder قبل المعاملة الحرارية ٢,٥ وبعدها بلغ ١,٩ ولـ micro powder قبل المعاملة الحرارية قد بلغ ١,١ وبعدها بلغ ٢,٤ ولـ ZnO nano powder قبل المعاملة الحرارية بلغ ١,٣ وبعدها بلغ ١,١ ولـ micro powder قبل المعاملة الحرارية بلغ ١,٩ وبعدها قد بلغ ١,٤ وقد وظفت البيانات المستحصلة من برنامج Fullprof في برنامج WinPLOTER لغرض رسم أطياف الحيود الملاحظة والمحسوبة بعد إجراء عملية التصفية للعينات ألتي تناولها البحث.

بتوظيف بيانات الشعاع السيني تم الحصول على الحجم الحبيبي باستخدام معادلة ديباي-شيرر والحجم الحبيبي والتوتر باستخدام معادلة ويليامسون-هول وقد وجد إن حجم الحبيبات يزداد بعد إجراء المعاملة الحرارية كما تم حساب عامل التشكيل لكل عينة من عينات البحث.

وأخيراً إجري فحص SEM لجميع العينات قبل وبعد معاملتها حرارياً وقد أظهرت الصور تغيراً في طبيعة اشكال الحبيبات(morphology) واحجامها.

جمهورية العراق
وزارة التعليم العالي والبحث العلمي
جامعة ديالى
كلية العلوم
قسم الفيزياء

مقارنة الخصائص التركيبية لبعض مساحيق الأكاسيد المعدنية (النانوية والمايكروية) بإستخدام طريقة ريتفيلد

رسالة مقدمة إلى

مجلس كلية العلوم - جامعة ديالى

وهي جزء من متطلبات نيل شهادة ماجستير علوم في الفيزياء

من قبل

نور عامر حميد الصفار

(بكالوريوس فيزياء - ٢٠٠٩)

بإشراف

الأستاذ المساعد	الأستاذ المساعد
د . نبيل علي بكر	د . تغريد مسلم مربوش

١٤٣٥ هـ

٢٠١٤ م